ISSN: 2639-7455

Research Article

Earth & Environmental Science Research & Reviews

No Gravitational Wave from Orbiting Supermassive Kerr Black Hole—a model of matter distribution and propagation of gravitational waves inside the event horizon

Hiroshi Oya*;

Geophysical Department, Graduate School for Science, Tohoku University; Space and Astrophysics Research Task, Seisa University Japan.

***Corresponding Author**
Hiroshi Oya*, Geophysical Department, Graduate School for Science, Tohoku University and Space and Astrophysics Research Task, Seisa University, Japan.

Submitted :19 Nov 2022; **Accepted**: 02 Dec 2022; **Published**: 03 Jan 2023

Citation: Oya H (2023) No Gravitational Wave from Orbiting Supermassive Kerr Black Hole—a model of matter distribution and propagation of gravitational waves inside the event horizon, *Eart & Envi Scie Res & Rev*. 6(1): 278-332.

Abstract

The matter distribution of the extremely high-energy and dense plasma inside a supermassive rotating black hole has been theoretically investigated, starting from Einstein's equation with the source term, in the coordinate close to the free-falling frame along the geodesics of interior matter, where the state of the force balance can be described with the formalism of modified Newtonian dynamics. For a model of equal-rotation velocity of matter, where the main component of plasma is rotating around a common axis with the same velocity close to the light velocity, with a high Lorentz factor (gamma rate), it is concluded that the matter distribution is condensed to a region with a much smaller radius than that of the event horizon of the Kerr spacetime. The gravitational waves that are generated from the condensed matter region due to the orbital motion of the binary, return towards the source, after ceasing at the critical sphere in the vacuum region of spinning Kerr spacetime. At the stage where returning waves encounter with foreword waves, the gravitational waves are deformed to standing waves that carry no energy outside of the event horizon. We conclude that no gravitational wave is radiated from the supermassive black hole binary.

Keywords: Super Massive Kerr Black Hole, Gravitational Wave, Binary Black Hole, Interior Matter, Kerr Spacetime

1. Introduction

1.1. Relation to Current Studies

Direct observations of gravitational waves (GWs) by LIGO [1,2,3] have opened a new avenue for the quest of GWs, after ,the first indication was made by Einstein [4]. The LIGO team has frequently reported the detection of GWs generated by the mergers of black hole (BH) binaries. The objects of mergers of BHs have been estimated to be in the mass range of a star or intermedium masses less than $120M_{\odot}$. Through the history of the progression of theoretical studies on GWs, the LIGO results meet the expectation of theorists, with no special room for argument. However, because BH mergers have not been directly confirmed by other means, except in the case of the neutron star merger [5], several works have attempted to investigate alternative objects such as the gravastar [6] or ultra-compact star [7,8] as mimics of a BH that has no event horizon, with similar density of matter to that of a BH. These alternatives have not yet been verified because of the current limits of the accuracy of observations. After a long history of studies on star tracking around SgrA* at the center of the Galaxy [9,10,11,12,13], the existence of the supermassive BH has been confirmed; recent results indicated a mass of $(4.31\pm0.42)\times10^6$ $M_{\odot}$ [14], which was further improved to $(4.28\pm0.31)\times10^6$ $M_{\odot}$ [15]. Different from the star-tracking methods of the quest for the supermassive BH, we have proposed evidence for the existence of the supermassive Kerr BH binary (SMBHB) based on results from observations of decameter radio wave pulses (DRWP) at 21.86 MHz from SgrA* [16]. Digitized data from observations whose signal-to-noise ratios are from 1/200 to 1/500 (i.e., extremely low) were transformed to Fourier-analyzed spectra; after sufficient averaging to eliminate background noise, the final data, called the BH code, were deciphered by applying the simulation technique to the original signals, which comprised two kinds of pulses; detected intrinsic pulse periods of (173±1) and (148±1) s show constant variation with common periods at 2,200±50 s. By attributing the pulses to spins of two Kerr BHs, we concluded that two supermassive BHs exist, temporarily called Gaa with the mass of $(2.27\pm0.02)\times10^6$ $M_{\odot}$ and Gab with the mass of $(1.94\pm0.01)\times10^6$ $M_{\odot}$ ($(4.21\pm0.03)\times10^6$ $M_{\odot}$ in total), forming a binary system with an orbital period of around ~2,200 s. The orbital velocities of Gaa and Gab were also calculated as 18% and 22%, respectively, of the velocity of light. Interpretation [17] has been carried out for the evidence of the time varying emissions with regular period

of 2150±2.5sec observed by 1.3mm wavelength radio VLBI [18] , with time variation model of 1,3 mm wavelength radio wave sources associated with SMBHB orbital motions [17] whose parameters are decided as results of DRWP[16]. By this study to confirm the orbits parameters by coincidence between VLBI observations and DRWP results, we can state the existence of SMBHB at Sgr A* with such extreme parameters.

Thus far, when we apply the currently established theory of the generation of GWs from the binary BH without distinguishing between a star-mass BH binary (STM-BHB) and SMBHB, the existence of the above-described SMBHB system may not be accepted at all because of the extremely high rate of energy loss of the orbital motion due to the generation of GWs. However, if we have room to argue for the difference in the generation mechanism of GWs between the cases of STM-BHB and SMBHB, we could not abandon the proposal of the existence of the SMBHB at SgrA*. Thus, we presently have evidence with which pursuing the present study can be considered to be meaningful; that is, there has been no report of the merger of a SMBHB by ongoing observations of GWs, despite frequent reports of the merger of BHs of a STM-BHB and an intermediate-mass BH binary [19]. The trial to observe the continuous GWs from the expected SMBHB has not been detected yet [20].

Currently we have thought that the most important references to the standpoint of claim of existence of SMBHB at SgrA* are the results of EHTC works [21,~26]. Though the EHTC forced to release the single image of BH shadow at SgrA* we are not able to accept the results because of clarifying discrepancy or erroneous conclusion. The erroneous conclusion is disclosed by Miyoshi et al [27] who pointed out that the EHTC made basic misunderstanding for their mapping processes of the VLBI data which resulted construction of wrong image for shadow of black hole M87*[28,~33]. Miyoshi et al claim [27] that there is an inherent hole , of the data distribution versus viewing angle, that coincides with a size resembling the shadow of the black hole caused due to biased locations of the global scale distribution of observation station of VLBI of the EHT. It is naturally adopted to the case of the SgrA* whose observation data are collected almost in the same periods with completely same VLBI system. Furthermore we consider that in the EHTC approach constructing image of the black hole shadow, the problem of the time variation of the observed data [34] is not solved even that is the principal cause for delaying the release of the image of the black hole shadow of SgrA* about three years compared with the rerelease of M87*.

1.2. The Purpose and Uniqueness of the Present Study

Thus, the purpose of the present study is to investigate a possible model that allows the stable existence of the extremely close case of the SMBHB without outward radiation of GWs. A significant step toward the purpose of the present study is to achieve a physically reasonable model for the distribution of collapsed matter as "inside matter" of the supermassive BH (IMSBH, hereafter). Current studies on the interior of the Kerr BH are described based on the anti-de-Sitter (Kerr-AdS) space time [e.g.35,36,37]. Such works for the interior of the Kerr BH generally concern with the stellar-mass BH, where the source energy tensor of the Einstein equation consist of the quantum dynamical wave equations for the quark–gluon plasma. In this work, for the case of the supermassive BH, the Kerr-AdS space time was not used. There are three reasons why we applied the present unique method without following the already established space time to investigate the interior of the Kerr BH. The first is because we are concerned with the supermassive BH, whose maximum possible density of interior matter is in a relatively tenuous state because the average density of the BH interior follows the inverse square law of the total mass. For example, in the case of a supermassive BH with mass of 10^6 $M_{\odot}$, the density becomes $10^{-8} \sim 10^{-12}$ that of the stellar-mass BH. Thus, we can apply classical dynamics to the rotating plasma as the interior matter of the BH. The second reason that we do not use the direct spacetime of the interior matter region of the BH, is in the coordinate system covering the wide range of space of the binary system. More specifically, the orbital motion of the binary can be described by Newtonian dynamics, while the generation of GWs caused by this orbital motion is exactly the subject of the general relativity governed by the spacetime around the source region. Rigorous connection of the dynamics of the two regimes is possible when we transform the physical processes to the quasi-Minkowsky coordinates that are selected as a common observation frame of the two regimes of physics. The third reason is that unlike the de-Sitter or anti-de-Sitter spacetime, whose curvature is controlled by vastly distributed inside matter, we seek the collapsed matter region, leaving a wide vacuum region on the inner side of the event horizon.

Accordingly, we selected observation coordinates that are not fixed to the BH but are close to the freefalling system following the geodesics of the corresponding BH interior. The analytical method to determine the force balance state is based on the quasi-Minkowsky spacetime (QMST) that starts from Einstein's gravity equation, setting the perturbation spacetime from the Minkowsky spacetime. The method to establish the forces follows that indicated by Einstein himself [38]. In the detailed phase, however, we have modified his processes from two aspects. First, contrary to the case of the present study with high-speed rotation of the inside plasma with a velocity close to that of light, Einstein selected in his lecture, the case of low-speed matter whose velocity is negligible compared to that of light. Second, regarding the function to set the source energy tensor, we applied the delta function for locally moving matter because the energy carried by moving matter works at the moment of mutual interaction only at a given point, unlike the case of gravity that shows effects of the interaction with matter located at remote places. The characteristic point of the present model is the assumption of the equal speed of matter rotation with quasi-light velocity, with a high relativistic gamma rate, in a range greater than 10, to increase momentum of the rotating matter. Then, in the model, the radius of the matter region is condensed from 1/10 to 1/100 of the radius of the event horizon, maintaining the

observed mass and rotation parameters to describe Kerr spacetime in a vacuum region as the same as the observed values.

The studies from Sec.2 to Sec.4 concern with formation of IMSBH that is located deep inside of BH contacting with the boundary of Kerr spacetime that is characterized as vacuum solution, of the Einstein field equation, which is constructed with the mass and angular momentum of IMSBH; It should be emphasized that contents in Sec.2 to Sec.4 are not purposed to modify the orthodox form of the Kerr spacetime but for IMSBH inside of the Kerr spacetime. Then, in Sec.5 and Sec.6, the generation and propagation of GWs are analyzed over a wide vacuum area inside the region of the event horizon of Kerr spacetime. Current studies on the radiation of a GW from a BH state that there is no definite distinction between neutron stars concerning either quasi-normal mode radiation [39,40] or radiation of GWs associated with the orbital motion or merger of compact objects [41,42]. More specifically, in the case of quasi-normal mode oscillation, the existence of the event horizon that distinguishes the BH from other compact stars such as neutron stars is considered. However, because there is no clear separation of the vacuum region from the matter distribution, oscillation of the event horizon is assumed simultaneously [43]. Thus, current studies on the radiation of a GW from a BH are not impeded by the existence of the event horizon; this may be accepted in the case of a stellar-mass BH, where the separation of the matter zone from the event horizon is not clearly discussed.

In this study, we analyze the generation and propagation of GWs, for the IMSBHs isolated deep inside of surrounding Kerr spacetime of a supermassive BH. It is important that the result of the present study reveals that the sources of GW are not available outside of the event horizon of BH a priory; GWs are generated by the acceleration of the quadruple moment source formed by the binary configuration and their orbital motions of IMSBHs, but the propagation of the GW is controlled due to the constraint of the Kerr spacetime inside the event horizon. The waves are deformed to standing waves that are unable to carry energy outside, as described in Sec. 5. Thus, we conclude that no GW is radiated from the SMBHB, as described in Sec. 6.

2. Classical Approach to Analyze the Internal State of IMSBH

2.1. State of Matter Distribution

The average density of possible matter inside of a BH generally becomes milder as the mass becomes larger. The average density of a BH, where the matter radius is assumed to be close to the Schwarzschild radius r_s with a spherically symmetric shape and total mass of M, can be simply estimated using:

$$\rho = \frac{M}{\left(\frac{4\pi}{3}\right) r_s^3} =\cdot \frac{\rho_\odot}{\left(M/M_\odot\right)^2} \ . \qquad (2.1)$$

where $M_\odot$ is the solar mass, and $\rho_\odot$ is the average density of the solar-mass BH with Schwarzschild radius $r_{s\odot}=2GM_\odot/c^2$. In Figure 1, the interior state of possible matter of a BH is given in terms of the estimated average density of the matter region (top panel) and the average separation distance of baryon (bottom panel) for the assumed matter radius close to the event horizon; furthermore, the average particle distance d is calculated from $d=N^{(1/3)}$ for the number density N of neutrons for regime I and ions for regime II. The mutual distance of particles in regime I covers the distance range less or close to the neutron radius r_n, reflecting the state of quark–gluon plasmas that are described by quantum mechanical theory; whereas, the particle distance in regime II is larger than 10^4 r_n, suggesting high-density plasma that can be described by classical plasma physics.

For the plasma state in regime II, we assume iron ions throughout this work, considering that the matter is in the final stages where energy is provided only by gravity; possible accreting components with atomic nuclei lighter than those of iron are considered to be fractional and to arrive at the final stage after a relatively short period of nuclear fusion. The mutual distance of particles in regime I in Figure 1 covers the state of a stellar-mass BH, while the particle distance in regime II is for the supermassive BH. These interior states of matter show a clear contrast to the states of the stellar-mass BH, regime I in the bottom panel of Figure 1, whose masses are smaller than $100M_\odot$, where the average separation distance of particles is less or close to the neutron radius r_n. This state is currently considered as quark–gluon plasma by quantum mechanics. To describe the interior state of a supermassive BH with a mass larger than 10^5 $M_\odot$, we can therefore consider states of plasma whose physics can be described using classical mechanics.

2.2. Description of Dynamics of IMSBH by Bridging Einstein's Equation to the Modified Newtonian Dynamics

2.2.1. Basic equations

We start with the Einstein equation to find the spacetime of the present study for the supermassive BH which consists of Kerr spacetime for vacuum solution of the Einstein equation and a spacetime for IMSBH which is located inside region of Kerr spacetime with assumed spherical boundary; that is.

$$R_{jk} - \frac{1}{2} g_{jk} R = \kappa T_{jk} \ . \qquad (2.2)$$

where R_{jk},R,g_{jk},and T_{jk} are the Ricci tensor, scalar Ricci, metric describing spacetime, and the source energy tensor, respectively; and κ is Einstein's coefficient that connects energy to the four-dimensional curvature providing forces. Because the regions of vacuum and distributed matter are clearly separated in the present model, we can rewrite eq.(2.2) as

$$R_{jk}^{(K)} - \frac{1}{2} g_{jk}^{(K)} R^{(K)} = 0 . \quad \text{and} \quad R_{jk}^{(M)} - \frac{1}{2} g_{jk}^{(M)} R^{(M)} = \kappa T_{jk} \qquad (2.3)$$

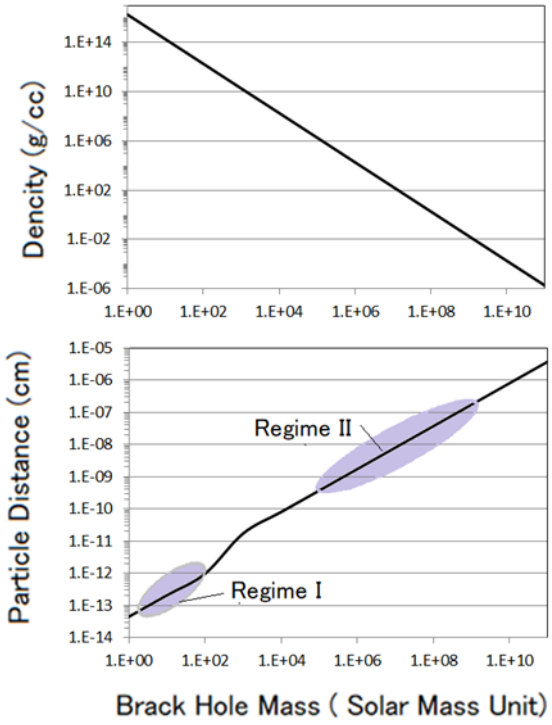

Figure 1: Interior state of the black hole (BH) in terms of the estimated average density of the matter region for an assumed radius close to the event horizon (top panel) and average separation distance of ions (bottom panel). The average separation distance d of particles is calculated from $d=N^{(1/3)}$ for the number density N of neutrons for regime I and ions for regime II; d in regime I covers a range less than or close to the neutron radius r_n, reflecting the state of quark–gluon plasmas described by the quantum mechanical theory, while d in regime II is larger than $10^4\, r_n$, suggesting the state of high-density plasma that can be described by classical plasma physics.

where superscripts (K) and (M) are for the Kerr spacetime and IMSBH, respectively. Hereafter we concentrate to the space time of IMSBH before arriving at Sub. Sec 3.5 where we consider the boundary of the Kerr spacetime and IMSBH.

To find the spacetime of IMSBH, we have started with a standpoint to search for suitable coordinates to describe the dynamics of plasma as IMSBH. Then, we select a coordinate close to the freefall system to observe the balance in the forces in the regime of classical dynamics; hence, the spacetime is expressed by perturbation of the Minkowsky spacetime. We determine the perturbation terms by following the methods of Einstein, who demonstrated the connection to Newtonian dynamics of matter, for weak fields, starting from the Einstein equation with source energy tensor [38].

When we express the anti-covariant vector in the coordinate of the IMSBH, as $x^{(M)i}$ (coordinate $x^{(M)i}$ hereafter) geodetics in the spacetime of the IMSBH can be written as:

$$\frac{d^2 x^{(M)i}}{ds^2} + \Gamma_{jk}^{(M)i} \frac{dx^{(M)j}}{ds} \frac{dx^{(M)k}}{ds} = 0, \qquad (2.4)$$

Further, when we select a coordinate slightly shifted from the coordinate of system that freefalls in the spacetime of IMSBH , we obtain the following geodesics:

$$\frac{d^2 x^{\alpha}}{ds^2} + \Gamma_{\mu\nu}^{\alpha} \frac{dx^{\mu}}{ds} \frac{dx^{\nu}}{ds} = 0, \qquad (2.5)$$

where

$$\Gamma_{\mu\nu}^{\alpha} = \frac{\partial x^{\alpha}}{\partial x^{(M)i}} \Gamma_{j\,k}^{(M)i} \frac{\partial x^{(M)j}}{\partial x^{\mu}} \cdot \frac{\partial x^{(M)k}}{\partial x^{\nu}} + \frac{\partial x^{\alpha}}{\partial x^{(M)\xi}} \frac{\partial^2 x^{(M)\xi}}{\partial x^{\mu} \partial x^{\nu}}. \qquad (2.6)$$

Then, the force F^{α} working on a portion with density ρ in the frame of the IMSBH is given by:

$$F^{\alpha} = \rho \frac{d^2 x^{\alpha}}{ds^2} = -\rho \Gamma^{\alpha}_{\mu\nu} \frac{dx^{\mu}}{ds} \frac{dx^{\nu}}{ds}. \tag{2.7}$$

Here, we can describe the spacetime using the perturbation metric γ_{jk} with respect to the Minkowsky spacetime η_{jk} because the observation system is close to a freefall system, i.e.,

$$g_{jk} = \eta_{jk} + \gamma_{jk}, \tag{2.8}$$

which is referred to as QMST(see Introduction).
As a solution to satisfy Einstein's equation, given in the second of Eq. (2.3) gives the relation:

$$R^{(M)}_{jk} = \frac{1}{2}\eta^{\beta\beta}\left(\frac{\partial^2 \gamma_{\beta j}}{\partial x^{\beta}\,\partial x^{k}} + \frac{\partial^2 \gamma_{\beta\beta}}{\partial x^{j}\,\partial x^{k}} - \frac{\partial^2 \gamma_{\beta j}}{\partial x^{\beta}\,\partial x^{k}}\right) - \frac{1}{2}\eta^{\beta\beta}\left(\frac{\partial^2 \gamma_{\beta j}}{\partial x^{k}\,\partial x^{\beta}} + \frac{\partial^2 \gamma_{\beta k}}{\partial x^{j}\,\partial x^{\beta}} - \frac{\partial^2 \gamma_{jk}}{\partial x^{\beta}\,\partial x^{\beta}}\right) + K, \tag{2.9}$$

where

$$K = \Gamma^{\beta}_{k\alpha}\Gamma^{\alpha}_{j\beta} - \Gamma^{\beta}_{j\alpha}\Gamma^{\alpha}_{k\beta} = 0. \tag{2.10}$$

We can rewrite Eq. (2.9) further defining $\gamma = \eta^{\beta\beta}\gamma_{\beta\beta}$, as:

$$R^{(M)}_{jk} = \frac{1}{2}\Box\gamma_{jk} + \frac{1}{2}\left(\frac{\partial^2 \gamma}{\partial x^{j}\,\partial x^{k}} - 2\eta^{\beta\beta}\frac{\partial^2 \gamma_{\beta k}}{\partial x^{\beta}\,\partial x^{k}}\right). \tag{2.11}$$

Here, we can find the generalized Lorentz condition as:

$$\frac{\partial^2 \gamma}{\partial x^{j}\,\partial x^{k}} - 2\eta^{\beta\beta}\frac{\partial^2 \gamma_{\beta k}}{\partial x^{\beta}\,\partial x^{k}} = 0. \tag{2.12}$$

Then, it follows that:

$$R^{(M)}_{jk} = \frac{1}{2}\Box\gamma_{jk}. \tag{2.13}$$

Setting $\gamma = \eta^{ij}\gamma_{ij}$, the scalar Ricci R is expressed as:

$$R^{(M)} = \eta^{jk}R^{(M)}_{jk} = \frac{1}{2}\eta^{jk}\Box\gamma_{jk} = \frac{1}{2}\Box\gamma, \tag{2.14}$$

and the second of Eq. (2.3) becomes:

$$\Box\gamma_{jk} - \frac{1}{2}\eta_{jk}\Box\gamma = \kappa T_{jk}. \tag{2.15}$$

2.2.2. Rationale of using the QMST

Before proceeding, we consider the appropriateness of our approach to find the state of force balance in the IMSBH, which has its own spacetime $g_{ij}^{(M)}$ that apparently differs from our assumed QMST. For the coordinate $x^{(M)i}$ fixed to IMSBH, we have a corresponding coordinate x^{i} in QMST that is related as:

$$x^{(M)i} = x^{(M)i}(x^0, x^1, x^2, x^3). \tag{2.16}$$

Then, by the transformation of the tensor, the relation between the QMST and the spacetime of IMSBH is given by:

$$\eta_{\mu\nu} + \gamma_{\mu\nu} = g^{(M)}_{jk} \frac{\partial x^{(M)j}}{\partial x^{\mu}} \cdot \frac{\partial x^{(M)k}}{\partial x^{\nu}} . \tag{2.17}$$

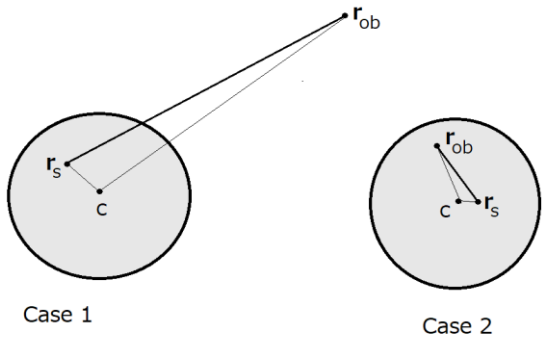

Figure 2: Configurations between the source point r_s and the observation point r_{0b}. Case 1: r_{0b} is located outside of the source region. Case 2: r_{0b} is located inside the source region; this is the case of the present study.

For the geodesic of IMSBH given by Eq. (2.4), we obtain the geodesic in Eq. (2.5) with the transformed affine coefficient given in Eq. (2.6), corresponding to the geodesic in our selected QMST. Then, we can observe the force balance acting on a group of test particles with density ρ from Eq. (2.7) as:

$$F^i = \rho \frac{d^2 x^i}{ds^2} = -\rho \Gamma^i_{\mu\nu} \frac{dx^{\mu}}{ds} \frac{dx^{\nu}}{ds} = 0. \tag{2.18}$$

As described in the following sections, the force balance detected in the QMST is endorsed as the true state of force balance in IMSBH. From the geodesics of the IMSBH given in Eq. (2.4), the forces working on test particles with density ρ and the force balance states are:

$$F^{(M)i} = \rho \cdot \frac{d^2 x^{(M)i}}{ds^2} = 0, \text{and } -\rho \cdot \Gamma^{(B)i}_{jk} \frac{dx^{(M)j}}{ds} \cdot \frac{dx^{(M)k}}{ds} = 0 . \tag{2.19}$$

For $d^2 x^{\alpha}/ds^2$ in Eq. (2.5), which expresses the geodesic in QMST, we can determine the following relation:

$$\frac{d^2 x^{\alpha}}{ds^2} = \frac{d}{ds}\left(\frac{\partial x^{\alpha}}{\partial x^{(M)\,i}}\right) \cdot \frac{dx^{(M)i}}{ds} + \frac{\partial x^{\alpha}}{\partial x^{(M)\,i}} \cdot \frac{d^2 x^{(M)i}}{ds^2} . \tag{2.20}$$

Considering the time-stationary condition (see Appendix A), the first term on the right-hand side of the above equation vanishes, as:

$$\frac{d}{ds}\left(\frac{\partial x^{\alpha}}{\partial x^{(B)\,i}}\right) = 0. \tag{2.21}$$

Then, Eq. (2.19), which reveals the force balance state in the IMSBH, produces the result to Eq. (2.20) as:

$$\frac{d^2 x^{\alpha}}{ds^2} = 0. \tag{2.22}$$

Once Eq. (2.22) is confirmed, we can further realize, for QMST, that:

$$\Gamma^{\alpha}_{\mu\nu} \frac{dx^{\mu}}{ds} \cdot \frac{dx^{\nu}}{ds} = 0. \tag{2.23}$$

The above-described logic indicates that the force balance of IMSBH is strictly reflected by the force balanced state described by QMST. Furthermore, because $dx^{(M)j}/ds$ and $dx^{(M)k}/ds$ are not necessarily zero for all of those terms, we should select the following in Eq. (2.19):

$$\Gamma_{jk}^{(B)i} = 0. \qquad (2.24)$$

More specifically, around the point of the force balance, we can describe the dynamics in the IMSBH by applying the approximation on the frame of QMST.

2.2.3. Einstein's approach [38].

Substituting η^{jk} to both sides of Eq. (2.15), we obtain the equation that was originally shown by Einstein as:

$$\Box\eta^{jk}\gamma_{jk} - \frac{1}{2}\eta^{jk}\eta_{jk}\Box\gamma = \kappa \cdot \eta^{jk}T_{jK} = \kappa T. \qquad (2.25)$$

Because $\eta^{ij}\,\eta_{ij}=4$, it follows from Eq. (2.25) that:

$$-\Box\,\gamma = \kappa T\ . \qquad (2.26)$$

Then, by inserting this $\Box\gamma$ into Eq. (2.15), it follows that

$$\Box\gamma_{jK} = \kappa T_{jk}^{*}\,, \qquad (2.27)$$

where

$$T_{jk}^{*} = T_{jk} - \frac{1}{2}\eta_{jk}T\,. \qquad (2.28)$$

By rewriting the d' Alembertian with respect to the coordinates (x,y,z,t) as:

$$\Box \equiv \eta^{\beta\beta}\frac{\partial^2}{x^\beta x^\beta} = \frac{\partial^2}{-c^2\,\partial t^2} + \frac{\partial^2}{\partial x^2} + \frac{\partial^2}{\partial y^2} + \frac{\partial^2}{\partial z^2}, \qquad (2.29)$$

the solution for γ_{jk} can be expressed by:

$$\gamma_{jk}(\mathbf{r}_{ob}) = \frac{\kappa}{2\pi}\iiint \frac{T_{jk}^{*}(\mathbf{r}_s, \mathbf{t} - r_{os}/c)}{r_{os}}\,dx_s dy_s dz_s \qquad (2.30)$$

where r_{0b} and r_s are the position vectors for the observation point and source position, respectively. Then, the scalar distance r_{os} between the observation point and source point is given as:

$$r_{os} = |\mathbf{r}_{0b} - \mathbf{r}_s| = \sqrt{(x_{ob} - x_s)^2 + (y_{ob} - y_s)^2 + (z_{ob} - z_s)^2}\ . \qquad (2.31)$$

With respect to the two categories of configurations between source $\boldsymbol{r}_s$ and observation point $\boldsymbol{r}_{0b}$ depicted in Figure 2, we are concerned with case 2. The perturbation metric $\gamma_{jk}(\mathbf{r}_{ob})$ given by Eq. (2.30) is subject to the condition of inside the source region; that is, we cannot avoid the point where $r_{os}=0$ in the processes of the integration to describe the metric of IMSBH.

2.3. Perturbation Metrics of IMSBH in QMST

2.3.1. Rotating state of IMSBH

We start with the metric in QMST given by Eq. (2.8) that is understood as spacetime transformed from that of IMSBH; by rewriting to the spherical coordinates, we obtain:

$$ds^2 = -(1-\gamma_{00})c^2dt^2 + (1+\gamma_{11})dr^2 + (1+\gamma_{22})r^2d\theta^2 + (1+\gamma_{33})r^2\sin^2\theta d\varphi^2. \qquad (2.32)$$

Further, we consider the case of a supermassive BH where the IMSBH rotates with a constant velocity v_φ, associated with additional components that have random thermal velocity $\mathbf{v}_{th}$. Then, for the rotating component, v_φ can be express by:

$$v_\varphi = r \cdot \sin\theta \cdot \Omega, \quad \text{with } \Omega = \frac{d\varphi}{dt}. \tag{2.33}$$

For this case, Eq. (2.32) is rewritten as:

$$ds^2 = -(1-\gamma_{00}^*)c^2dt^2 + (1+\gamma_{11})dr^2 + (1+\gamma_{22})r^2d\theta^2, \tag{2.34}$$

where

$$\gamma_{00}^* = \gamma_{00} + (1+\gamma_{33})\left(\frac{v_\varphi}{c}\right)^2. \tag{2.35}$$

When we find ds for dr=0, and dθ=0, considering $\gamma_{33} \ll 1$, under the condition $v_\varphi \approx c$, it follows that:

$$ds^2 = -\left(1-\left(v_\varphi/c\right)^2 - \gamma_{00}\right)\cdot c^2dt^2 \quad . \tag{2.36}$$

The present study is carried out in a coordinate system $1 - (v_\varphi/c)^2 \gg \gamma_{00}$. Hereafter, we take ds^2 as:

$$ds^2 = -\left[1-\left(\frac{v_\varphi}{c}\right)^2\right]c^2t^2. \tag{2.37}$$

2.3.1. Setting of source function for rotating IMSBH

The setting of the energy as the source function in the second of Eq. (2.3) is basically guided by Einstein's concept [38], where the energy expression is generalized from the case of special relativity as:

$$T_{jk} = g_{j\mu}g_{k\nu}\rho\frac{dx^\mu}{ds}\cdot\frac{dx^\nu}{ds} - g_{jk}p, \tag{2.38}$$

where ρ and p are the density at rest for ponderable matter and total pressure, which constitute the hydrodynamic component and magnetic energy, respectively. Considering the case of high velocity where $(v_\varphi/c)^2 \approx 1$, we can define the energy density of plasma dynamics p for the IMSBH in the QMST frame as:

$$c^2\,p = \rho\cdot(1-\zeta)\gamma_{th}^*\frac{v_{th}^2}{2} + \frac{B^2}{2\mu_0}, \tag{2.39}$$

where ζ is the ratio of the plasma component, which is responsible for systematic flow, while the ratio (1-ζ) is for the themal component; B^2/μ_0 , with permittivity μ_0 of the magnetic field in vacuum, is the energy density of the magnetic field generated by possible electric currents in the plasma distributed in IMSBH. Because generation of the magnetic field energy is directly related to the stage of the charge separation in the plasma, the existence of the magnetic energy is independently given to the mass of the matter. In addition, relating to Eqs. (2.37) and (2.39), we define Lorentz factors, γ_φ^* and γ_{th}^* as:

$$\gamma_\varphi^* = \frac{1}{\sqrt{1-\left(\frac{v_\varphi}{c}\right)^2}} \quad \text{and} \quad \gamma_{th}^* = \frac{1}{\sqrt{1-\left(\frac{v_{th}}{c}\right)^2}}, \tag{240}$$

i.e., the plasma components of the rate ζ take systematic motion in the azimuthal direction φ with velocity v_φ, which is close to the velocity of light c, while components with rate (1-ζ) are in a state of thermal motion with thermal velocity v_{th}, which is also close to c. The dynamics of these plasma components are all under the effects of the magnetic field B and intense gravitational force.

We start with the Cartesian coordinates for space, which are transformed to spherical coordinates as subsidiary coordinates in cases when the expression becomes tractable. To set the source energy density following Einstein's constant, given in the second of Eq. (2.3), we consider that room remains to modify the coefficient with a related function to connect the energy tensor T_{jk} to match the description of Newtonian dynamics of the plasma. The modification also remains for the effects of source terms that have two categories. The first category is for the gravity that has remote effects; and the second is for local dynamical forces in plasma that have no remote influence. In the latter case, the source tensor T_{jk} is selected for local effects at $\mathbf{r}_s$ by introducing$\delta(\mathbf{r}-\mathbf{r}_s)$, where $\mathbf{r}$ and $\mathbf{r}_s$ are, respectively, the general position vector and the vector to indicate a specific position within the source plasma.

We follow Eqs. (2.38) and (2.39) to obtain:

$$T_{00} = \rho\gamma_{\varphi}^{*2} - \frac{\lambda}{\kappa c^2}\cdot(1-\zeta)\nu\left(\frac{\rho\delta(\boldsymbol{r}-\boldsymbol{r}_s)\gamma_{th}^{*2}v_{th}^2}{2}+\frac{B^2}{2\mu_0}\right) \quad \ldots\ldots\ldots\ldots\ldots\ldots\ldots (2.41)$$

where λ is a factor introduced to bridge the result of Einstein's gravity equation and modified Newtonian dynamics. Further, we use plasma β to describe the relation between the kinetic and magnetic pressure, defined as follows:

$$\beta = \left(\rho\gamma_{\mathrm{th}}^{*2}\frac{v_{\mathrm{th}}^2}{2}\right)\Big/\left(\frac{B^2}{2\mu_0}\right). \quad (2.42)$$

Considering the rotation of plasma as described in Sec. 2.3.1., the other terms of T_{jk} are:

$$T_{11} = \frac{\lambda}{\kappa}\rho\delta(\mathbf{r}-\mathbf{r}_s)\gamma_{\varphi}^{*2}\left(v_{\varphi}^2/c^2\right)\cdot\sin^2\varphi\,, \quad (2.43)$$

$$T_{22} = \frac{\lambda}{\kappa}\rho\delta(\mathbf{r}-\mathbf{r}_s)\gamma_{\varphi}^{*2}\left(v_{\varphi}^2/c^2\right)\cdot\cos^2\varphi\,, \quad (2.44)$$

$$T_{12} = T_{21} = -\frac{1}{2}\cdot\frac{\lambda}{\kappa}\rho\delta(\mathbf{r}-\mathbf{r}_s)\gamma_{\varphi}^{*2}\left(v_{\varphi}^2/c^2\right)\cdot\sin 2\varphi\,, \quad (2.45)$$

$$T_{33} = 0\,. \quad (2.46)$$

The effects of the rotating plasma are also expressed by T_{0i} for i=1,2 as:

$$T_{0i} = T_{i0} = \delta(\mathbf{r}-\mathbf{r}_s)\cdot\frac{\lambda}{\kappa}\rho\cdot\zeta\gamma_{\varphi}^{*2}\frac{dx^i}{cdt}. \quad (2.47)$$

In Eqs. (2.43)–(2.47), $\delta(\mathbf{r}\text{-}\mathbf{r}_s)$ is defined as:

$$\delta(\mathbf{r}-\mathbf{r}_s) = \delta\left(x^{(1)}-x_s^{(1)}\right)\cdot\delta\left(x^{(2)}-x_s^{(2)}\right)\cdot\delta\left(x^{(3)}-x_s^{(3)}\right). \quad (2.48)$$

We start solving the Einstein equation with the form given in Eq. (2.27), which is deduced by changing Eq. (2.15), with Eq. (2.28), following Einstein's original method. The source tensor T_{jk} is transformed to T_{jk}^{*} (see Appendix B) as:

$$(T_{jk}^{*}) = \begin{pmatrix} T_{00}^{*} & T_{01}^{*} & T_{02}^{*} & 0 \\ T_{10}^{*} & T_{11}^{*} & T_{12}^{*} & 0 \\ T_{20}^{*} & T_{21}^{*} & T_{22}^{*} & 0 \\ 0 & 0 & 0 & T_{33}^{*} \end{pmatrix}, \quad (2.49)$$

where $T_{0i}^{*}=T_{i0}^{*}=T_{0i}=T_{i0}$ because $\eta_{i0}=\eta_{0i}=0$. The elements of the source tensor are then given by:

$$T_{00}^{*} = \frac{1}{2}\left[\left(\rho\gamma_{\varphi}^{*2}-A_f\right)+\frac{\lambda}{\kappa}\rho\delta(\mathbf{r}-\mathbf{r}_s)\gamma_{\varphi}^{*2}\left(v_{\varphi}^2/c^2\right)\right], \quad (2.50)$$

$$T_{11}^{*} = \frac{1}{2}\left[\left(\rho\gamma_{\varphi}^{*2}-A_f\right)-\frac{\lambda}{\kappa}\rho\delta(\mathbf{r}-\mathbf{r}_s)\gamma_{\varphi}^{*2}\left(v_{\varphi}^2/c^2\right)\cos 2\varphi\right], \quad (2.51)$$

$$T_{22}^{*} = \frac{1}{2}\left[\left(\rho\gamma_{\varphi}^{*2}-A_f\right)+\frac{\lambda}{\kappa}\rho\delta(\mathbf{r}-\mathbf{r}_s)\gamma_{\varphi}^{*2}\left(v_{\varphi}^2/c^2\right)\cos 2\varphi\right], \quad (2.52)$$

and

$$T_{33}^{*} = \frac{1}{2}\left[\left(\rho\gamma_{\varphi}^{*2} - A_f\right) - \frac{\lambda}{\kappa}\rho\delta(\mathbf{r}-\mathbf{r}_s)\gamma_{\varphi}^{*2}\left(v_{\varphi}^2/c^2\right)\right]. \tag{2.53}$$

Because $\eta^{12}=\eta^{21}=0$, it follows from Eq. (2.45) that:

$$T_{12}^{*} = T_{21}^{*} = -\frac{1}{2}\cdot\frac{\lambda}{\kappa}\rho\delta(\mathbf{r}-\mathbf{r}_s)\gamma_{\varphi}^{*2}\left(v_{\varphi}^2/c^2\right)\cdot\sin 2\varphi\,. \tag{2.54}$$

In Eqs. (2.50)–(2.53), the term A_f is given by:

$$A_f = \frac{\lambda}{\kappa}\cdot(1-\zeta)\frac{\rho\delta(\mathbf{r}-\mathbf{r}_s)\gamma_{th}^{*2}v_{th}^2}{2c^2}\left(1+\frac{1}{\beta}\right). \tag{2.55}$$

2.3.3. Calculation of perturbation metrics γ_{jk}.

Corresponding to case 2, inside the IMSBH, as shown in Figure 2, where dt ($=r_{os}/c$) $\ll$ r_g/c, the solution given by Eq. (2.30) is rewritten as:

$$\gamma_{ij}(\mathbf{r}_{ob}) = \frac{\kappa}{2\pi}\iiint\frac{T_{ij}^{*}(\mathbf{r}_s)}{r_{os}}dx_s dy_s dz_s, \tag{2.56}$$

where $x_s^{(1)} = x_s$, $x_s^{(2)} = y_s$,and $x_s^{(3)} = z_s$. For the case of $i=j$ and for $i = 0$ and 3, it follows that:

$$\gamma_{ii}(\mathbf{r}_{ob}) = \cdot\frac{\kappa}{4\pi}\iiint\frac{\gamma_{\varphi}^{*2}\rho(\mathbf{r}_s)}{r_{os}}dx_s dy_s dz_s$$
$$-\frac{\kappa}{4\pi}\iiint\frac{\delta(\mathbf{r}-\mathbf{r}_s)\cdot\frac{\lambda}{\kappa}\rho\cdot(1-\zeta)\cdot\gamma_{th}^{*2}\frac{\left(v_{th}^2/c^2\right)}{2}\left(1+\frac{1}{\beta}\right)}{r_{os}}dx_s dy_s dz_s$$
$$\pm\frac{\kappa}{4\pi}\iiint\frac{\lambda}{\kappa}\frac{\rho\delta(\mathbf{r}-\mathbf{r}_s)\gamma_{\varphi}^{*2}\left(v_{\varphi}^2/c^2\right)}{r_{os}}dx_s dy_s dz_s, \tag{2.57}$$

where the + sign of ± is for the case of $i = 0$ and the – sign is for $i = 3$; and for $i = 1$ and 2, it follows that:

$$\gamma_{ii}(\mathbf{r}_{ob}) = \frac{\kappa}{4\pi}\iiint\frac{\gamma_{\varphi}^{*2}\rho(\mathbf{r}_s)}{r_{os}}dx_s dy_s dz_s$$
$$-\frac{\kappa}{4\pi}\iiint\frac{\delta(\mathbf{r}-\mathbf{r}_s)\cdot\frac{\lambda}{\kappa}\rho\cdot(1-\zeta)\gamma_{th}^{*2}\frac{\left(v_{th}^2/c^2\right)}{2}\left(1+\frac{1}{\beta}\right)}{r_{os}}dx_s dy_s dz_s$$
$$\mp\frac{\kappa}{4\pi}\iiint\frac{\lambda}{\kappa}\frac{\rho\delta(\mathbf{r}-\mathbf{r}_s)\gamma_{\varphi}^{*2}\left(v_{\varphi}^2/c^2\right)\cos 2\varphi}{r_{os}}dx_s dy_s dz_s, \tag{2.58}$$

where the – sign of $\mp$ is for i=1 and the + sign is for i=2. The last term of the right-hand side of Eq. (2.58) can be rewritten, taking a spherical coordinate transformation, as:

$$\mp\frac{\kappa}{4\pi}\iiint\frac{\lambda}{\kappa}\frac{\rho\delta(\mathbf{r}-\mathbf{r}_s)\gamma_\varphi^{*2}\left(v_\varphi^2/c^2\right)\cos 2\varphi}{r_{os}}dx_s dy_s dz_s$$

$$=\mp\frac{\kappa}{4\pi}\iiint\frac{\lambda}{\kappa}\frac{\rho\delta(\mathbf{r}-\mathbf{r}_s)\gamma_\varphi^{*2}\left(v_\varphi^2/c^2\right)\cos 2\varphi}{r_{os}}r_s^2\sin\theta dr_s d\theta\cdot d\varphi. \qquad (2.59)$$

Then, as the result of integration by φ, under the condition $r_{os}\to 0$, Eq. (2.59) vanishes. Similarly, for γ_{12} and γ_{21}:

$$\gamma_{12}(\mathbf{r}_{ob})=\gamma_{21}(\mathbf{r}_{ob})=-\frac{\kappa}{4\pi}\iiint\frac{\lambda}{\kappa}\frac{\rho\delta(\mathbf{r}-\mathbf{r}_s)\gamma_\varphi^{*2}\left(v_\varphi^2/c^2\right)\cdot\sin 2\varphi}{r_{os}}dx_s dy_s dz_s$$

$$=-\frac{\kappa}{4\pi}\iiint\frac{\lambda}{\kappa}\frac{\rho\delta(\mathbf{r}-\mathbf{r}_s)\gamma_\varphi^{*2}\left(v_\varphi^2/c^2\right)\cdot\sin 2\varphi}{r_{os}}r_s^2\sin\theta dr_s d\theta\cdot d\varphi=0\,. \qquad (2.60)$$

For $\gamma_{0i}(\mathbf{r}_{ob})$, we have:

$$\gamma_{0i}(\mathbf{r}_{ob})=\frac{\lambda}{2\pi}\iiint\frac{\rho\delta(\mathbf{r}-\mathbf{r}_s)\zeta\cdot\gamma_\varphi^{*2}\frac{dx^i}{cdt}}{r_{os}}dx_s dy_s dz_s\,. \qquad (2.61)$$

We are concerned with the case in which $\boldsymbol{r}_{0b}=\boldsymbol{r}_s$.;when integrating the second and third terms of the right-hand side of Eq. (2.57), and the second terms of the right-hand sides of Eqs. (2.58) and (2.61), all these terms are subject to the singularity problem where r_{ob} approaches asymptotically close to $\boldsymbol{r}_s$ in the denominator of the integrand. Specifically, for an example case of the second term on the right-hand side of Eq. (2.57), the result is obtained by applying the method of the Cauchy integral (see Appendix C), as:

$$\frac{\kappa}{2\pi}\iiint\frac{\delta(\mathbf{r}-\mathbf{r}_s)\cdot\frac{\lambda}{\kappa}\rho\cdot(1-\zeta)\gamma_{th}^{*2}\frac{\left(v_{th}^2/c^2\right)}{2}\left(1+\frac{1}{\beta}\right)}{r_{os}}dx_s dy_s dz_s$$

$$=\frac{i}{4}\rho\lambda(1-\zeta)\cdot\gamma_{th}^{*2}v_{th}^2\left(1+\frac{1}{\beta}\right), \qquad (2.62)$$

where i is the imaginary unit. Using the same procedure to realize Eq. (2.62), Eq. (2.61) can be rewritten (see also Appendix C) as:

$$\gamma_{0i}(\mathbf{r}_{ob},t)=\cdot\frac{i}{4}\rho\lambda\cdot\zeta\gamma_\varphi^{*2}\frac{dx^i}{cdt} \qquad (2.63)$$

Because the right-hand sides of Eqs. (2.62) and (2.63) are expressed as imaginary quantities, we should select the coefficient λ such that $i\ \rho\lambda$ is real, as will be discussed in the next section.

3. Calculation of the Distribution Limit of IMSBH

3.1. Force Balance in IMSBH with Formulae Bridged to Modified Newtonian Dynamics

3.1.1. Basic current to find the force balance formulae from the geodesics in QMST

The dynamics working in IMSBH cannot be described unless we use the exact coordinate system fixed to IMSBH. However, we can observe the state of the force balance in IMSBH in the coordinate by which the geodesic is expressed in Eq. (2.5), which is close to the freefalling system in IMSBH, though the expressions of forces are modified from the actual forces operating on the plasma. The forces F^i observed in the coordinate system corresponding to Eq. (2.5), that is modified from real forces working in IMSBH, can be then realized as:

$$F^i = \rho \frac{d}{d\tau}\left(\frac{dx^i}{d\tau}\right) = -\rho\Gamma^i_{jk}\frac{dx^j}{d\tau}\cdot\frac{dx^k}{d\tau}, \tag{3.1}$$

where τ is defined as $-ds^2=d\tau^2$. Before proceeding, we rewrite Eq. (3.1) as:

$$\rho \frac{d}{dt}\left(\frac{dx^i}{dt}\right) = -\rho\Gamma^i_{jk}\frac{dx^j}{dt}\cdot\frac{dx^k}{dt}. \tag{3.2}$$

Using the resultant γ_{jk} (see Sec 2.3.3.), Eq. (3.2) is expanded to find the dynamic balance for plasma with density ρ, as:

$$\rho\frac{d}{dt}\frac{dx^i}{dt} = \frac{1}{2}\rho\frac{\partial\gamma_{00}}{\partial x^i}\left(\frac{dx^0}{dt}\right)^2 + \frac{1}{2}\rho\sum_{k=1}^{3}\frac{\partial\gamma_{kk}}{\partial x^i}\left(\frac{dx^k}{dt}\right)^2 - \rho\cdot\frac{\partial\gamma_{0i}}{\partial x^0}\left(\frac{dx^0}{dt}\right)^2$$
$$-\rho\sum_{k=1}^{3}\left(\frac{\partial\gamma_{i0}}{\partial x^k}-\frac{\partial\gamma_{k0}}{\partial x^i}\right)\frac{dx^k}{dt}\frac{dx^0}{dt} - \rho\sum_{k=1}^{3}\frac{\partial\gamma_{ii}}{\partial x^k}\frac{dx^k}{dt}\frac{dx^i}{dt} - \frac{1}{2}\rho\frac{\partial\gamma_{ii}}{\partial x^i}\frac{dx^i}{dt}\frac{dx^i}{dt} = 0\ . \tag{3.3}$$

The first term of the right-hand side of Eq. (3.3) is expressed by setting $i = 0$ in Eq. (2.56) as:

$$\frac{1}{2}\rho\frac{\partial\gamma_{00}}{\partial x^i}\left(\frac{dx^0}{dt}\right)^2 =$$
$$\rho\left\{\frac{\kappa c^2\rho}{8\pi}\mathrm{grad}\left[\iiint\frac{\rho(\mathbf{r}_s)\gamma_\varphi^{*2}}{r_{os}}dx_s dy_s dz_s\right] - \frac{i}{8}\lambda\rho(1-\zeta)\mathrm{grad}\left[\cdot\,\gamma_{th}^{*2}\frac{v_{th}^2}{2}\left(1+\frac{1}{\beta}\right)\right]\right.$$
$$\left. + \frac{i}{8}\rho\lambda\,.\zeta\mathrm{grad}\left(\gamma_\varphi^{*2}v_\varphi^2.\right)\right\}. \tag{3.4}$$

In the present case, because of the situation:

$$\frac{dx^3}{d\tau} = 0, \tag{3.5}$$

the second term of the right-hand side of Eq. (3.3) is expressed as:

$$\frac{1}{2}\rho\sum_{k=1}^{2}\frac{\partial\gamma_{kk}}{\partial x^i}\left(\frac{dx^k}{dt}\right)^2$$
$$= \rho\left\{\frac{\kappa c^2}{8\pi}\mathrm{grad}\left[\iiint\frac{\rho(\mathbf{r}_s)\gamma_\varphi^{*2}}{r_{os}}dx_s dy_s dz_s\right] - \frac{i}{8}\lambda(1-\zeta).\mathrm{grad}\left[\gamma_{th}^{*2}\frac{v_{th}^2}{2}\left(1+\frac{1}{\beta}\right)\right]\right\}$$
$$\times\frac{v_\varphi^2}{c^2}\,. \tag{3.6}$$

Considering Eq. (2.60), the third term of the right-hand side of Eq. (3.3) is expressed as:

$$-\rho\cdot\zeta\frac{\partial\gamma_{i0}}{\partial x^0}\left(\frac{dx^0}{dt}\right)^2=-\frac{i}{4}\rho^2\lambda\cdot\zeta\,\gamma_\varphi^{*2}\frac{\partial}{\partial t}\left(\frac{dx^i}{dt}\right). \tag{3.7}$$

Then, we can rewrite the equation using the regular vector expression as:

$$-\rho\cdot\zeta\frac{\partial\gamma_{i0}}{\partial x^0}\left(\frac{dx^0}{dt}\right)^2=-\frac{i}{4}\rho^2\lambda\cdot\zeta\,\gamma_\varphi^{*2}\frac{\partial\mathbf{v}}{\partial t}. \tag{3.8}$$

Considering Eq. (2.62), the fourth term of the right-hand side of Eq. (3.3) can be expressed as:

$$-\rho\cdot\zeta\sum_{k=1}^{3}\left(\frac{\partial\gamma_{i0}}{\partial x^k}-\frac{\partial\gamma_{k0}}{\partial x^i}\right)\frac{dx^k}{dt}\frac{dx^0}{dt}$$

$$=-\frac{i}{4}\rho^2\lambda\cdot\zeta\gamma_\varphi^{*2}\sum_{k=1}^{3}\left(\frac{\partial v^i}{\partial x^k}-\frac{\partial v^k}{\partial x^i}\right)v^k. \tag{3.9}$$

As explained in Appendix D, Eq. (3.9) can be rewritten using expressions for regular vector analyses as:

$$-\rho\cdot\zeta\sum_{k=1}^{3}\left(\frac{\partial\gamma_{i0}}{\partial x^k}-\frac{\partial\gamma_{k0}}{\partial x^i}\right)\frac{dx^k}{dt}\frac{dx^0}{dt}=-\frac{i}{4}\rho^2\lambda\cdot\zeta\gamma_\varphi^2\mathrm{rot}\mathbf{v}\times\mathbf{v}, \tag{3.10}$$

i.e., the fourth term on the right-hand side of Eq. (3.3) represents the Coriolis force when we select the coordinate system on the rotating frame.

Moreover, the last two terms on the right-hand side of Eq. (3.3) vanish because γ_{ii} terms are time-stationary, i.e.,

$$-\rho\sum_{k=1}^{3}\frac{\partial\gamma_{ii}}{\partial x^k}\frac{dx^k}{dt}\frac{dx^i}{dt}-\frac{1}{2}\rho\frac{\partial\gamma_{ii}}{\partial x^i}\frac{dx^i}{dt}\frac{dx^i}{dt}=-\rho\sum_{k=1}^{3}\frac{\partial\gamma_{ii}}{\partial t}\frac{dx^i}{dt}-\frac{1}{2}\rho\frac{\partial\gamma_{ii}}{\partial t}\frac{dx^i}{dt}=0. \tag{3.11}$$

Collecting the first to fourth terms on the right-hand side of Eq. (3.3), the force ***F*** working on the IMSBH, i.e., iron plasma, is expressed considering homogeneously distributed v_φ as:

$$\mathbf{F}=\rho\cdot\frac{\kappa c^2}{8\pi}\left(1+\frac{v_\varphi^2}{c^2}\right)\mathrm{grad}\left[\int\frac{\rho(\mathbf{r}_s)\gamma_\varphi^{*2}}{r_{os}}dV_s\right]$$

$$+\frac{i}{4}\rho^2\lambda\zeta\gamma_\varphi^{*2}\cdot\left(\frac{\partial\mathbf{v}}{\partial t}+\mathrm{rot}\mathbf{v}\times\mathbf{v}\right)-\frac{i}{8}\rho\lambda\left[(1-\zeta)\cdot\gamma_{th}^{*2}\mathrm{grad}\cdot P\left(1+\frac{1}{\beta}\right)\right], \tag{3.12}$$

where the velocity vector is $\boldsymbol{v}=(dx^1/dt, dx^2/dt, dx^3/dt\,(=0))$,and $P=\rho((v_{th}^2/2)$. For the first term on the right-hand side of Eq. (3.12), which corresponds to the Newtonian gravitational force and is intensified by $(1+(v_\varphi/c)^2)$ times as a result of the modification of general relativity; we can find the gravity constant as:

$$G=\frac{\kappa c^2}{8\pi}. \tag{3.13}$$

That is,

$$\kappa=\frac{8\pi G}{c^2}, \tag{3.14}$$

and κ becomes the same as that in Einstein's lecture [38].

We understand that the manipulation of λ follows the concept of the selection of Einstein's κ value, i.e., we can redefine κ depending on γ_{ij} for consistency with Newtonian dynamics, to bridge the results of Einstein's equation to modified Newtonian dynamics. For smooth bridging to the modified Newtonian dynamics of the expression regarding the second and third terms on the right-hand side of Eq. (3.12), we require:

$$\frac{i}{4}\rho\lambda = 1, \text{i.e.}, \lambda = -\frac{i}{}\frac{4}{\rho}\ . \tag{3.15}$$

3.1.2. Freedom of selection of coefficient of the source term in Einstein equation

At this stage, we are allowed further freedom to consider the Lorentz factor γ_{φ}^{*2} at each term of Eq. (3.12); the constraint to our selection within the freedom will be given by parameters of the BH. Regarding the first term in Eq. (3.12), we separate γ_{φ}^{*2} by introducing constants $\gamma_{\varphi G}^{*}$ and $\gamma_{\varphi M}^{*}$, as:

$$\gamma_{\varphi}^{*2} = \gamma_{\varphi}^{*} \cdot \gamma_{\varphi G}^{*} \cdot \gamma_{\varphi M}^{*}. \tag{3.16}$$

Then, applying the newly selected constants given by Eqs. (3.14) and (3.15), we can rewrite Eq. (3.12) as the relation:

$$\mathbf{F} = \rho\gamma_{\varphi}^{*}\left(1+\frac{v_{\varphi}^{2}}{c^{2}}\right)\gamma_{\varphi G}^{*}\text{grad}\left[G\int\frac{\rho_{M}(\mathbf{r}_{s})}{r_{os}}dV_{s}\right] + \rho\zeta\gamma_{\varphi}^{*2}\cdot\left(\frac{\partial\mathbf{v}}{\partial t}+\text{rot}\mathbf{v}\times\mathbf{v}+\text{grad}\cdot v_{\varphi}^{2}\right)$$
$$-\left[(1-\zeta)\left(\gamma_{th}^{*2}/2\right)\text{grad}\cdot P\left(1+\frac{1}{\beta}\right)\right], \tag{3.17}$$

where $\rho_{M}=\rho\gamma^{*}_{\varphi M}$. Under the freedom of the mathematical selection to share the coefficient γ_{φ}^{*2} at each term in Eq. (3.12), we selected one of the possible cases that corresponds to the increment of the matter density ρ to ρ_{M} due to the relativistic effects of the high-speed rotation of the matter with velocity close to that of light. Because v_{φ} is close to c, the gravity term in Eq. (3.16) increases to $2\gamma^{*}_{\varphi G}$; this difference from the pure Newtonian expression of gravity is also attributed to the effect of the general relativity that reflects the QMST selected for the observation of dynamics of IMSBH.

3.2. Detail of Balance of Forces in IMSBH

3.2.1. Modified Newtonian gravity

By setting F=0 in Eq. (3.17), we realize the situation of force balance in the IMSBH as follows:

$$\rho_{M}\left(1+\frac{v_{\varphi}^{2}}{c^{2}}\right)\gamma_{\varphi G}^{*}\text{grad}\left[G\int\frac{\rho_{M}(\mathbf{r}_{s})}{r_{os}}dV_{s}\right]$$
$$-\left[(1-\zeta)\left(\gamma_{th}^{*2}/2\gamma_{\varphi G}^{*}\right)\text{grad}\cdot P\left(1+\frac{1}{\beta}\right)+\rho_{M}\zeta\cdot\gamma_{\varphi}^{*}\left(\frac{\partial\mathbf{v}}{\partial t}+\text{rot}\mathbf{v}\times\mathbf{v}\right)\right]=0. \tag{3.18}$$

The first term on the left-hand side expresses the gravity field $2\gamma^{*}_{\varphi G}\, g_{r}$, which is radially directed toward the center of the spherically distributed IMSBH, and can be expressed for $v_{\varphi}\approx c$ as follows:

$$g_{r} = \text{grad}\left[\int\frac{G\rho_{M}(\mathbf{r}_{s})}{r_{os}}dV_{s}\right]. \tag{3.19}$$

Instead of calculating this directly, we employ the analysis method of Gauss's theorem for integration, starting from Poisson's formalism for flux of gravity field **g**, expressed by:

$$\text{div}\mathbf{g} = -4\pi G\rho_{M}, \tag{3.20}$$

which gives a relation of volume integration as:

$$\iiint \text{div}\mathbf{g}\cdot dV_{S} = -\iiint 4\pi G\rho_{M}\cdot dV_{S}\ . \tag{3.21}$$

For the gravity field **g**, we can apply the Stokes theorem:

$$\iiint \mathrm{div}\mathbf{g}\cdot \mathrm{d}V_S = \iint \mathbf{g}\cdot \mathrm{d}\mathbf{S} = 4\pi r^2 g_r. \tag{3.22}$$

Then, from Eqs. (3.18), (3.20), and (3.21), it follows that:

$$\mathrm{grad}\left[\int \frac{G\rho_M(\mathbf{r}_s)}{r_{os}}\mathrm{d}V_s\right] = g_r = -\frac{\iiint G\rho_M(\mathbf{r}_s)\cdot \mathrm{d}V_S}{r^2}, \tag{3.23}$$

where r is the radial distance defined in the local spherical coordinates, whose origin is set at the center of the IMSBH.

3.2.2. Lorentz force due to rotating plasma of IMSBH

Because plasma creates toroidal flow, the toroidal electric current I_φ is raised due to possible differential velocities of the average motion between iron ions and electrons, as follows:

$$I_\varphi \hat{\boldsymbol{\varphi}} = \left(nN_i e v_{i\varphi} - N_e e v_{e\varphi}\right)\hat{\boldsymbol{\varphi}}, \tag{3.24}$$

where N_i, N_e,n,$v_{i\varphi}$, $v_{e\varphi}$,e, and $\hat{\boldsymbol{\varphi}}$ are the number density of iron ions, number density of electrons, ionization number of iron ions, rotation velocity of ions, rotation velocity of electrons, electric charge unit, and unit vector in the φ direction of the spherical coordinate, respectively. Because of the charge neutrality, $nN_i=N_e$, Eq. (3.24) is rewritten as:

$$I_\varphi \hat{\boldsymbol{\varphi}} = nN_i e\left(v_{i\varphi} - v_{e\varphi}\right)\hat{\boldsymbol{\varphi}}\,. \tag{3.25}$$

We here propose a ratio α_c (r)= $(v_{i\varphi}-v_{e\varphi})/v_{i\varphi}$ for the electric current generation efficiency due to differences in the velocities between ions and electrons; furthermore, we assume that the ratio α_c (r) depends on distance r in general. Using this ratio, the toroidal current i (=$I_\varphi \hat{\boldsymbol{\varphi}}$) is given by:

$$\mathbf{I} = nN_i e\cdot \alpha_c(r) v_{i\varphi}\hat{\boldsymbol{\varphi}}. \tag{3.26}$$

For this **I** and generated poloidal magnetic field $\mathbf{B}_p$ (see Appendix E), the Lorentz force $\mathbf{F}_L$ is generated as follows:

$$\mathbf{F}_L = \mathbf{I}\times\mathbf{B}_P = I_\varphi I_0\left(\frac{A^*_\varphi}{r}+\frac{\partial A^*_\varphi}{\partial r}\right)\hat{\mathbf{r}} + I_\varphi I_0\left(\frac{\cos\theta}{\sin\theta}\cdot\frac{A^*_\varphi}{r}+\frac{\partial A^*_\varphi}{r\,\partial\theta}\right)\cdot\hat{\boldsymbol{\theta}}, \tag{3.27}$$

where $\hat{\mathbf{r}}$ and $\hat{\boldsymbol{\theta}}$ are unit vectors in the radial and polar angle directions, respectively; and I_φ is given by Eq. (3.26). In Eq. (3.27), the modified vector potential A^*_φ is A_φ/I_0 with respect to the vector potential A_φ and current density I_0 at $r = r_{Mc}$; these are described in detail in Appendix E, where values of A^*_φ/r, $\partial A^*_\varphi/\partial r$, B_r,and B_θ are given normalized by $\mu_0 I_0 r_{Mc}$, with the unit $4\pi\times10^{-7}$ V s/m^2 for $\mu_0=4\pi\times10^{-7}$ H/m, with current density I_0 (A/m^2) and core radius r_{Mc} (m) of the IMSBH, i.e., the plasma region. As also described in Appendix E, the density of plasma distribution is assumed to be:

$$N_i = N_0\left(\frac{r_{Mc}}{r}\right)^2, \tag{3.28}$$

where N_0 is the ion number density at $r = r_{Mc}$. Furthermore, we assume the electric current generation coefficient as:

$$\alpha_c(r) = \alpha_0\left(\frac{r_{Mc}}{r}\right)^\delta \tag{3.29}$$

with a constant rate α_0 and power index δ in the range of $0 \le \delta \le 1$. Then, the plasma density and the current density are expressed as $\rho_M=\rho_{0M}(r_{Mc}/r)^2$ and $I_\varphi = I_0(r_{Mc}/r)^{2+\delta}$, respectively.

For the generated magnetic fields, we set a constraint that the fields are frozen in the rotating plasma, i.e., magnetic field **B** satisfies the frozen-in condition with respect to $v = v_\varphi\ \hat{\boldsymbol{\varphi}}$ as follows:

$$\frac{\partial \mathbf{B}}{\partial t} + \mathrm{rot}(\mathbf{B} \times \mathbf{v}) = 0\,. \qquad (3.30)$$

In the case of the frozen-in magnetic field, the toroidal motion of plasma moves with the magnetic field. Thus, there is no electric field without raising relative motion between the plasma and the magnetic field.
The second term on the right-hand side of Eq. (3.17) is rewritten as follows:

$$\mathbf{F}_p = -\rho_M \zeta \cdot \gamma_\varphi^* \left(\frac{\partial \mathbf{v}}{\partial t} + \mathrm{rot}\mathbf{v} \times \mathbf{v}\right) = -\rho_M \zeta \cdot \gamma_\varphi^* \frac{d\mathbf{v}}{dt} = \rho_M \zeta \gamma_\varphi^* \left(\frac{v_\varphi^2}{r}\right)\left[\hat{\mathbf{r}} + \frac{\cos\theta}{\sin\theta}\hat{\boldsymbol{\theta}}\right]. \qquad (3.31)$$

Then, we can express the total force $\boldsymbol{F}_T$ working on the rotating plasmas as follows:

$$\mathbf{F}_T = -\rho_M \cdot \zeta \cdot \gamma_\varphi^* \frac{d\mathbf{v}}{dt} + \mathbf{I} \times \mathbf{B}_p$$
$$= \frac{\rho_M \cdot v_\varphi^2}{r}\left\{\left[\zeta\gamma_\varphi^* + \eta\frac{r}{r_{Mc}} \cdot \left(\frac{A_\varphi^*}{r} + \frac{\partial A_\varphi^*}{\partial r}\right)\right]\hat{\mathbf{r}}\right.$$
$$\left. + \left[\frac{\cos\theta}{\sin\theta}\left(\zeta\gamma_\varphi^* + \eta\frac{r}{r_{Mc}} \cdot \frac{A_\varphi^*}{r}\right) + \eta\frac{\partial A_\varphi^*}{\partial\theta}\right]\hat{\boldsymbol{\theta}}\right\}, \qquad (3.32)$$

where

$$\eta = \frac{\alpha_c(r)\alpha_0 e^2 n N_0 r_{Mc}^2 \mu_0}{m_i} = \frac{\alpha_c(r)\alpha_0 \omega_{pi}^2 r_{Mc}^2}{c^2} \qquad (3.33)$$

with ion plasma angular frequency ω_{pi}, which is given by $5.61\pi\sqrt{(nN_i)}\times10^{-2}$ / s for N_i indicated with the unit $1/m^3$. The normalized magnetic field intensities B_r and B_θ are given in Figure 3.
As the first step to construct a model for the total force balance of the plasma in the IMSBH, Eq. (3.18) can be further rewritten considering the Lorentz term with condition $v_\varphi \approx c$ as:

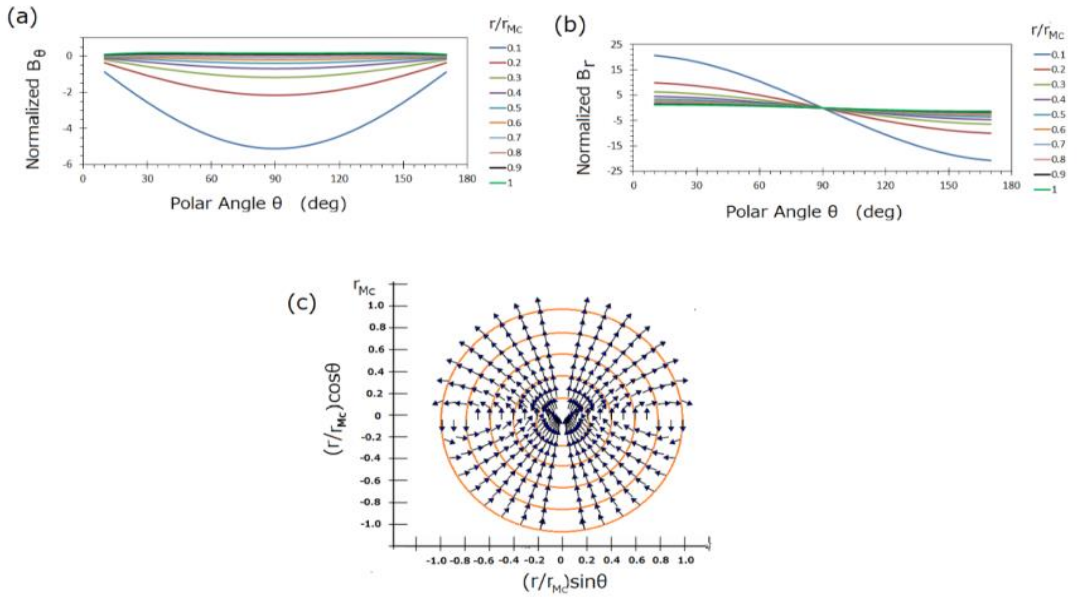

Figure 3: Poloidal magnetic field generated by toroidal current in IMSBH for the case of $\alpha_c=\alpha_{c0}$,δ=0: (a) magnitude of θ component B_θ normalized by $\mu_0 I_0 r_{Mc}$, which has unit $4\pi\times10^{-7}$ Wb/m² for $\mu_0 = 4\pi\times10^{-7}$ H⁄m, with current density I_0 (A⁄m²) and core radius r_{Mc} (m); (b) magnitude of the radial component B_r, also normalized by $\mu_0 I_0 r_{Mc}$; (c) direction of magnetic field expressed in *r*–*θ* plane in terms of vectors normalized by the magnitude at each given point, indicated by the orange circles. The magnetic field lines are drawn approximately by connecting the tip to the end of the nearest vectors with each other.

$$\mathbf{F} \cdot = 2\gamma^*_{\varphi G}\rho \cdot \mathrm{grad}\left[\int \frac{G\rho_M(\mathbf{r}_s)}{r_{os}} dV_s\right] + \left[(1-\zeta)(\gamma^*_{th}/2)\mathrm{grad}\ \cdot P\left(1+\frac{1}{\beta}\right)\right]$$

$$+\frac{\rho \cdot v_\varphi^2}{r}\left\{\left[\zeta\gamma^*_\varphi + \eta\frac{r}{r_{Mc}}\cdot\left(\frac{A^*_\varphi}{r}+\frac{\partial A^*_\varphi}{\partial r}\right)\right]\hat{\mathbf{r}} + \left[\frac{\cos\theta}{\sin\theta}\left(\zeta\gamma^*_\varphi + \eta\frac{r}{r_{Mc}}\cdot\frac{A^*_\varphi}{r}\right) + \eta\frac{\partial A^*_\varphi}{\partial\theta}\right]\hat{\boldsymbol{\theta}}\right\} = 0\,. \qquad (3.34)$$

3.3. Solution of Dynamic Balance Equations

3.3.1. Balance in r-direction

From Eq. (3.32), we can obtain equations of the force balance for the r-direction:

$$-\frac{2\gamma^*_{\varphi G}GM(r)\rho}{r^2} - \frac{\partial}{\partial r}\left[\rho(1-\zeta)\gamma^*_{th}\cdot\xi\frac{c^2}{2}+\frac{B^2_{th}}{2\mu_0}\right] + \frac{\rho v^2_\varphi}{r}\left[\zeta\gamma^*_\varphi + \eta\frac{r}{r_{Mc}}\left(\frac{A^*_\varphi}{r}+\frac{\partial A^*_\varphi}{\partial r}\right)\right] = 0\,, \qquad (3.35)$$

where $\xi = v_{th}{}^2/c^2$ with respect to the thermal velocity v_{th}. We will describe GM(r) in detail at the end of this section.
Considering diamagnetic effects for the thermal components of plasma, we assume r dependence of the total thermal pressure P as:

$$P = \rho(1-\zeta)\cdot\xi\gamma^*_{th}\frac{c^2}{2}+\frac{B^2_{th}}{2\mu_0} = \left(\frac{r^2_{Mc}}{r^2}\right)P_0c^2, \qquad .(3.36)$$

where P_0c^2 is the total pressure at $r=r_{Mc}$. Then, we can rewrite Eq. (3.35) as:

$$-\frac{2\gamma^*_{\varphi G}GM(r)\rho}{r^2} + \frac{r^2_{Mc}}{r^3}P_0c^2 + \frac{\rho v^2_\varphi}{r}\left[\zeta\gamma^*_\varphi + \eta\frac{r}{r_{Mc}}\left(\frac{A^*_\varphi}{r}+\frac{\partial A^*_\varphi}{\partial r}\right)\right] = 0\,. \qquad (3.37)$$

3.3.2. Balance in θ-direction.

Because we assume that $\partial\rho/\partial\theta = 0$, the force balance in the θ-direction, obtained from Eq. (3.34), is given by:

$$-\frac{\partial}{r\,\partial\theta}\cdot\left[\frac{B^2_{th}}{2\mu_0}\right] + \frac{\rho_M v^2_\varphi}{r}\cdot\left[\zeta\gamma^*_\varphi\frac{\cos\theta}{\sin\theta} + \eta(r)\frac{r}{r_{Mc}}\left(\frac{A^*_\varphi}{r}\frac{\cos\theta}{\sin\theta}+\frac{\partial A^*_\varphi}{r\,\partial\theta}\right)\right] = 0\,, \qquad .(3.38)$$

Here, we use an approximation form with assumption $\eta = \eta_0\,(r/r_{Mc})^\delta$ (see Appendix F), as:

$$\eta(r)\frac{r}{r_{Mc}}\left(\frac{A^*_\varphi}{r}\frac{\cos\theta}{\sin\theta}+\frac{\partial A^*_\varphi}{r\,\partial\theta}\right) = \eta_0K_B\frac{\cos\theta}{\sin\theta}\,. \qquad (3.39)$$

Then,

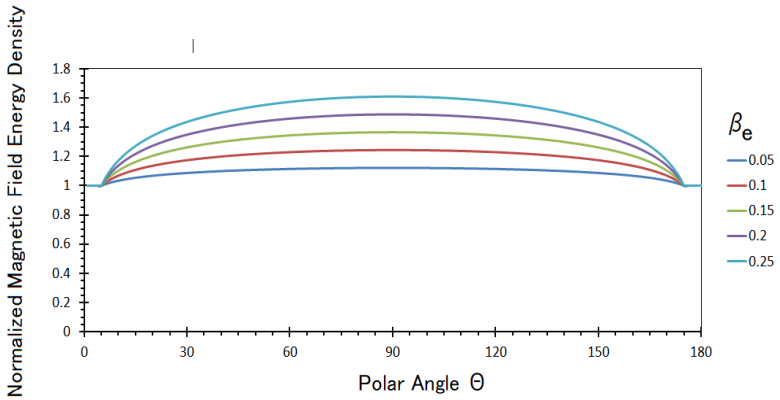

Figure 4: Magnetic field energy density $B_H^2(\theta)/\mu_0$ versus polar angle θ, taking $\beta_e = \rho_M v_\varphi^2 \cdot [\zeta\gamma_\varphi^* + \eta_0 K_B]/[B_{H0}^2 \theta_0/2\mu_0]$ as a parameter. We consider results corresponding to β_e less than 0.2 to be acceptable as approximately independent to θ in Eq. (3.34).

$$-\frac{\partial}{r\,\partial\theta}\cdot\left[\frac{B_{th}^2}{2\mu_0}\right]+\frac{\rho v_\varphi^2}{r}\cdot\left(\zeta\gamma_\varphi^*+\eta_0 K_B\right)\frac{\cos\theta}{\sin\theta}=0\,, \qquad (3.40)$$

where K_B is a constant that takes a value of 1.3 for $(\pi/6 \le \theta \le 5\pi/6)$ and 0.5 in other ranges of θ (see Appendix F).
Thus, we can solve Eq. (3.40) as:

$$\frac{B_{th}^2(\theta)}{2\mu_0}=\frac{B_{th}^2(\theta_0)}{2\mu_0}+\rho v_\varphi^2\cdot\left(\zeta\gamma_\varphi^*+\eta_0 K_B\right)\cdot\ln\left(\frac{\sin\theta}{\sin\theta_0}\right). \qquad (3.41)$$

Because Eq. (3.41) includes singularities at θ=0 and θ=π, we should modify the expression for a realistic model of the magnetic field energy caused by the thermal component of plasma. Specifically, we assume that the θ dependence of $B_{th}^2(\theta)/(2\mu_0)$ is:

$$\frac{B_{th}^2(\theta)}{2\mu_0}=\frac{B_{th}^2(\theta_0)}{2\mu_0}+\rho v_\varphi^2\cdot\left(\zeta\gamma_\varphi^*+\eta_0 K_B\right)\cdot\ln\left(\frac{\sin\theta}{\sin\theta_0}\right), \quad \text{for } \theta_0 \le \theta \le \pi-\theta_0,$$

and

$$\frac{B_{th}^2(\theta)}{2\mu_0}=\frac{B_{th}^2(\theta_0)}{2\mu_0} \text{ for } 0 \le \theta < \theta_0 \text{ and } \pi-\theta_0 < \theta \le \pi. \qquad (3.42)$$

As an allowable approximation for this setting of the model using Eq. (3.42), we select θ_0=5°. In this model, it is favorable that the $B_{th}^2(\theta)/2\mu_0$ value is less dependent on θ to endorse a spherical shape of IMSBH. In Figure 4, examples for low-β cases where $\rho v_\varphi^2 \cdot (\zeta\gamma_\varphi^* + \eta_0 K_B)/[B_{th}^0(\theta_0)/2\mu_0]$ is in the range of 0.05–0.25 are presented. For these cases, we observe a weak θ dependence, where we expect to simplify the force balance condition in the r-direction by approximating independence of θ.

3.3.3. Radius of IMSBH r_{Mc}.

Corresponding to Eq. (3.28), the density in the IMSBH is:

$$\rho_M=\rho_{M0}\left(\frac{r_{Mc}}{r}\right)^2, \qquad (3.43)$$

and

$$M(r)=2\pi\int_0^r\int_0^\pi \rho_{M0}\left(\frac{r_{Mc}}{r_S}\right)^2 r_S^2\sin\theta_S\,dr_S\,d\theta_S\,. \qquad (3.44)$$

Integrating Eq. (3.44), we obtain:

$$M(r) = 4\pi\rho_{M0} \cdot r_{Mc}^2 r, \qquad (3.45)$$

which provides a total BH mass of M by $M(r_{Mc})$; and Eq. (3.35) is rewritten as:

$$-\frac{\gamma_{\varphi G}^* r_g}{r_{Mc} r^3} \cdot \rho_{M0} r_{Mc}^2 + \frac{r_{cM}^2}{r^3} P_0 + \frac{\rho_{M0} r_{Mc}^2 \cdot (v_\varphi^2/c^2)}{r^3} \cdot \left[\zeta\gamma_\varphi^* + \eta \frac{r}{r_{Mc}} \left(\frac{A_\varphi^*}{r} + \frac{\partial A_\varphi^*}{\partial r}\right)\right] = 0, \qquad (3.46)$$

where $r_g = 2GM/c^2$. As discussed in Appendix F, in detail, we apply the approximation regarding the last term in the bracket of the third term on the left-hand side of Eq. (3.46) as:

$$\eta \frac{r}{r_{Mc}} \left(\frac{A_\varphi^*}{r} + \frac{\partial A_\varphi^*}{\partial r}\right) \approx 0. \qquad (3.47)$$

As will be discussed in Sec 4.2., the systematic rotation flow of plasma is tightly controlled by the extremely intense gravity in IMSBH. Therefore, we consider an extremely low rate for α_c, which also produces a low η.

From Eq. (3.46), we obtain:

$$\gamma_{\varphi G}^* r_g = \left[\frac{P_0}{\rho_{M0}} + (v_\varphi^2/c^2)\zeta\gamma_\varphi^*\right] \cdot r_{Mc}. \qquad (3.48)$$

Taking $v_\varphi \approx c$, it follows that:

$$r_{Mc} = \frac{\gamma_{\varphi G}^* r_g}{\zeta\gamma_\varphi^* + (P_0/\rho_{M0})}. \qquad (3.49)$$

3.4. Calculation of the Rotation Parameter *a*

In the present model, the rotation parameter *a* is expressed relative to the angular momentum J of the IMSBH, considering γ_φ^* and ρ_{M0} to be constant, as follows:

$$a = \frac{J}{Mc} = \frac{2\pi \int_0^{r_{Mc}} dr_s \int_0^\pi d\theta_S \cdot \gamma_\varphi^* c \sqrt{1 - \frac{1}{\gamma_\varphi^{*2}}} \cdot \zeta\rho_{M0} \left(\frac{r_{Mc}}{r_S}\right)^2 r_S^3 \sin^2\theta_S}{2\pi \int_0^{r_{Mc}} dr_S \int_0^\pi d\theta_S \rho_{M0} \left(\frac{r_{Mc}}{r_S}\right)^2 r_S^2 \sin\theta_S}. \qquad (3.50)$$

Then, the rotation parameter is calculated from Eq. (3.50), with Eq. (3.49) for r_{Mc}, as follows:

$$a = \frac{J}{Mc} = \left(\frac{\pi}{4}\right) \sqrt{1 - \frac{1}{\gamma_\varphi^{*2}}} \cdot \frac{\gamma_{\varphi G}^* \cdot \gamma_\varphi^* \zeta \cdot (r_g/2)}{\zeta\gamma_\varphi^* + (P_0/\rho_{M0})} \quad . \quad (3.51)$$

In the case of a Kerr BH, the maximum rotation takes place at $r_g/2 = r_E$, where $a = r_E$. As the observational result [16], the supermassive BHs at SgrA* are in the state of maximum rotation. Then, we can set the condition of the maximum rotation for Eq. (3.51) as:

$$\frac{a}{r_E} = \left(\frac{\pi}{4}\right) \sqrt{1 - \frac{1}{\gamma_\varphi^{*2}}} \cdot \frac{\gamma_{\varphi G}^* \cdot \gamma_\varphi^* \zeta \cdot}{\zeta\gamma_\varphi^* + (P_0/\rho_{M0})} = 1 \cdot \qquad (3.52)$$

For a sufficiently high γ_{φ}^{*} value, Eq. (3.49) gives the result as follows:

$$r_{Mc} = \frac{8}{\pi} \cdot \frac{r_E}{\gamma_{\varphi}^{*} \zeta}. \qquad (3.53)$$

3.5. Angular Velocity of Vacuum in Kerr Spacetime

For a vacuum region, which envelops IMSBH, we are concerned with the Kerr spacetime [44] that is given in spherical coordinates, in space as follows:

$$ds^2 = -c^2\left(1 - \frac{rr_g}{\Sigma}\right)dt^2 - \frac{2carr_g \sin^2\theta}{\Sigma} dt d\varphi + \frac{\Sigma}{\Delta} dr^2 + \Sigma d\theta^2 + \left(r^2 + a^2 + \frac{a^2 rr_g \sin^2\theta}{\Sigma}\right)\sin^2\theta d\varphi^2, \qquad (3.54)$$

where $r_g = 2GM/c^2$, $a = \alpha = J/Mc$, $\Sigma = r^2 + a^2\cos^2\theta$, and $\Delta = r^2 - rr_g + a^2$. When we consider an extremely collapsed IMSBH radius r_{Mc}, Eq. (3.54) is expressed as an asymptotic case where r approaches r_{Mc} ($\ll a$) , except for a polar angle range $,(\pi/2 + r/a) > \theta > \pi/2 - r/a,$ as follows:

$$ds^2 = -c^2 dt^2 + \cos^2\theta dr^2 + a^2\cos^2\theta \cdot d\theta^2 + a^2 \sin^2\theta d\varphi^2. \qquad (3.55)$$

Introducing rotation of vacuum space of Kerr spacetime Ω, the spacetime can be deduced from Eq. (3.55) at a given point with the condition $dr = d\theta = 0$ as :

$$ds^2 = -c^2\left(1 - \frac{a^2}{c^2}\sin^2\theta \Omega^2\right) dt^2. \qquad (3.56)$$

The angular velocity Ω_{Mc} of the rotation of IMSBH described in the spaceteime of IMSBH should harmonize with the angular velocity of vacuum space of Kerr spacetime Ω; that is, when we observe the rotation of the IMSBH in the frame of the QMST, as is the case of the present study of plasma, the proper four-dimensional distance ds corresponding to the surface of the IMSBH for time passage dt_{QM} has a common relation to ds of the contacting vacuum region described in the Kerr spacetime for dt_B. Then, it follows that :

$$-c^2\left[1 - \left(\frac{v_\varphi}{c}\right)^2\right] dt_{QM}^2 = -c^2\left[1 - \left(\frac{a}{c}\right)^2 \sin^2\theta \cdot \Omega^2\right] dt_B^2 , \qquad (3.57)$$

where $v_\varphi = \Omega_{Mc} r_{Mc} \sin\theta.$

In the present study, we assumed fast rotation of the IMSBH with velocity $v_\varphi \approx c$ on the left-hand side of Eq. (3.57); we can find angular velocity Ω of the rotation of the vacuum. Kerr spacetime at the boundary extremely close to the singular point of the spacetime as:

$$\Omega \approx \frac{c}{a \cdot \sin\theta} \quad . \qquad (3.58)$$

We understand that the high angular velocity Ω_{Mc} ($= v_\varphi / (r_{Mc} \sin\theta)$) observed in QMST corresponding to the spacetime of the IMSBH occurs as the low angular rotation velocity given by Eq. (3.58) in vacuum spacetime due to differences in time passages between

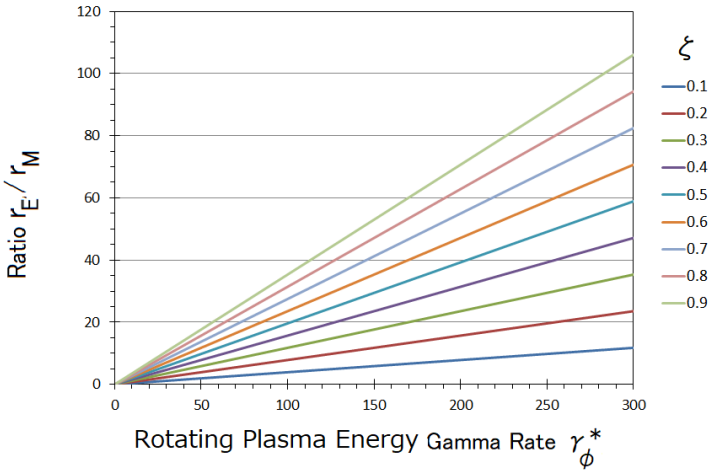

Figure 5: Results of numerical calculation for the ratio of radii r_E/r_M based on Eq. (3.53) versus the Lorentz factor γ_φ^*, which is proportional to the energy of the rotating iron ion energy Ɛ as Ɛ = $\gamma_\varphi^*\times$ (5.6×10^{10}) eV, related to the angular momentum of rotating plasma with velocity extremely close to that of light, and considering ζ, the rate of the rotating plasma component to the total plasma, as a parameter.

dt_{QM} in QMST observing the IMSBH and that in the vacuum region dt_B in vacuum region Kerr spacetime.

That is, we have relation for the angular velocities between the discussing two systems as

$$\Omega \equiv \frac{d\varphi}{dt_B} = \frac{\sqrt{1-\left(\frac{a}{c}\right)^2 \sin^2\theta \cdot \Omega^2}}{\sqrt{1-\left(\frac{v_\varphi}{c}\right)^2}} \cdot \frac{d\varphi}{dt_{QM}}. \qquad (3.59)$$

4. Numerical Results of the Ratio of IMSBH Radius and Event Horizon Radius

4.1. Possible Rotating Plasma Energy

In Figure 5, the ratio of the event horizon radius r_E and that of IMSBH r_{Mc} is presented as a result of Eq. (3.53), with ζ (= 0.1~ 0.9) as a parameter that shows the rate of the rotating plasma component in total plasma. IMSBH radius r_{Mc} decreases when the rotation velocity increases with a larger gamma rate; furthermore, the ratio also depends on the rate of the rotation component ζ. The abscissa of Figure 5 expressed by the Lorentz factor (gamma rate γ_φ^*), in the case of velocity extremely close to c, is proportional to the energy of the rotating iron plasma in IMSBH; i.e., the energy Ɛ is given by:

$$Ɛ = \frac{m_{iron}c^2}{\sqrt{1-\left(\frac{v_\varphi}{c}\right)^2}} = m_{iron}c^2\gamma_\varphi^*, \qquad (4.1).$$

for iron ion mass m_{iron}. Taking m_{iron} c^2 as approximately 56 GeV, Ɛ of the rotating plasma for γ_φ^* is Ɛ = $\gamma_\varphi^*\times(5.6\times10^{10}$) eV. Therefore, in the case of ζ=0.7 at γ_φ^*=175, where r_E/r_{Mc} becomes 50 (r_{Mc} is condensed to 1/50 of r_E), the condensed plasmas are rotating with energy 9.80×10^{12} eV. For the case of the condensed plasma region of the IMSBH, the density and average mutual distance of the iron ions are calculated as given in Figures 6 and 7, respectively. As shown in Figure 6, the density for the above-described case of ζ=0.7, r_E/r_{Mc} = 50 at γ_φ^*=175 becomes 3.59×10^{31}/cm^3. We can confirm, for this extremely high-density state, that the plasma is still in a gaseous state where particles are not bound by each other, as revealed in Figure 7, where the mutual distance of the ions is indicated as 3.03×10^{-11} cm, i.e., approximately 2.4×10^6 times the quantum mechanically estimated iron ion radius with energy 9.80×10^{12} eV.

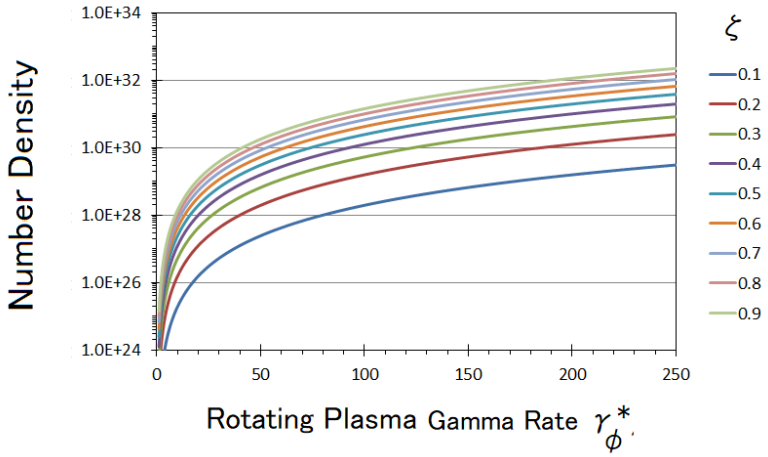

Figure 6: Density of ions versus the gamma rate of rotating iron plasma, taking the rate of the rotating component ζ as a parameter. The abscissa is the same as that in Figure 5, which corresponds to iron ion energy Ɛ as $Ɛ=\gamma_\varphi^*\times(5.6\times10^{10})$ eV.

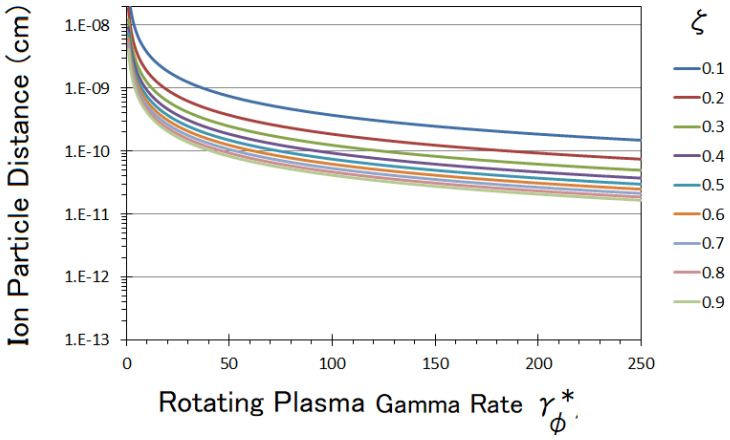

Figure 7: Average mutual distance of ions taking the rate of the rotating component ζ as a parameter. The abscissa corresponds to the energy Ɛ of the rotating iron plasma, $Ɛ = \gamma_\varphi^*\times(5.6\times10^{10})$ eV. It is confirmed that the plasma is still in a gaseous state, where the mutual distance of ions with energy 9.80×10^{12} eV, for example, is indicated to be 3.03×10^{-11} cm, or approximately 2.4×10^{6} times the quantum mechanically estimated iron ion radius.

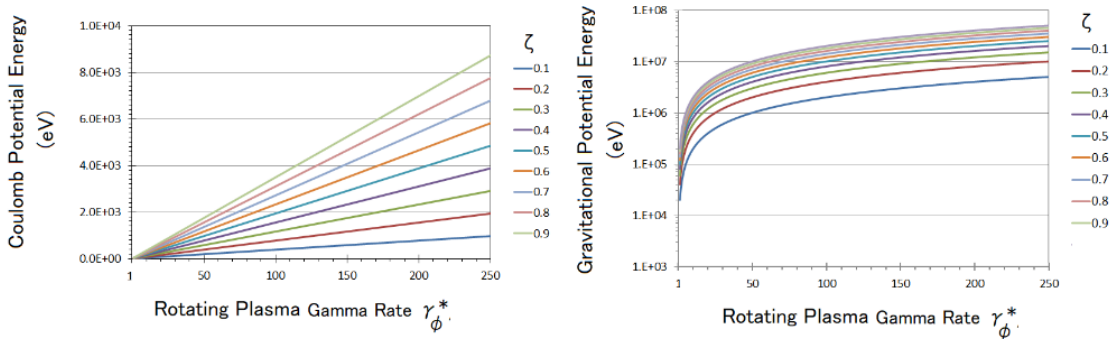

Figure 8: Comparison of the Coulomb potential energy and gravitational potential energy working on the electrons of rotating plasma in IMSBH. The left-hand panel shows the Coulomb potential energy between an electron and the nearest ion or electron versus the rotation energy of plasma given by the gamma rate γ_φ^* that gives energy $Ɛ = \gamma_\varphi^*\times(5.6\times10^{10})$ eV. The right-hand panel shows the gravitational potential energy working on an electron of rotating plasma, with the same abscissa as the left-hand panel.

4.2. Intense Gravity and Low η

Figure 8 presents a comparison of the potential energies of the Coulomb force and the gravity working on an electron of the rotating plasma in the IMSBH. It is remarkable that the motion of electrons is absolutely governed by gravity. Specifically, when we select the example case where ζ=0.7 and γ_φ^*=175 with r_E/r_{Mc} =50, the Coulomb potential energy is 4.75 keV, whereas the gravitational potential energy is 24.6 MeV. Because of the basic nature of gravity, particles move with the same velocity when the dynamics is controlled by gravity. From Eq. (3.33), η ≈1 by α_c=2.73×10^{-14} for the same example case of ζ=0.7 and γ_φ^*=175 with r_E/r_{Mc} =50. We may use this low rate of the current generation as a reference point to consider the effects of the Lorentz force in the IMSBH.

5. Generation of GW

5.1. Solution of GW under Transverse Traceless Gauge

5.1.1. Start point

As motivation for the present study, we are concerned with the generation of GWs, focusing on the possible SMBHB that we have proposed for SgrA* at the center of the Milky Way Galaxy. The configuration of the Kerr SMBHB is depicted in Figure 9 where the relations of the radii of the IMSBHs are estimated to be in the range of 1/10 to 1/100 of the radii of the event horizons based on the results of the present study (see Eq. (3.53) and Figure 5). As the source of GWs, IMSBHs are at positions far from the event horizons in the interior of the BH; the effect of orbital motion on the source does not arrive at the event horizon directly. We should separate the dynamical processes that may be raised at the event horizon and the processes that initiate GWs in the source region, which is not like the case of the stellar-mass BH where generation of a GW is considered without separation of the source matter and the existing event horizon. When we consider a possible case raised by our observation of the SMBHB at SgrA*[16], the speed of the source movement is less than 21% of the velocity of light; then, we can follow the classical quadrupole moment theory, as presented by Einstein, rather than the current post-Newtonian or post-Minkowskian expansion theory [42]. We begin with the orthodox GW generation theory by following the established method of the GW theory, albeit with some differences in details.

5.1.2. Description with transverse traceless gauge

In the main two fields of the theory of the generation of GW from compact objects, i.e., the quasi-normal mode oscillation and the merger of spiraling compact objects, the present study of GW generation belongs to the latter case. However, we are seeking the possibility of no GW for the case of a SMBHB. Unlike most of the current works, we consider the interior of a supermassive BH as propagation media of GWs. Before focusing on the coordinates to describe the real configuration given in Figure 9, we start with an arbitrary coordinate in the Minkowsky spacetime η_{ij} with Cartesian coordinate (x^0,x^1,x^2,x^3). This is possible when we observe a freefall system that moves along the geodesic of the BH spacetime. In this coordinate, the linearized perturbation of the spacetime metric h_{ij} of GW, related to the spacetime metric g_{ij}, is expressed as:

$$g_{ij} = \eta_{ij} + h_{ij} . \qquad (5.1)$$

By following the procedure of the deduction of the spacetime to describe GWs, as given in Appendix G, we approach the basic equation as:

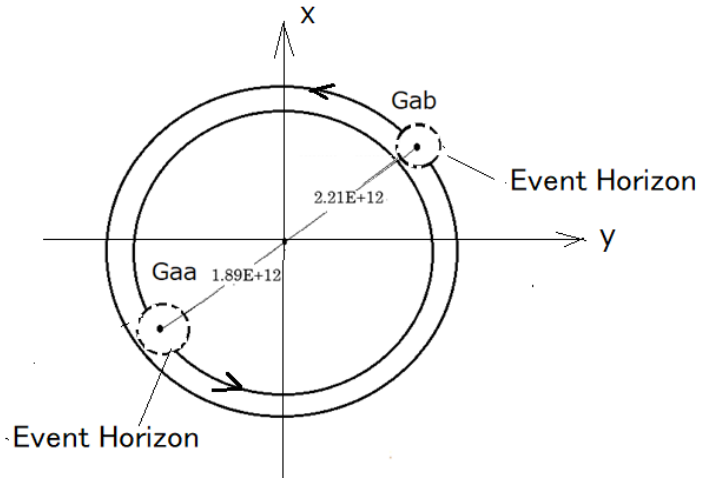

Figure 9: Configuration of the SMBHB system at SgrA* for investigation of generation of GW in the present study. Members of binary Gaa with mass (2.27±0.02)×10^6 $M_\odot$ and Gab with mass (1.94±0.01)×10^6 $M_\odot$ orbit with period of 2,200±50 s and velocities of (5.40±0.15)×10^4 km/s (0.18c)and(6.31±0.03)×10^4 km/s (0.21c) , respectively. The orbital radii of Gaa and Gab were estimated to be 1.89×10^7 and 2.21×10^7 km, respectively; Gaa and Gab are associated with event horizons with radii of 3.83×10^6 and 3.21×10^6 km, respectively [16]

$$\Box\varphi_{ij} = -\frac{16\pi G}{c^4} T_{ij}\,, \qquad (5.2)$$

where

$$\varphi_{ij} = h_{ij} - \frac{1}{2}\eta_{ij} h\ , \qquad (5.3)$$

with trace $h = \eta^{ij} h_{ij}$. To approach Eq. (5.3), we apply the Lorentz gauge:

$$\frac{\partial \varphi_{ij}}{\partial x^j} = 0, \qquad (5.4)$$

considering the freedom for φ_{ij}.
When we seek a coordinate where h'=0 for the transformed trace h' corresponding to h in Eq. (5.3), a new coordinate system (x'^0,x'^1,x'^2,x'^3) that is introduced with a small deviation ξ^μ is required as:

$$x'^\mu = x^\mu + \xi^\mu \qquad (5.5)$$

(see Appendix H). For the requirement of the Lorentz gauge in the transformed coordinate,

$$\frac{\partial \varphi'_{ij}}{\partial x'^j} = 0, \qquad (5.6)$$

it follows that:

$$\Box\xi^\mu = 0. \qquad (5.7)$$

Associated with this additional constraint, we find the basic equation of the GW components in a traceless (h'=0) frame (see Appendix G).

As given in Eq. (G6) in Appendix G, Eq. (5.3) is transformed to the new coordinates as:

$$\varphi'_{\mu\nu} = h_{\mu\nu} - \eta_{ij}\delta^i_\mu \frac{\partial \xi^j}{\partial x^\nu} - \eta_{ij}\delta^j_\nu \frac{\partial \xi^i}{\partial x^\mu} - \frac{1}{2}\eta'_{\mu\nu} h'\,. \qquad (5.8)$$

The trace is given by:

$$\varphi' = \eta^{\mu\nu}\varphi'_{\mu\nu} = \eta^{\mu\nu} h_{\mu\nu} - \eta^{\mu\nu}\eta_{ij}\delta^i_\mu \frac{\partial \xi^j}{\partial x^\nu} - \eta^{\mu\nu}\eta_{ij}\delta^j_\nu \frac{\partial \xi^i}{\partial x^\mu} - \frac{1}{2}\eta^{\mu\nu}\,\eta'_{\mu\nu} h'\,. \qquad (5.9)$$

Further, φ' is given (see eq. (H7) in Appendix H) as:

$$\varphi' = \frac{1}{2} h'. \qquad (5.10)$$

When we establish the condition φ'=0, then h'=0 ; therefore, the equation transformed from Eq. (5.3) is expressed as:

$$\varphi'_{ij} = h'_{ij} - \frac{1}{2}\eta_{ij} h', \qquad (5.11)$$

giving the result:

$$\varphi'_{ij} = h'_{ij} \qquad (5.12)$$

(see Appendix H). In this context, we set the solution of Eq. (5.2), a priori, as well as that of the equation in the transformed coordinate $\Box\,\varphi_{ij}' = -(16\pi G/c^4)\, T_{ij}'$; that is:

$$\varphi_{ij} = A_{ij}\exp\left(\underline{i}k_m x^m\right) \qquad (5.13)$$

and

$$\varphi'_{ij} = A'_{ij}\exp\left(\underline{i}k'_m x'^m\right), \qquad (5.14)$$

where $\underline{i}$ is the imaginary unit, and k_m and k_m' are four-dimensional vectors to express harmonic waves. Then, the processes to set φ'=0 and h'=0 are carried out in the frame given by Eqs. (5.9) and (5.10), as described in Appendix H. It is indicated that $A_{0\nu}$'= 0, and only two independent components are allowed among $A_{\mu\nu}$'. When we select A_{11}' and A_{12}' as independent amplitudes to decide φ_{11}' and φ_{12}', the other amplitudes are given by:

$$\left.\begin{aligned} A'_{13} &= -\frac{k'_1A'_{11} + k'_2A'_{12}}{k'_3} \\ A'_{22} &= -\frac{(k'^2_1 + k'^2_3)A'_{11} + 2k'_1k'_2A'_{12}}{k'^2_2 + k'^2_3} \\ A'_{23} &= -\left(\frac{k'_2}{k'_3}\right)\frac{(k'^2_1 + k'^2_3)A'_{11} + k'_1k'_2A'_{12}}{k'^2_2 + k'^2_3} \\ A'_{33} &= \frac{(k'^2_1 + k'^2_2)A'_{11} + 2k'_1k'_2A'_{12}}{k'^2_2 + k'^2_3} \end{aligned}\right\} \qquad (5.15).$$

In the case of a plane wave (k_1'=0 and k_2'=0), for the propagation of GWs in the region located a long distance away from the source, it is indicated from Eq. (5.15) that A_{13}'=0, A_{13}'= -A_{11}', A_{23}'=0, and A_{33}'=0. From the symmetry of the spacetime tensor A_{21}'=A_{12}', we can see the commonly known characteristics of the transverse traceless (TT) expression. Because we are concerned with the propagation near the source region, it would be accurate to use Eq. (5.15) without the plane wave approximation, but we assume the local plane wave front for each propagating direction.

5.2. Generation of GWs from Quadrupole Source

We now consider the system depicted in Figure 9 for binary BHs whose IMSBH regions are condensed to radii ranging from 1/10 to 1/100 of the event horizons (see Sec. 3), i.e., we set the final coordinate system described in Sec. 5.1.2 as identical to that describing the generation of GW, which is associated here with the configuration in Figure 9; hereafter, we express the member BH as Gam that represents Gaa and Gab, by taking "m" as " a " and "b" ,respectively.

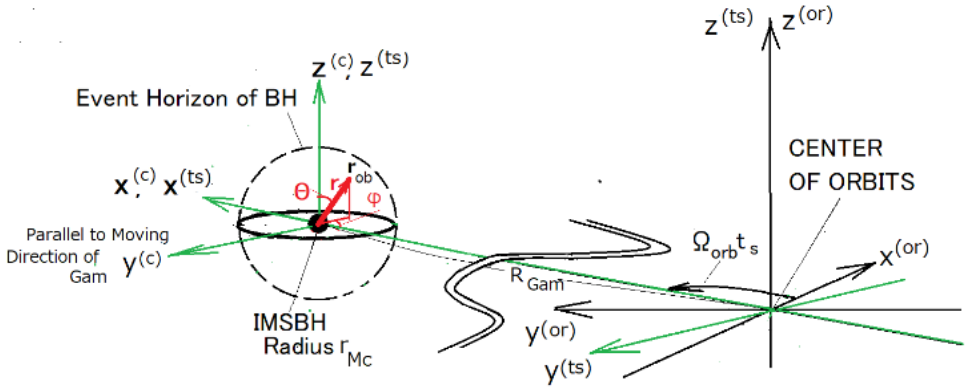

Figure 10: Coordinate systems of orbiting binary Gam (m indicates a or b) to describe the generation and propagation of GWs. The basic configuration of the Gaa and Gab orbits in Figure 9 are described as Gam in the Cartesian coordinate system ($x^{(or)}$,$y^{(or)}$,$z^{(or)}$), whose origin is at the center of the orbits. The orbiting IMSBH of Gam moves in the direction of the $y^{(ts)}$ axis of the Cartesian coordinate system ($x^{(ts)}$,$y^{(ts)}$,$z^{(ts)}$), where the center of the IMSBH of Gam, with radius r_{Mc}, is located in the direction of the $x^{(ts)}$ axis where Gam has orbital radius R_{Gam}. The position in the interior of the Kerr BH within the event horizon is expressed by vector $\mathbf{r}_{ob}$, defined from the center of the IMSBH, as described by the Cartesian coordinate system ($x^{(c)}$,$y^{(c)}$,$z^{(c)}$), whose origin is at the center of the IMSBH; axes $x^{(c)}$,$y^{(c)}$,and $z^{(c)}$ are defined in parallel directions to $x^{(ts)}$,$y^{(ts)}$ and $z^{(ts)}$, respectively. The vector $\mathbf{r}_{ob}$ is also described in spherical coordinates (r,θ,φ), as transformed from the coordinate system ($x^{(c)}$,$y^{(c)}$,$z^{(c)}$).

Further, we follow the established expression of the generation of GWs, projecting φ_{ij}' to the TT gauge given by Eq. (5.15) that is connected to:

$$\Box\varphi'_{ij} = \Box h_{ij}^{TT} = -\frac{16\pi G}{c^4} T_{ij} \ . \quad \ldots\ldots\ldots\ldots\ldots\ldots\ldots\ldots\ldots\ldots\ldots\ldots\ldots\ldots\ldots (5.16)$$

Then, in Eq. (5.16), h_{ij}^{TT} is expressed for the Gam system following the standard method, where the source function is expressed by the retarded function as:

$$h_{ij}^{TT}(\mathbf{r}_{ob}) = -\frac{4G}{c^4}\int_{orb} \frac{T_{ij}\left(\mathbf{r}_{ob}^{(or)}, t_{ob} - \frac{r_{os}}{c}\right)\cdot\delta\left(\mathbf{r}_{ob}^{(or)} - \mathbf{r}_{s}^{(or)}\right)}{r_{os}} dV_s^{(or)}, \qquad (5.17)$$

where $\mathbf{r}_{ob}^{(or)}$ and $\mathbf{r}_{s}^{(or)}$ are vectors of the observation point and source position, respectively, in the orbiting system defined from the origin of the coordinate at the center of the binary orbits; and $\Gamma_{os} = |\Gamma_{ob}^{(or)} - \Gamma_{s}^{(or)}|$. Integration of Eq. (5.17) is carried out, with:

$$dV_s^{(or)} = dx_s^{(or)} dy_s^{(or)} dz_s^{(or)} \ . \qquad (5.18)$$

Following Einstein's original expression, it becomes standard procedure to consider the quadruple moment for the source of GW. In the present work, we cannot simply apply the remote approximation for the proximity to the source but it becomes clear after a mathematical manipulation that we can use the same formula for the case of remote source approximation, as commonly utilized in the general formula of GW generation (see Appendix I). Specifically:

$$h_{ij}^{TT}(\mathbf{r}_{ob}) = -\frac{2G}{c^6}\cdot\frac{\partial^2}{\partial t_{ob}^2}\int_s \frac{T_{00}\left(\mathbf{r}_s^{(or)}, t_{ob} - \frac{r_{os}}{c}\right)x^i x^j}{r_{ob}} dV_s^{(or)} \ , \qquad (5.19)$$

where $\mathbf{r}_{ob} = |\mathbf{r}_{ob}|$, $\mathbf{r}_s = |\mathbf{r}_s|$, and $\mathbf{r}_{os} = |\mathbf{r}_{ob} - \mathbf{r}_s|$. In Eq. (5.19), all vectors are defined from the center of the IMSBH, and t_{ob} is the time passage at the observation point. Concerning the time passage t_s at the source point, we have the alternative expression:

$$h_{ij}^{TT}(\mathbf{r}_{ob}, t_{ob}) = -\frac{2G}{c^6}\int_s \frac{\partial^2}{\partial t_s^2}\left[\frac{T_{00}\left(\mathbf{r}_s^{(or)}, t_s\right)x^i x^j \cdot}{r_{ob}}\right] dV_s^{(or)} \ , \qquad (5.20)$$

where $t_{ob} = t_s + r_{os}/c$.

5.3. Case of SMBHB

We apply the results given by Eq. (5.19) (or Eq. (5.20), which are equivalent) to the case of the supermassive BH shown in Figure 9, taking the Cartesian coordinate for space with the origin at the center of the orbits of the two members of the BH Gam. Further, for detailed description of GW propagation in the Kerr BH interior, we depict additional coordinate systems in Figure 10, where the coordinates for Gam orbital system and for the interior vacuum region of the Kerr BH located outside of each IMSBH of Gam are indicated together.

As discussed in Sec. 5.1.2 for determining a TT gauge, we concentrated on the two basic spacetimes $h_{xx}^{TT}(r_{ob})$ and $h_{xy}^{TT}(r_{ob})$ to express the generated GW, as follows:

$$h_{xx}^{TT}(\mathbf{r}_{ob}) = -\frac{2G}{c^6}\int_s \frac{\partial^2}{\partial t_s^2}\left[\frac{\rho c^2 \delta\left(x_s^{(or)} - x,\ y_s^{(or)} - y,\ t_{ob} - \frac{r_{os}}{c}\right)\cdot x^2}{r_{ob}}\right] dV_s^{(or)} \quad \ldots (5.21)$$

and

$$h_{xy}^{TT}(\mathbf{r}_{ob}) = -\frac{2G}{c^6}\int_s \frac{\partial^2}{\partial t_s^2}\left[\frac{\rho c^2 \delta\left(x_s^{(or)} - x,\ y_s^{(or)} - y,\ t_{ob} - \frac{r_{os}}{c}\right)\cdot xy}{r_{ob}}\right] dV_s^{(or)} \ , \quad \ldots (5.22)$$

where x and y are the same as $x^{(or)}$ and $y^{(or)}$, respectively, as components of $r_{orb}^{(or)}$.
In Eqs. (5.21) and (5,22), $x_s^{(or)}$ and $y_s^{(or)}$ can be rewritten as:

and

$$x_s^{(or)} = R_{Gam}\cos(\Omega_{orb}t_s) + x_s^{(c)}$$
$$y_s^{(or)} = R_{Gam}\sin(\Omega_{orb}t_s) + y_s^{(c)}, \qquad .(5.23)$$

where $x_s^{(c)}$ and $y_s^{(c)}$ are components of the source position vector measured from the center of the IMSBH in the new coordinates $(x^{(c)},y^{(c)},z^{(c)})$ (see Appendix I), and R_{Gam} and Ω_{orb} are the orbital radius and angular velocity, respectively, of the orbiting BH Gam. Following the configuration in Figure 10, we obtain the relations:

$$x_s^{(c)} = r\sin\theta \cdot \cos\varphi \qquad (5.24)$$

and

$$y_s^{(c)} = r\sin\theta \cdot \sin\varphi. \qquad (5.25).$$

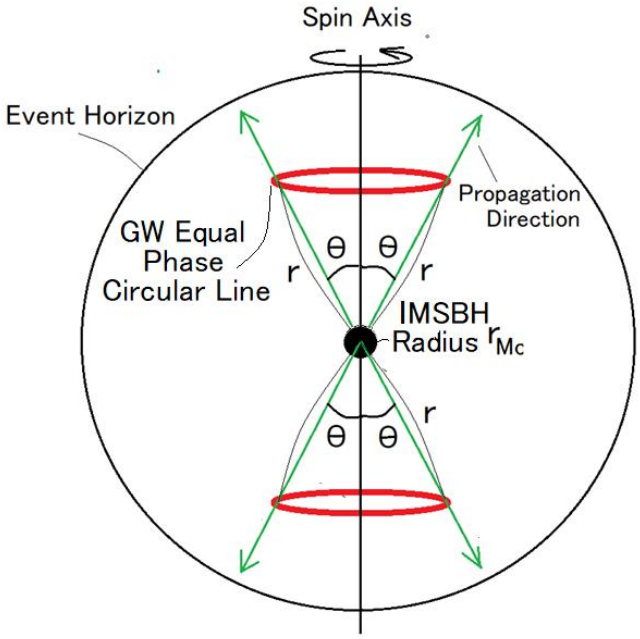

Figure 11: Equal-phase circle of GW propagating at polar angle $\boldsymbol{\theta}$, generated from IMSBH. GWs that propagate radially in the $\boldsymbol{\theta}$ (0–$\boldsymbol{\pi/2}$) direction take the same phase for a given $\boldsymbol{\theta}$ homogeneously without dependence on the rotation direction $\boldsymbol{\varphi}$, i.e., equal-phase lines form a circle. The spin axis of IMSBH is directed perpendicular to the orbital plane of the binary; then, the azimuth is $\varphi = \Omega_s t + \varphi_0$ for angular velocity Ω_s and phase angle φ_0.

As described in Appendix J, the integrations of Eqs. (5.21) and (5.22) are given as functions of the observation point at distance r_{ob}, measured from the center of the IMSBH at time t_{ob}, as:

$$h_{xx}^{TT}(t_{ob},r_{ob}) = 2\frac{r_g}{r_{ob}}\cdot\left(\frac{v_{Gam}}{c}\right)^2\cdot\cos\left[2\Omega_{orb}\left(t_{ob}-\frac{r_{ob}}{c}\right)+\Phi_I\right], \qquad (5.26)$$

and

$$h_{xy}^{TT}(t_{ob},r_{ob}) = 2\frac{r_g}{r_{ob}}\cdot\left(\frac{v_{Gam}}{c}\right)^2\cdot\sin\left[2\Omega_{orb}\left(t_{ob}-\frac{r_{ob}}{c}\right)+\Phi_I\right], \qquad (5.27)$$

where v_{Gam} is the orbital velocity of Gam. The initial average phase $((2\Omega_{orb}\,\alpha_{Mc}\,r_{Mc})/c$ is given by $\Phi_I = 2\alpha_{Mc}\,\pi$, with a factor $\alpha_{Mc}(0<\alpha_{Mc}<1)$ to be calculated to give the representative source position in IMSBH within radius r_{Mc}.

6. Propagation of GW in the Interior Region of a Kerr BH

6.1. GW in the Rotating Frame of Kerr BH

To investigate the propagation characteristics of the generated GW, we introduce a vector $\mathbf{k}_{ob}$ to describe the wave number for h_{xx}^{TT} and h_{xy}^{TT}, given by Eqs. (5.26) and (5.27) as:

$$h_{xx}^{TT}(t_{ob}, \mathbf{r}_{ob}) = A_{xx}\cos[2\Omega_{orb}t_{ob} - \mathbf{k}_{ob}\mathbf{r}_{ob} + \Phi_I] \quad \ldots\ldots\ldots\ldots\ldots\ldots\ldots\ldots\ldots (6.1)$$

and

$$h_{xy}^{TT}(t_{ob}, \mathbf{r}_{ob}) = A_{xy}\sin[2\Omega_{orb}t_{ob} - \mathbf{k}_{ob}\mathbf{r}_{ob} + \Phi_I], \ldots\ldots\ldots\ldots\ldots\ldots\ldots\ldots\ldots (6.2)$$

where

$$A_{xx} = A_{xy} = 2\frac{r_g}{r_{ob}} \cdot \left(\frac{v_{Gam}}{c}\right)^2, \quad \ldots\ldots\ldots\ldots\ldots\ldots\ldots\ldots (6.3)$$

and

$$\boldsymbol{k}_{ob}\boldsymbol{r}_{ob} = 2\Omega_{Gam}\frac{r_{ob}}{c}. \quad \ldots\ldots\ldots\ldots\ldots\ldots\ldots\ldots\ldots\ldots\ldots\ldots\ldots\ldots (6.4)$$

To describe the propagation of a GW in the interior region of the Kerr BH, we follow the spherical coordinates describing Eq. (3.54). At this stage, however, we rewrite Eq. (3.54) for the observation system where we can observe the spinning angular velocity of the BH as:

$$ds^2 = -\left\{\left(1 - \frac{rr_g}{\Sigma}\right) + \frac{2carr_g\sin^2\theta}{\Sigma}\left(\frac{\Omega}{c}\right) - \left(r^2 + a^2 + \frac{a^2rr_g\sin^2\theta}{\Sigma}\right)\sin^2\theta\left(\frac{\Omega}{c}\right)^2\right\}c^2dt^2 + \frac{\Sigma}{\Delta}dr^2 + \Sigma d\theta^2, \quad (6.5)$$

defining $\Omega = d\varphi/dt$ with respect to coordinate φ (see Eq. (3.54)); the coordinate to describe Eq. (6.5) becomes consistent with those of Eqs. (6.1) and (6.2) when we translate from the Cartesian to spherical coordinates (see Appendix K); that is:

$$h_{rr}^{TT}(t_{ob}, \mathbf{r}_{ob}) = A\cos[2\Omega_{Gam}t_{ob} - \mathbf{k}_{ob}\mathbf{r}_{ob} + \Phi_I - 2\varphi_{0b}], \quad (6.6)$$

and

$$h_{r\varphi}^{TT}(t_{ob}, \mathbf{r}_{ob}) = A\sin[2\Omega_{Gam}t_{ob} - \mathbf{k}_{ob}\mathbf{r}_{ob} + \Phi_I - 2\varphi_{0b}], \quad (6.7)$$

where $A=A_{xx}=A_{xy}$, and φ_{0b} is a φ value corresponding to a given observation position. Considering Eqs. (6.6) and (6.7), Eq. (6.4) is rewritten to describe the propagation through the interior region of BH, as follows:

$$\mathbf{k}_{ob}\mathbf{r}_{ob} = k_{\perp}r\sin\theta + k_Z r\cos\theta = k(\theta)r \quad (6.8)$$

where $k(\theta)$ is a newly introduced function that satisfies relations $k_{\perp}=k(\theta)\sin\theta$ and $k_Z = k(\theta)\cos\theta$.

With the configuration in Figure 11, the propagation of the wave front of GW was analyzed as a function of the distance r from the center of IMSBH of radius r_{Mc} with the wavelength characterized by a propagating direction given by the polar angle θ; the equal-phase line of the propagating GW forms a circle along the direction of the azimuth φ.

We do not address the calculation processes of energy transport or the work action of the generated GW but simply discuss the propagation of GW in terms of h_{rr}^{TT} and $h_{r\varphi}^{TT}$. Therefore, we construct a function to simplify the description for the propagation of GW with spacetime h_{rr}^{TT} and $h_{r\varphi}^{TT}$, as follows:

$$H = h_{rr}^{TT} + \underline{i}\, h_{r\varphi}^{TT} = A \cdot \cos(2\Omega_{orb} t_{ob} - \mathbf{k}_{ob}\mathbf{r}_{ob} + \Phi_I - 2\varphi_{0b}) + \underline{i}\, A \cdot \sin(2\Omega_{orb} t_{ob} - \mathbf{k}_{ob}\mathbf{r}_{ob} + \Phi_I - 2\varphi_{0b}) = A \cdot \exp\left[\underline{i}(2\Omega_{orb} t_{ob} - k(\theta) r + \Phi_I - 2\varphi_{0b})\right] \quad (6.9).$$

where $\underline{i}$ is the unit of the complex quantity again.

The velocity of the generated GW propagating through a vacuum region of the interior Kerr BH is calculated. Eqs. (6.6), (6.7), and (6.9) are described by the coordinate close to the freefall system where we apply QMST, which becomes the observation platform following the geodesic of BH. Then, transformation to the spacetime for the vacuum region in the interior of Kerr BH is required. With respect to the four-dimensional proper length described by Eq. (6.5) for the Kerr BH spacetime, we can find the common proper length given in the QMST as follows:

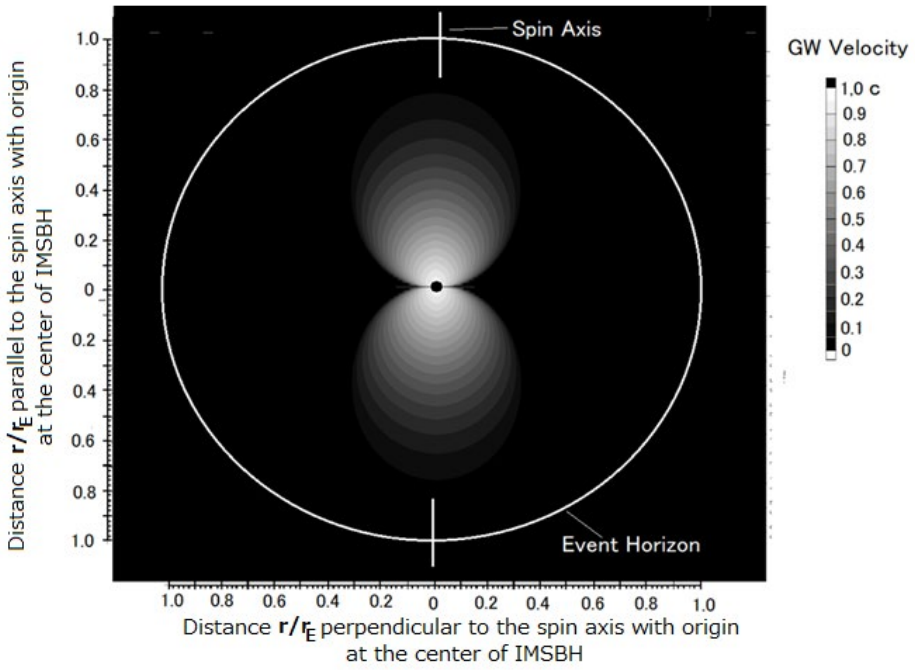

Figure 12: Calculated velocity of GW propagating in the interior region of Kerr BH. Results are given in r–θ cross section, including spin axis for AΩ= 8 (see Eq. (6.17) and Figure 13), with IMSBH radius r_{Mc}/r_E =1⁄50. The GW velocity is indicated as gray code, from pure white for light velocity to pure black for null velocity. The GWs that propagate radially in the direction of the polar angle θ cease to propagate at (r, θ_F), corresponding to F^2=0 (see Eq. (6.12)) before arriving at the event horizon.

$$-c^2\left(1 - \frac{v_\varphi^2}{c^2}\right) \cdot dt_{ob}^2 + dr^2 = -c^2 dt_B^2 \cdot F^2 + \frac{\Sigma}{\Delta} dr_B^2, \quad (6.10)$$

where t and r in Eq. (6.5) are rewritten as t_B and r_B, respectively, for the case of BH, and dθ is set to zero because the phase of the GW varies as a function of t_B and r_B propagating in the direction with fixed angle θ. In Eq. (6.10), F^2 is defined to simplify the expression of Eq. (6.5), as follows:

$$F^2 = \left(1 - \frac{r r_g}{\Sigma}\right) + \frac{2 c a r r_g \sin^2\theta}{\Sigma}\left(\frac{\Omega}{c}\right) - \left(r^2 + a^2 + \frac{a^2 r r_g \sin^2\theta}{\Sigma}\right)\sin^2\theta\left(\frac{\Omega}{c}\right)^2. \quad (6.11)$$

When we try to find the relation of the linear transformation, it follows that:

$$\begin{pmatrix} dr \\ dt_{ob} \end{pmatrix} = \begin{pmatrix} a_{11} & a_{12} \\ a_{21} & a_{22} \end{pmatrix} \begin{pmatrix} dr_B \\ dt_B \end{pmatrix}. \qquad (6.12)$$

Based on Eq. (6.10), the result is given by:

$$a_{11} = \sqrt{\frac{\Sigma}{\Delta}}, \quad a_{12} = 0, \quad a_{21} = 0 \quad \text{and} \quad a_{22} = \gamma_{\varphi}^{*} F \qquad (6.13)$$

(see Eq. (2.40) for γ_{φ}^{*}). Using the transformation relations given by Eqs. (6.12) and (6.13), the propagating GW given by Eq. (6.9) is expressed, in the interior region of the BH that is given by the Kerr spacetime, with the form of the WKB approximation, as follows:

$$H_B = A_B \cdot \exp\left[\underline{i}\left(\int_{t_s}^{t_{ob}} 2\Omega_{orb}\gamma_{\varphi}^{*} F dt_B - \int_{r_{Mc}}^{r} k(\theta)\sqrt{\frac{\Sigma}{\Delta}} dr_B + \Phi_I - 2\varphi_{0b}\right)\right]. \qquad (6.14)$$

As discussed in Appendix L, the normalized amplitude A_B observable in Kerr spacetime is estimated as:

$$A_B = \frac{\Sigma}{\Delta} A = 4\frac{\Sigma}{\Delta} \cdot \frac{r_g}{r_{ob}} \left(\frac{v_{Gam}}{c}\right)^2. \qquad (6.15)$$

The propagation velocity $V(t_{ob}, r, \theta)$ of this GW at point $t = t_{ob}$ at r in the direction with polar angle θ that is measured from the direction of the spin axis is then given by:

$$V(t_{ob}, r, \theta) = \frac{2\Omega_{orb}\gamma_{\varphi}^{*} F}{k(\theta)} \sqrt{\frac{\Delta}{\Sigma}} = cF\sqrt{\frac{\Delta}{\Sigma}}, \qquad (6.16)$$

where $2\Omega_{orb}\, \gamma_{\varphi}^{*} / k(\theta) = c$. It is clear that $V(t_{ob}, r, \theta)$ becomes zero at two characteristic points, at F=0 and the event horizon that is given by Δ=0. In Figure 12, the GW velocity given by Eq. (6.16) is shown with gray code from 0 to near light velocity for the case in which the radius of IMSBH is r_{Mc}/r_E =1/50. All GWs radiated from IMSBH stop before arriving at the event horizon. Before arriving at the stopping point, GWs propagate in the range from the direction of the spin axis to its vertical; the calculated results show that the propagation distance in the vertical direction is shorter than in the direction parallel to the rotation axis. To express the stopping points of GWs clearly, the lines where we can see F=0 are presented in Figure 13, where the lines are indicated in r,θ domain with the parameter A_Ω, which describes the spatial dependence of Ω given with the following function (see both the top and bottom panels of Figure 13)

$$\frac{\Omega}{2\Omega_E} = \frac{\Omega \cdot r_E}{c} = 1 - \frac{1}{2}\exp\left[A_\Omega \left(\frac{r}{r_E} - 1\right)\right]. \qquad (6.17)$$

where Ω_E is the angular velocity at the event horizon.

As given by Eq. (6.15), the amplitude of a GW diverges to infinity at the event horizon. The calculated results given in the top panel of Figure 13 show, however, that in all cases, GWs stop before approaching the event horizon by encountering F=0 lines.

6.2. Return of GW from Stopping Points

The GWs propagating in the direction of the polar angle range $0 \le \theta \le 90^{\circ}$ start returning from the point where they cease to proceed, taking reciprocal paths with the wave function given by:

$$H_{B,R} = A \cdot \exp\left[\underline{i}\left(\int_{t_s}^{t_{ob,R}} 2\Omega_{orb}\gamma_{\varphi}^{*} F dt_B + \int_{r_{Mc}}^{r,R} k(\theta)\sqrt{\frac{\Sigma}{\Delta}} dr_B + \Phi_{IR} - 2\varphi_{0bR}\right)\right]. \quad \ldots\ldots\ldots\ldots (6.18)$$

It is a significant principle that the propagating wave does not accumulate the phase value because the wave maintains progress with the condition of the phase, as:

$$\int_{t_{sF}}^{t_{ob,R}} 2\Omega_{orb}\gamma_{\varphi}^{*}Fdt_B - \int_{r_{Mc}}^{r,R} k(\theta)\sqrt{\frac{\Sigma}{\Delta}}dr_B = 0. \quad \ldots\ldots\ldots\ldots\ldots\ldots\ldots\ldots\ldots\ldots\ldots\ldots\ldots (6.19)$$

At a given time and space, the return wave $H_{B,R}$ encounters the outgoing wave:

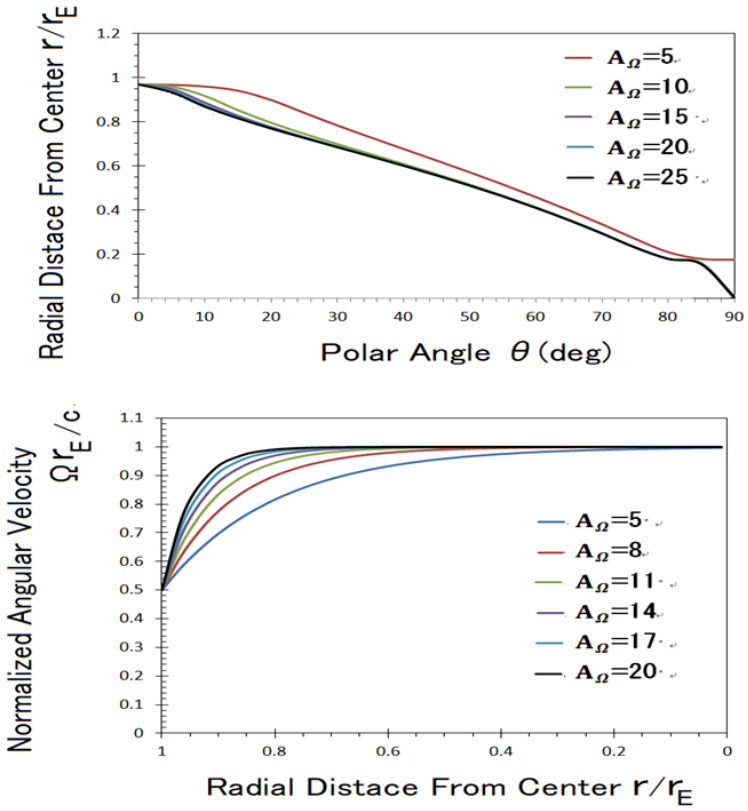

Figure 13: Top panel: Stopping line F=0 of GW plotted in the r-θ plane in the interior region of Kerr BH, where the radial distance r is given in the ordinate in terms of the ratio to the event horizon r_E. The parameter A_Ω of the stopping lines represents the spatial dependence of the spin angular velocity. Bottom panel: Spatial dependence of the spin angular velocity with A_Ω of 5–20, showing the range of variation of the spin angular velocity from the value at the event horizon to the rotation at the position of IMSBH.The radial distance is given in the abscissa in terms of r/r_E along the spin axis.

$$H_{B,F} = A \cdot \exp\left[\underline{i}\left(\int_{t_{sF}}^{t_{ob,R}} 2\Omega_{orb}\gamma_{\varphi}^{*}Fdt_B - \int_{r_{Mc}}^{r,R} k(\theta)\sqrt{\frac{\Sigma}{\Delta}}dr_B + \Phi_{IF} - 2\varphi_{0bF}\right)\right]. \quad \ldots\ldots\ldots\ldots (6.20)$$

Then, the forward-progressing wave encounters the returning waves at each moment, as:

$$H_{B,R} + H_{B,F} = A \cdot \exp\left[\underline{i}\left(2\Omega_{orb}\gamma_{\varphi}^{*}Fdt_B + k(\theta)\sqrt{\frac{\Sigma}{\Delta}}dr_B + \Phi_{IR} - 2\varphi_{0bR}\right)\right]$$

$$+A \cdot \exp\left[\underline{i}\left(2\Omega_{orb}\gamma_{\varphi}^{*}Fdt_B - k(\theta)\sqrt{\frac{\Sigma}{\Delta}}dr_B + \Phi_{IF} - 2\varphi_{0bF}\right)\right]. \quad \ldots\ldots (6.21)$$

At this encounter state, the initial phases of each wave, Φ_{IR} - $2\varphi_{0bR}$ and Φ_{IF} - $2\varphi_{0bF}$, are generally independent. In the present situation, however, Φ_{IR} and Φ_{IF} are defined as the average propagation time differences around a sphere-shaped source within IMSBH that always give the same values; the phase angles $2\varphi_{0bR}$ and $2\varphi_{0bF}$ are also the same because they are selected from the spinning IMSBH, which is assumed to be in complete symmetry with the azimuth direction. Then, Eq. (6.21) gives the result:

$$H_{B,R} + H_{B,F} = 2A \cdot \exp\left[i(2\Omega_{orb}Fdt_B + \Phi_I - 2\varphi_{0b})\right] \cos\left(k(\theta)\sqrt{\frac{\Sigma}{\Delta}}dr_B\right), \quad \ldots\ldots (6.22)$$

which shows that GWs are deformed to standing waves that can no longer carry energy.

7. Discussion

7.1. Problem of Angular Momentum to Describe Kerr Spacetime

In the present study, one of the significant points is that GW forms a standing wave, so dissipation of the orbiting energy of the binary is avoided; this fact is strictly related to the existence of the wide vacuum region inside the Kerr BH, as suggested in the present work for the condensation of IMSBH. The essence of the argument of condensation is in the property of the rotation parameter as α defined in Eq. (3.50), which is repeated in a simple form here as:

$$a = \frac{J}{Mc}. \qquad (7.1)$$

When we assume a homogeneous rigid state model rotating with angular velocity Ω and with a constant density ρ, the expression of Eq. (7.1) is given, normalized by the Schwarzschild radius r_g, as follows:

$$\frac{a}{r_g} = \frac{8\pi r_{Mc}^5 \rho\Omega/15}{(4\pi r_{Mc}^3\rho/3)c} \cdot \frac{1}{r_g} = \frac{2}{5}\left(\frac{v_\varphi}{c}\right)\left(\frac{r_{Mc}}{r_g}\right), \qquad (7.2)$$

where r_{Mc} and v_φ are the radius of the assumed IMSBH and the representative rotation velocity selected at the equator surface, respectively. In so far as we maintain the constraint of the low-velocity model, we have arg<1/5 ,considering the case of matter distribution where the radius is close to the event horizon r_E =(r_g/2); thus, we cannot approach the case of the maximum rotation where (a/r_g)=1/2.

To lose this constraint, we selected a fast rotation model that comprises a fluid with constant rotation velocity v_φ and angular momentum that admits the relativistic approach to realize the same rotation parameter a, even though the radius r_{Mc} of IMSBH becomes small because of condensation. Specifically:

$$J = \int_0^{r_{Mc}}\int_0^{\pi}\int_0^{2\pi} \frac{\rho v_\varphi r\sin\theta}{\sqrt{1-(v_\varphi/c)^2}} r^2\sin\theta dr d\theta d\varphi, \qquad (7.3)$$

where $1/\sqrt{1-(v_\varphi/c)^2}$ is given by γ_φ^* (see Eq.(2.40)). However, the rationale to accept the concept expressed by Eq. (7.3) is not simple because there is the question of what is increased to maintain α constant rotation parameter under the situation of shrinking r_{Mc}. Considering only J in Eq. (7.3), the angular momentum increases because the Lorentz factor γ_φ^* increases matter density from ρ to $\rho\gamma_\varphi^*$ as relativistic effects. However, in Eq. (7.1), it becomes a subject of argument that the mass M could also be increased as $M\gamma_\varphi^*$; therefore, the rotation parameter α would neither be increased nor would it remain constant for decreasing matter region radius r_{Mc}, even in the case of high-speed rotation of the IMSBH.

When the equal-rotation velocity model is selected, as is the case in this study, the rotation parameter corresponding to Eq. (7.3) is:

$$a = \frac{(3/4)Mr_{Mc}v_\varphi\gamma_\varphi^*}{Mc}, \qquad (7.4)$$

where $M = (4\pi R^3/3)\rho$ assuming homogeneous ρ. Because Eq. (7.4) is simply expressed ,for $v_\varphi \approx c$,as:

$$a = (3/4)r_{Mc}\gamma_\varphi^*, \qquad (7.5)$$

there is no room for explicit expression of ρ^* (= $\rho/\sqrt{(1-(v_\varphi/c)^2}$) in Eqs. (7.4) and (7.5). We must then consider the rotation parameter a without the relation to the increase in density; that is, it should be understood that a is realized only in the form $r_{Mc}\ \gamma_\varphi^*$, which is also endorsed in the present study as given by Eq. (3.53). The underlying physics of the constancy of $r_{Mc}\ \gamma_\varphi^*$ for high-speed rotation is, therefore, the Lorentz shortening of the length of the distributing range of the matter along the rotation direction.

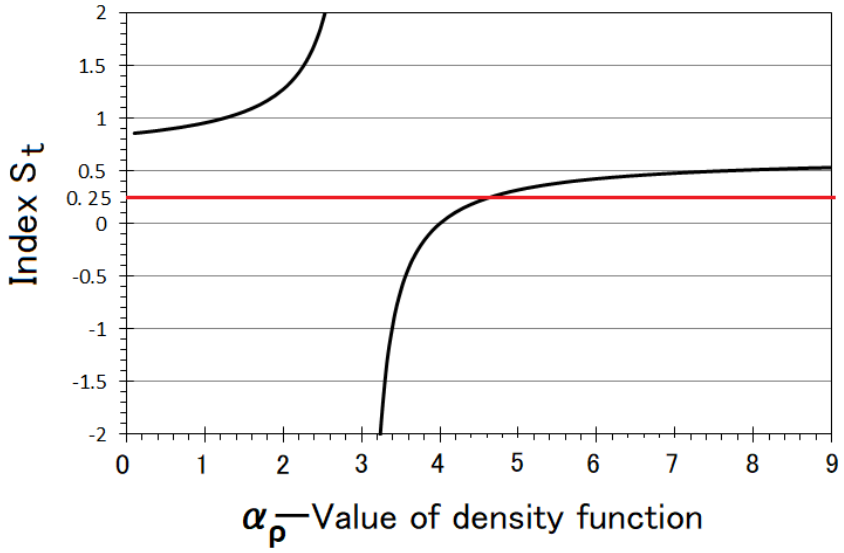

Figure 14: Index S_t versus power index α showing the density distribution of IMSBH as $\rho = \rho_0 (r_{Mc}/r)^\alpha$.$S_t$ is given by Eq. (7.10) under the constraint of the maximum rotation ($a = r_E$), which indicates a critical point at 0.25 where the IMSBH radius r_{Mc} becomes equal to the event horizon radius r_E, with γ_φ^*=1 and v_φ/c=0.5. The differential length dl of an arc on rotating matter that is set in a parallel direction to the rotation direction is expressed by:

$$d\ell = \left(1/\gamma_\varphi^*\right) d\ell_0 \,, \qquad (7.6)$$

where dl_0 is the differential arc length in the case of non-rotation that can be expressed as $dl_0 = r_{Mc0}\, d\varphi$ for the radius r_{Mc0} of the matter region in the static case with differential azimuth angle dφ. Then, the radius r_{Mc} of the rotating matter region is given as:

$$2\pi r_{Mc} = \int_0^{\ell} d\ell = \int_0^{2\pi} \left(1/\gamma_\varphi^*\right) r_{Mc0}\, d\varphi. \qquad (7.7)$$

This shows that:

$$r_{Mc}\gamma_\varphi^* = r_{Mc0}. \qquad (7.8)$$

7.2. Effect of Matter Distribution on the Rotation Parameter

Although we assume a case of constant and homogeneous density distribution in Eqs. (7.2), (7.4), and (7.5), to simplify the discussion, we need to consider the cases of the density distribution functions $\rho = \rho_0 (r_{Mc}/r)^2$ in the present study. Therefore, the general case must be discussed here, with $\rho = \rho_0 (r_{Mc}/r)^{\alpha_\rho}$ (where α_ρ is an arbitrary constant), which reflects the spacetime of IMSBH and affects the calculations of the rotation parameter and the radius of the IMSBH.

When we assume a constant rotation velocity v_φ, the rotation parameter depending on the density distribution function is given as a ratio to r_g by:

$$a/r_g = \frac{\pi(3-\alpha_\rho)}{4(4-\alpha_\rho)} \cdot \frac{r_{Mc}\gamma_\varphi^*}{r_g}\left(\frac{v_\varphi}{c}\right). \qquad .(7.9)$$

For the case of maximum rotation (a/r_g=1/2) of a Kerr BH, we define an index S_t, corresponding to Eq. (7.9), as:

$$S_t \equiv \frac{r_{Mc}\gamma_\varphi^*}{r_g}\left(\frac{v_\varphi}{c}\right) = \left(\frac{1}{2}\right) \cdot \frac{4(4-\alpha_\rho)}{\pi(3-\alpha_\rho)}. \qquad (7.10)$$

The index S_t is 0.25 when r_{Mc} is extremely close to the event horizon at which $r_{Mc} \approx r_E$, $r_g = 2r_E$,$\gamma_\varphi^* \approx 1$,and $v_\varphi / c = 0.5$. If $S_t > 0.25$, we can find the solution for $v_\phi / c \approx 1$, such as $\gamma_\varphi^* > 1$ with $r_{Mc} < r_E$, i.e., the surface of the IMSBH is clearly inside the event horizon and apart from the event horizon even for the maximum case of r_{Mc}. In Figure 14, S_t is exhibited as a function of α_ρ. Passing the boundary formed by the singular point at α_ρ=3, the features of S_t reveal different α_ρ dependences. That is, for α_ρ higher than 3, the index remains in a range from ≈ 0.25 to 0.5, over most of the range; and at α_ρ=4.646, it is exactly 0.25 where $r_{Mc} \approx r_E$. We should note that for this high α_ρ value, there exist an extremely high intensity of the gravity that would be completely different from the orthodox Newtonian gravity which results distribution of matter with density distribution function $\rho = \rho_0 (r_{Mc}/r)^{\alpha_\rho}$.

7.3 . Role of QMST

To solve the state of local force balance in the IMSBH starting from the Einstein equation given in the second of Eq.(2.3), we have employed the QMST that is set in the frame close to a system of free falling system following the geodesics in IMSBH. As has been described in Sub Sec. 2.2.2 , we can observe the state of the force balance in IMSBH even though we cannot obtain the real spacetime of IMSBH; as has been described in Sub Sec.3.3.3, we are able to find the key relation to find r_{Mc} as consequence of the quest to find the force balance in IMSBH observed from QMST. It should be noted that the usage of QMST in Sec.2 is, therefore, not to be purposed to construct the spacetime of IMSBH but to describe the geodesic observed from a frame close to the freefalling system ; that is, we have derived formulae to express the force balance in IMSBH observed in QMST based on the metrics to describe the geodesics.

In Sec.5, we utilized QMST to describe the GWs which are generated from IMSBH and propagate through internal vacuum region of Kerr BH. In this case, we take QMST as a frame of observation where the gravity is observed as weak field even that is intense enough in the frame of the spacetime of IMSBH and in Kerr. spacetime. Due to this rationale we have translated the expression for time and space as given from Eqs. (6.10) to (6.15) to describe the phase and amplitude of the propagating GWs inside of the BH with intense gravity fields.

8. Conclusion

The motivation of the present study was to investigate the proposal of the existence of a SMBHB at SgrA* based on the observation of decameter radio wave pulses independent of the established method of tracking stars surrounding Sgr A*. The most critical issue of the present study relating to our observed SMBHB with an extremely close situation is energy dissipation due to the generation of GW. When we apply the current GW theory and evidences of the generation of GW reported by LIGO to the observed system, SMBHB will merge within a few hours[45]. However, before we abandon the observed SMBHB as erroneous, we have reinvestigated the present concept of the generation of GWs from a BH. The following questions remain for studies of the generation of GWs from a BH: 1) all results reported by LIGO at present are GWs from the mergers of star mass objects; 2) sources endorsed by theory assume star mass binaries of less than 200 solar masses; and 3) all theories of GWs tacitly assume no remarkable separation between the distribution of matter as GW sources and positions of the event horizons of BHs. We restricted our argument to the case of a supermassive BH whose possible matter density becomes milder than that of a stellar-mass BH so that we could apply the classical theory of plasma dynamics and try to find the possibility of separation of the matter region (IMSBH) from the event horizon, where GWs generated at matter sources cease to propagate toward the outside so as not to cross the event horizon. Various studies have addressed the interior of a BH using a family of spacetime AdS_3, for example, but we selected a unique way aiming to find a collapsed matter region deep inside of vacuum space in the interior region of a Kerr BH (IMSBH). To investigate the separation of the IMSBH within the event horizon, we selected a coordinate QMST, which is close to the freefall system in IMSBH where the spacetime can be described as perturbation from the Minkowsky spacetime. Although we could not express the exact form for forces described in the spacetime of IMSBH, we could observe a state of force balances that strictly reflect radius of matter distribution region in IMSBH. The results of the force balance were obtained through methods of analysis of classical plasma physics characterized by modified Newtonian dynamics, arriving eventually from Einstein's equation for weak gravity fields given with QMST. The result shows that the collapsed radius of the IMSBH depends on the increased rotation energy of matter as $m_i c^2 \gamma_\varphi^*$ for the iron ion mass m_i with Lorentz factor γ_φ^* .with rotation velocity close ot the light velocity.

From the expression of the force balance state in the IMSBH, we obtained results of the collapsed radius r_{Mc} for matter distribution with respect to the radius of the event horizon r_E, for Kerr spacetime which envelop the IMSBH thickly in the end point of inside vacuum region, as $r_{Mc} = (8/\pi\zeta) \cdot r_E \sqrt{(1-(v_\varphi / c)^2}$ for the rotating velocity v_φ that is assumed close to the light velocity c and rate ζ of rotating plasma. The original cause of the contraction of IMSBH is the gravity by which the matter is condensed, finding a balance point by the centrifugal force due to systematic rotation of plasma and the pressure that gains energy converted from increased gravity. For the balance system consisting of pure kinetic forces, however, we cannot endorse the final balance point. The present study suggests that the runaway state of the contraction of the IMSBH is avoided as associated with the generated Lorentz force induced by electric currents that are raised in parallel to the toroidal motion of the plasma. The investigation to determine the precise limit for the final stable state will be deferred for future work considering the electric current formations with many possible effects. We assumed a range of contractions of the matter radius from 1/10 to 1/100 of the event horizon radius by considering a high Lorentz factor γ_φ^* corresponding to the systematic rotation of the iron ion with energy from approximately 500 Gev to 10 TeV. This high plasma energy is thought to have only kinetic origin, including the Lorentz force without nuclear fusion, because of the assumption of the final stage of matter as iron plasma.

From the member of the binary BH orbiting with speeds of 18 and 21% of the light, GWs are generated starting from the IMSBH. We followed the established generation theory of GWs, starting from Einstein's quadruple pole source description. The theory of the generation of GWs has proceeded independently of the recently developing advanced theory relating to post-Newtonian or post-Minkowskian approaches because the orbiting speeds of the sources are still in the range in which we can apply the non-relativistic case.

Although the generated GWs expressed with the TT gauge consist of two fundamental components, these are expressed by one wave formula using a complex exponential function because the present study is focused on the propagation features rather than actions of GWs. After generation from condensed IMSBH sources, the waves propagate through the vacuum spacetime of the interior region of the Kerr BH toward the event horizon from the sources at IMSBH located deep inside. In rotating Kerr vacuum spacetime, there are two characteristic points where the propagation of GWs cease. One is the exact event horizon, and the other is the characteristic zone controlled by the angular velocity of the vacuum region, as indicated by the F or F^2 function (see Eq. (6.11)), that is expressed in terms of the radial distance r and polar angle θ. Although the wave amplitude transformed to the interior Kerr spacetime shows singularity to journey to infinity at the event horizon, GWs are stopped at the F zero point before approaching the event horizon. The GWs meet with the F zero point returning toward the starting points associated with the initial phase; the returning and forwarding GWs interact to form standing waves at each encounter point. Thus, the GWs in the interior region of the Kerr BH are unable to carry energy from the source. Therefore, for the case of a supermassive BH, we can determine a model where generated GWs are not radiated outside the event horizon and do not damp the orbital motion even for extremely close binaries.

Acknowledgement

The present research was accomplished in the science department of the graduate school of Tohoku University. The author is grateful to Prof. Y. Katoh, Dr. A. Kumamoto, and Dr. Y. Kawazura for their interest and valuable discussions for the present work. Financial support to continue the present work was provided with deep understanding of the standpoint of the present work; the author thanks to President Y. Miyazawa of Seisa Group and Prof. H. Inoue of Seisa University.

References

1. Abbott, B. P., Abbott, R., Abbott, T. D., Abernathy, M. R., Acernese, F., Ackley, K., …& Zweizig, J. (2016). Observation of Gravitational Waves from a Binary Black Hole Merger. Phys. Rev. Lett,116, 061102.
2. Abbott, B. P., Abbott, R., Abbott, T. D., Abernathy, M. R., Acernese, F., Ackley, K., …& Zweizig, J. (2016). GW151226: Observation of Gravitational Waves from a 22-Solar-Mass Binary Black Hole Coalescence. Phys. Rev. Lett,116, 241103
3. Abbott, B. P., Abbott, R., Abbott, T. D., Acernese, F., Ackley, K., Adams, C., …& Zweizig, J. (2017). GW179104:Observation of a 50-Solar-Mass Binary Black Hole Coalescence at Redshift 0.2. Phys. Rev. Lett,118, 221101
4. Einstein, A . (1916). Naeherungsweise Integration der Feldgleishungen der Gravitation. Preuss. Acad. Wiss. Berlin, 688.
5. Abbott, B. P., Abbott, R., Abbott, T. D., Acernese, F., Ackley, K., Adams, C., …& Zweizig, J. (2017). GW170817: Observation of Gravitational Waves from a Binary Neutron Star Inspiral. Phys. Rev. Lett,119, 161101
6. Chirenti, C. & Rezzolla, L.. (2016). Did GW150914 Produce a Rotating Gravastar ? Phys. Rev. D94, 084016
7. Cardoso, V. & Pani, P.. (2017). Tests for the Existence of Horizons Through Gravitational Wave Echoes. [gr-qc] arXiv:1709.01525 vol 1.
8. Glampedakis, K. & Pappas, G. (2018). How Well Can Ultracompact Bodies Imitate Black Hole Ringdowns? Phys. Rev. D97, 041502
9. Schödel, R., Ott, T., Genzel, R., Hofmann, R., Lehnert, M., Eckart, A., ….& Menten, K. M..(2002). A Star in a 15.2-Year Orbit around the Supermassive Black Hole at the Center of the Milky Way.Nature 419 694–6 [doi: 10.1038/nature01121]
10. Gehz, A., Duchene, G., & Mathews, K. (2003).The first Measurement of Spectral Lines in a Short-Period Star Bound to the Galaxy's Central Black Hole. Astrophys. J. Lett, 586,127
11. Ghez, A. M. , Salim, S. , Hornstein, S. D. , Tanner, A. , Lu, J. R., Morris, M. , …& Duchêne, G.(2005). Stella Orbits around the Galactic Center Black Hole. Astrophys. J., 620, 744
12. Eisenhauer, F., Genzel, R., Alexander, T., Abuter, R., Paumard, T., Ott, T., …& Zucker, S. (2005). SINHONIA in the Galactic Center: Young Stars and Infrared Flares in the Central Light-Month. Astrophys. J., 628, 246
13. Gillessen S, Eisenhauer F, Fritz T K, Bartko, H., Dodds-Eden, K., Pfuhl, O.,…& Genzel, R.. (2009). The Orbit of the Star S2 around SgrA* from Very Large Telescope and Keck Data. Astrophys. J. Lett., 707, 114
14. Gillessen, S., Eisenhauer. F,, Trippe, S., Alexander, T., Genzel, R., Martins, F., & Otto, T. (2009) Monitoring Stellar Orbits around the Massive Black Hole in the Galactic Center. Astrophys. J., 692,1075
15. Gillessen1, S., Plewa1, P. M., Eisenhauer, F., Sari, R., Waisberg, I., Habibi, M., & Genzel1, R. (2017) .An update on monitoring stellar orbits in the Galactic center, Astrophys. J., 837,30
16. Oya, H.(2019) Detection of Decameter Radio Wave Pulses from the Center Part of Our Galaxy Suggesting Sources at Rotating Super Massive Black Hole Binary, TERRAPUB, e-Lab, http://hdl.handle.net/10097/00126480
17. Oya, H.(2022). Interpretation of time-varying radio emissions of Sgr□* observed by 1.3 millimeter wavelength VLBI with black hole binary concluded by decameter radio wave pulse observations, Eart & Envi Scie Res & Rev. 5(4): 185-216.
18. Fish,V.,L.,Doeleman,S.,Beaudoin,C.,Blundell,R.,Bolin,D.E.,Bower,G.C., …& Friberg,P. (2011). The 1.3 mm Wavelength

VLBI of Sagittarius A*:Detection of Time-Variable Emission on Event Horizon Scales, Astrophys. Journ. Lett., 727 ,L36
19. Mehta, A., Buonanno, A., Gair, J., Miller, C., Deboer, R.,Wiescher, M.,…& Farag, E. (2021). Measurement of Intermediate Mass Black Hole Binaries Including the Mass Gap in the Upcoming LIGO-Virgo Observations. arXiv:2105.06366v1[gr-qc]
20. Arzoumanian, Z., Brazier, A., Burke-Spolaor, S., Chamberlin, S. J.,Chatterjee, S., Cordes, J. …& Zhu,W. W.. (2014). Gravitational Waves from Individual Supermassive Black Hole Binaries in Circular Orbits: Limits from the North American Nanohertz Observatory for Gravitational Waves. Astrophys. J. 794 ,141
21. Akiyama, K.; Alberdi, A., Alef,W., Algaba, J.C., Anantua, R.,Asada, K., … & Zebaros, M.(2022). First Sagittarius A* Event Horizon Telescope Results. I. The Shadow of the Supermassive Black Hole in the Center of the Milky Way, Astrophys. J. Lett, 930; L12
22. Akiyama, K.; Alberdi, A., Alef,W., Algaba, J.C., Anantua, R.,Asada, K., … & Wouterloot, J.G.A. (2022). First Sagittarius A* Event Horizon Telescope Results. II. EHT and Multiwavelength Observations, Data Processing, and Calibration, Astrophys. J. Lett. 930; L13
23. Akiyama, K.; Alberdi, A., Alef,W., Algaba, J.C., Anantua, R.,Asada, K., … & Zhao, S.-S. (2022). First Sagittarius A* Event Horizon Telescope Results. III. Imaging of the Galactic Center Supermassive Black Hole, Astrophys. J. Lett. (2022). 930; L14
24. Akiyama, K.; Alberdi, A., Alef,W., Algaba, J.C., Anantua, R.,Asada, K., … & Chang, D. O. (2022). First Sagittarius A* Event Horizon Telescope Results. IV. Variability, Morphology, and Black Hole Mass, Astrophys. J. Lett. 930; L15
25. Akiyama, K.; Alberdi, A., Alef,W., Algaba, J.C., Anantua, R.,Asada, K., … & White,C. (2022). First Sagittarius A* Event Horizon Telescope Results. V. Testing Astrophysical Models of the Galactic Center Black Hole, Astrophys. J. Lett., 930; L16
26. Akiyama, K.; Alberdi, A., Alef,W., Algaba, J.C., Anantua, R.,Asada, K., … & Zhao, S.-S. (2022).First Sagittarius A* Event Horizon Telescope Results. VI. Testing the Black Hole Metric, Astrophys. J. Lett., 930; L17,
27. Miyoshi, M. Kato, Y.. & Makino, J. (2022). The Jet and Resolved Features of the Central Supermassive Black Hole of M87 Observed with the Event Horizon Telescope (EHT) Astrophys. J., 933,36
28. Akiyama,K., Alberdi, A. Alef,W., Asada, K., Azulay,R , Baczko,A.-K.,...& Ziurys, L. (2019). First M87 Event Horizon Telescope Results. I: The Shadow of the Supermassive Black Hole, Astrophys. J. Lett., 875,L1
29. Akiyama,K., Alberdi, A. Alef,W., Asada, K., Azulay,R , Baczko,A.-K.,...& Ziurys, L. (2019). First M87 Event Horizon Telescope Results. II: Array and Instrumentation, Astrophys. J. Lett., 875,L2
30. Akiyama,K., Alberdi, A. Alef,W., Asada, K., Azulay,R , Baczko,A.-K.,…. & Yamaguti, P. (2019). First M87 Event Horizon Telescope Results. III. Data Processing and Calibration, Astrophys. J. Lett., 875, L3
31. Akiyama,K., Alberdi, A. Alef,W., Asada, K., Azulay,R , Baczko,A.-K.,…. & Yamaguti, P. (2019).First M87 Event Horizon Telescope Results. IV.:,Imaging the Central Supermassive Black Hole, Astrophys. J. Lett.875:L4
32. Akiyama,K., Alberdi, A. Alef,W., Asada, K., Azulay,R , Baczko,A.-K.,…& Zhang, S. (2019). First M87 Event Horizon Telescope Results. V.: Physical Origin of the Asymmetric Ring , Astrophys J. Lett., 875,L5
33. Akiyama,K., Alberdi, A. Alef,W., Asada, K., Azulay,R , Baczko,A.-K.,…. & Yamaguti, P. (2019).First M87 Event Horizon Telescope Results. VI.;The Shadow and Mass of the Central Black Hole., Astrophys. J. Lett., 875:,L6-ab1141
34. Fish,V,L.,Johnson,M.D.,Doeleman1,S.S., Broderick,A,E., Psaltis, D., Lu.R.-S., …& Ziurys,L.M.(2016). Persistent asymmetric structure of Sagittarius A* on event horizon scales, Astrophys, J., 820,90
35. McInnes, B. & Ong, Y. C., (2015). A Note on Physical Mass and the Thermodynamics of AdS-Kerr Black Holes, arXiv:1506.01248v2[gr-qc] 8.
36. Chew, X. Y. & Ong, Y. C.(2020). Interior Volume of Kerr-AdS Black Holes. Phys. Rev. D101, 104026
37. Pandya, A. & Pretorius, F. (2020). The Rotating Black Hole Iinterior: Insights from gravitational collapse in AdS3 spacetime. Phys. Rev. D 101, 104026
38. Einstein A (1922) The Meaning of Relativity, Lecture Note , Princeton University Press.
39. Kokkotas, K. D. & Schmidt, B. G. (1999). Quasi-Normal Modes of Stars and Black Holes , Living Reviews in Relativity volume 2, Article number: 2
40. Emanuele ,B., Cardoso,V., Starlinets,O .(2009). Qusinormal Modes of Black Holes and Black Branes., Class. Quantum. Grav.. 26, 163001
41. Epstein, R . & Wagoner, R.. V. (1975). Post-Newtonian Generation of Gravitational Waves., Astrophys. J., 197, 717
42. Blanchet, L. (1996). Energy Losses by Gravitational Radiation in Inspiraling Compact Binaries to 5/2 Post-Newtonian Order. Phys. Rev. D 54, 1417
43. Thorne, K. S. & Campolattaro, A. (1967). Non-Radial Pulsation of General-Relativistic Stellar Models. I. Analytic Analysis for L >= 2., Astrophys.J., 149 ,591.
44. Kerr, R. P. (1963). Gravitational Field of a Spinning Mass as an Example of Algebraically Special Metrics., Phys. Rev. Lett. 11, 237
45. Landau.L.D. and Lifshitz, E.M.(1967). Classical Theory of Fields (Third revised English Edition),Pergamon Press, Oxford, New York, P 325 .

Appendix A

We start with Eq. (2.16) in the main text by changing tensor index from (μ,ν) to (*α,β*) as:

$$\eta_{\alpha\beta} + \gamma_{\alpha\beta} = {}^{(M)}g_{ij}\,\frac{\partial x^{(M)i}}{\partial x^{\alpha}}\cdot\frac{\partial x^{(M)j}}{\partial x^{\beta}}\,. \qquad (A1)$$

This relation can be inversely transformed as:

$$g_{ij}^{(M)} = \left(\eta_{\alpha\beta} + \gamma_{\alpha\beta}\right)\frac{\partial x^{\alpha}}{\partial x^{(M)i}}\cdot\frac{\partial x^{\beta}}{\partial x^{(M)j}}. \qquad (A2)$$

Four-dimensional time derivatives of the metrics of the above equation are expressed as:

$$\frac{dg_{ij}^{(M)}}{ds} = \frac{dg_{\mu\nu}^{QM}}{ds}\left(\frac{\partial x^{\alpha}}{\partial x^{(M)i}}\cdot\frac{\partial x^{\beta}}{\partial x^{(M)j}}\right) + g_{\mu\nu}^{QM}\frac{d}{ds}\left[\frac{\partial x^{\alpha}}{\partial x^{(M)i}}\cdot\frac{\partial x^{\beta}}{\partial x^{(M)j}}\right], \qquad (A3)$$

where $g_{\mu\nu}^{QM} = \eta_{\mu\nu} + \gamma_{\mu\nu}$.

Because the metrics are time-stationary, Eq. (A3) can be rewritten as:

$$\frac{d}{ds}\left[\frac{\partial x^{\alpha}}{\partial x^{(M)i}}\cdot\frac{\partial x^{\beta}}{\partial x^{(M)j}}\right] = 0\,\cdot \qquad (A4)$$

Then, the term in the bracket in Eq. (A4) is expressed by:

$$\frac{\partial x^{\alpha}}{\partial x^{(M)i}}\cdot\frac{\partial x^{\beta}}{\partial x^{(M)j}} = K_{ij}^{\alpha\beta} \qquad (A5)$$

where $K_{ij}^{\alpha\beta}$ is a function independent of s for all combinations of (α,*i*) and (*β,j*) Then, we find logically that $\partial x^{\alpha}/\partial x^{(B)i}$ and $\partial x^{\beta}/\partial x^{(B)j}$ are functions independent of s.Thus,

$$\frac{d}{ds}\left(\frac{\partial x^{\alpha}}{\partial x^{(M)i}}\right) = 0. \quad \ldots\ldots\ldots\ldots\ldots\ldots\ldots\ldots\ldots\ldots\ldots\ldots\ldots\ldots (A6)$$

This is given in Eq. (2.20) of the main text.

Appendix B

Following Eq. (2.28) in the main text, which is repeated here as:

$$T_{jk}^{*} = T_{jk} - \frac{1}{2}\eta_{jk}T\,, \qquad (B1)$$

we calculate T_{jk}^{*}, starting with T_{jk}, as given from Eqs. (2.41)–(2.47) in the main text. The scalar T in Eq. (B1) is given as:

$$T = \eta^{00}T_{00} + \eta^{11}T_{11} + \eta^{22}T_{22} + \eta^{33}T_{33}\,. \quad \ldots\ldots\ldots\ldots\ldots\ldots (B2)$$

It follows that:

$$T = -\left(\rho\gamma_{\varphi}^{*2} - A_f\right) + \frac{\lambda}{\kappa}\rho\delta(\mathbf{r}-\mathbf{r}_s)\gamma_{\varphi}^{*2}\cdot\frac{v_{\varphi}^2}{c^2} \ldots\ldots\ldots\ldots\ldots\ldots\ldots\ldots (B3)$$

where

$$A_f = \frac{\lambda}{\kappa c^2}(1-\zeta)\left(\frac{\rho\delta(\mathbf{r}-\mathbf{r}_s)\gamma_{th}^{*2}v_{th}^2}{2} + \frac{B_T^2}{2\mu_0}\right). \quad \ldots\ldots\ldots\ldots\ldots\ldots\ldots (B4)$$

Inserting T in Eq. (B1), we have T_{jk}^{*} as follows:

$$T_{00}^{*} = \rho\gamma_{\varphi}^{*2} - A_f + \frac{1}{2}\left[-\left(\rho\gamma_{\varphi}^{*2} - A_f\right) + \frac{\lambda}{\kappa}\rho\delta(\mathbf{r}-\mathbf{r}_s)\gamma_{\varphi}^{*2}\cdot\frac{v_{\varphi}^2}{c^2}\right]$$

$$= \frac{1}{2}\left[\left(\rho\gamma_{\varphi}^{*2} - A_f\right) + \frac{\lambda}{\kappa}\rho\delta(\mathbf{r}-\mathbf{r}_s)\gamma_{\varphi}^{*2}\cdot\frac{v_{\varphi}^2}{c^2}\right]. \quad (B5)$$

$$T_{11}^{*} = \frac{\lambda}{\kappa}\rho\delta(\mathbf{r}-\mathbf{r}_s)\gamma_{\varphi}^{*2}\cdot\frac{v_{\varphi}^2}{c^2}\cdot\sin^2\varphi - \frac{1}{2}\left[-\left(\rho\gamma_{\varphi}^{*2} - A_f\right) + \frac{\lambda}{\kappa}\rho\delta(\mathbf{r}-\mathbf{r}_s)\gamma_{\varphi}^{*2}\cdot\frac{v_{\varphi}^2}{c^2}\right]$$

$$= \frac{1}{2}\left[\left(\rho\gamma_{\varphi}^{*2} - A_f\right) - \frac{\lambda}{\kappa}\rho\delta(\mathbf{r}-\mathbf{r}_s)\gamma_{\varphi}^{*2}\cdot\frac{v_{\varphi}^2}{c^2}\cos2\varphi\right], \quad \ldots\ldots (B6)$$

$$T_{22}^{*} = \frac{\lambda}{\kappa}\rho\delta(\mathbf{r}-\mathbf{r}_s)\gamma_{\varphi}^{*2}\cdot\frac{v_{\varphi}^2}{c^2}\cdot\cos^2\varphi - \frac{1}{2}\left[-\left(\rho\gamma_{\varphi}^{*2} - A_f\right) + \frac{\lambda}{\kappa}\rho\delta(\mathbf{r}-\mathbf{r}_s)\gamma_{\varphi}^{*2}\cdot\frac{v_{\varphi}^2}{c^2}\right]$$

$$= \frac{1}{2}\left[\left(\rho\gamma_{\varphi}^{*2} - A_f\right) + \frac{\lambda}{\kappa}\rho\delta(\mathbf{r}-\mathbf{r}_s)\gamma_{\varphi}^{*2}\cdot\frac{v_{\varphi}^2}{c^2}\cos2\varphi\right], \quad \ldots\ldots (B7)$$

and

$$T_{33}^{*} = \frac{1}{2}\left[\left(\rho\gamma_{\varphi}^{*2} - A_f\right) - \frac{\lambda}{\kappa}\rho\delta(\mathbf{r}-\mathbf{r}_s)\gamma_{\varphi}^{*2}\cdot\frac{v_{\varphi}^2}{c^2}\right]. \quad \ldots\ldots\ldots\ldots\ldots\ldots\ldots (B8)..$$

Because $\eta^{12}=\eta^{21}=0$, it follows from Eq. (2.45) in the main text that:

$$T_{12}^{*} = T_{21}^{*} = -\frac{1}{2}\cdot\frac{\lambda}{\kappa}\rho\delta(\mathbf{r}-\mathbf{r}_s)\gamma_{\varphi}^{*2}\cdot\frac{v_{\varphi}^2}{c^2}\cdot\sin2\varphi\,. \quad \ldots\ldots\ldots\ldots\ldots\ldots\ldots (B9)$$

Appendix C

When we set $y_s = y_{ob}$ and $z_s = z_{ob}$, the integrations of the second and third terms on the right-hand side of Eq. (2.57) in the main text can be rewritten by introducing $\gamma_{ii}(\mathbf{r}_{ob})_{2\&3}$ as:

$$\gamma_{ii}(\mathbf{r}_{ob})_{2\&3}$$

$$= \frac{\lambda}{4\pi}\int_{-x_{se}}^{x_{se}} \frac{\rho\delta(x_{ob}-x_s)\left\|\left[\pm\zeta\cdot\gamma_{\varphi}^{*}\cdot\frac{v_{\varphi}^2}{c^2} + (1-\zeta)\frac{\gamma_{th}^{*2}}{\gamma_{\varphi}^{*}}\frac{v_{th}^2}{2c^2}\right] + \frac{B^2}{2\mu_0\rho}\right|_{y_s=y_{ob}\,;\,z_s=z_{ob}}}{(x_{ob}-x_s)}dx_s\,, \quad (C1)$$

where $-x_{se}$ and x_{se} are the limits of the source region for the coordinate x_s. Therefore, we can define the existence of matter with density ρ confined within the source region as:

$$\rho\,\delta\,(x_{ob}-x_s)\left|\left[\pm\zeta\cdot\gamma_{\varphi}^{*}\cdot\frac{v_{\varphi}^{2}}{c^{2}}+(1-\zeta)\frac{\gamma_{th}^{*2}}{\gamma_{\varphi}^{*}}\frac{v_{th}^{2}}{2c^{2}}\right]+\frac{B^{2}}{2\mu_{0}\rho}\right|_{\text{out side of Source}}$$

$$=0. \quad \ldots\ldots\ldots\ldots\ldots\ldots (C2)$$

We can further rewrite Eq. (C1) as:

$$\gamma_{ii}(r_{ob})_{2\&3}$$

$$=\frac{\lambda}{4\pi}\int_{-\infty}^{\infty}\frac{\rho\delta(x_{ob}-x_s)\left|\left[\pm\zeta\cdot\gamma_{\varphi}^{*}\cdot\frac{v_{\varphi}^{2}}{c^{2}}+(1-\zeta)\frac{\gamma_{th}^{*2}}{\gamma_{\varphi}^{*}}\frac{v_{th}^{2}}{2c^{2}}\right]+\frac{B^{2}}{2\mu_{0}\rho}\right|_{y_s=y_{ob}\,;\,z_s=z_{ob}}}{(x_{ob}-x_s)}dx_s\,. \quad (C3)$$

By applying the residue theorem to the integration of Eq. (C3), which can be considered as a loop integral with Eq. (C2), we have:

$$\gamma_{ii}(r_{ob})_{2\&3}=\underline{i}\frac{\lambda}{4}\rho\left|\left[\pm\zeta\cdot\gamma_{\varphi}^{*}\cdot\frac{v_{\varphi}^{2}}{c^{2}}+(1-\zeta)\frac{\gamma_{th}^{*2}}{\gamma_{\varphi}^{*}}\frac{v_{th}^{2}}{2c^{2}}\right]+\frac{B^{2}}{2\mu_{0}\rho}\right|_{x_s=x_{ob}\,;y_s=y_{ob}\,;\,z_s=z_{ob}}, \quad \ldots\ldots (C4)$$

where $\underline{i}$ is the imaginary unit. In the main text, Eq. (C4) is simply expressed as:

$$\gamma_{ii}(\mathbf{r}_{ob})_{2\&3}=\underline{i}\frac{\lambda}{4}\rho\left[\left[\pm\zeta\cdot\gamma_{\varphi}^{*}\cdot\frac{v_{\varphi}^{2}}{c^{2}}+(1-\zeta)\frac{\gamma_{th}^{*2}}{\gamma_{\varphi}^{*}}\frac{v_{th}^{2}}{2c^{2}}\right]+\frac{B^{2}}{2\mu_{0}\rho}\right]. \quad (C5)$$

Appendix D

The right-hand side of Eq. (3.9) in the main text can be rewritten when we Please compare with eq.(C4) which is in a same current. i to α

$$-\frac{\underline{i}}{4}\rho^{2}\lambda\cdot\zeta\gamma_{\varphi}^{*2}\sum_{k=1}^{3}\left(\frac{\partial v^{\alpha}}{\partial x^{k}}-\frac{\partial v^{k}}{\partial x^{\alpha}}\right)v^{k}$$

$$=-\frac{\underline{i}}{4}\rho^{2}\lambda$$

$$\cdot\zeta\gamma_{\varphi}^{*2}\left[\left(\frac{\partial v^{\alpha}}{\partial x}-\frac{\partial v_x}{\partial x^{\alpha}}\right)v_x+\left(\frac{\partial v^{\alpha}}{\partial y}-\frac{\partial v_y}{\partial x^{\alpha}}\right)v_y+\left(\frac{\partial v^{\alpha}}{\partial z}-\frac{\partial v_z}{\partial x^{\alpha}}\right)v_z\right], \quad .(D1).$$

where arguments are rewritten as $x^1=x$, $x^2=y$, $x^3=z$, $v^1=v_x$,$v^2=v_y$,and $v^3=v_z$.

Starting from Eq. (D1), we can raise the regular vector form by introducing the unit vectors $\hat{x}$,$\hat{y}$, and $\hat{z}$ directed in the x, y, and z axes, respectively; specifically, we form a vector, -($\underline{i}/4$) $\rho^2\,\lambda\cdot\zeta\gamma_{\varphi}^{*2}$ **V** that is equivalent to the right-hand side of Eq. (D1), as follows:

$$\mathbf{V}=\left[\left(\frac{\partial v_x}{\partial x}-\frac{\partial v_x}{\partial x}\right)v_x+\left(\frac{\partial v_x}{\partial y}-\frac{\partial v_y}{\partial x}\right)v_y+\left(\frac{\partial v_x}{\partial z}-\frac{\partial v_z}{\partial x}\right)v_z\right]\hat{x}$$

$$+\left[\left(\frac{\partial v_y}{\partial x}-\frac{\partial v_x}{\partial y}\right)v_x+\left(\frac{\partial v_y}{\partial y}-\frac{\partial v_y}{\partial y}\right)v_y+\left(\frac{\partial v_y}{\partial z}-\frac{\partial v_z}{\partial y}\right)v_z\right]\hat{y}\,.$$

$$+\left[\left(\frac{\partial v_z}{\partial x}-\frac{\partial v_x}{\partial z}\right)v_x+\left(\frac{\partial v_z}{\partial y}-\frac{\partial v_y}{\partial z}\right)v_y+\left(\frac{\partial v_z}{\partial z}-\frac{\partial v_z}{\partial z}\right)v_z\right]\hat{z}\,. \quad \text{(D2)}$$

This is further rewritten as:

$$\mathbf{V}=\left[\left(\frac{\partial v_x}{\partial z}-\frac{\partial v_z}{\partial x}\right)v_z-\left(\frac{\partial v_y}{\partial x}-\frac{\partial v_x}{\partial y}\right)v_y\right]\hat{x}+\left[\left(\frac{\partial v_y}{\partial x}-\frac{\partial v_x}{\partial y}\right)v_x-\left(\frac{\partial v_z}{\partial y}-\frac{\partial v_y}{\partial z}\right)v_z\right]\hat{y}$$

$$+\left[\left(\frac{\partial v_z}{\partial y}-\frac{\partial v_y}{\partial z}\right)v_y-\left(\frac{\partial v_x}{\partial z}-\frac{\partial v_z}{\partial x}\right)v_x\right]\hat{z}\,. \quad \text{(D3)}$$

When we apply the basic relationship of vector analyses, it follows that:

$$\mathrm{rot}\mathbf{v}\times\mathbf{v}=\left[\left(\frac{\partial v_x}{\partial z}-\frac{\partial v_z}{\partial x}\right)v_z-\left(\frac{\partial v_y}{\partial x}-\frac{\partial v_x}{\partial y}\right)v_y\right]\hat{x}$$

$$+\left[\left(\frac{\partial v_y}{\partial x}-\frac{\partial v_x}{\partial y}\right)v_x-\left(\frac{\partial v_z}{\partial y}-\frac{\partial v_y}{\partial z}\right)v_z\right]\hat{y}$$

$$+\left[\left(\frac{\partial v_z}{\partial y}-\frac{\partial v_y}{\partial z}\right)v_y-\left(\frac{\partial v_x}{\partial z}-\frac{\partial v_z}{\partial x}\right)v_x\right]\hat{z}\,. \quad \text{(D4)}$$

We can confirm that Eq. (D1) is equivalent to $-(i/4)\,\rho^2\,\lambda\cdot\zeta\gamma_\varphi^{*2}\,\mathrm{rot}\mathbf{v}\times\mathbf{v}$, as described by Eq. (3.10) in the main text.

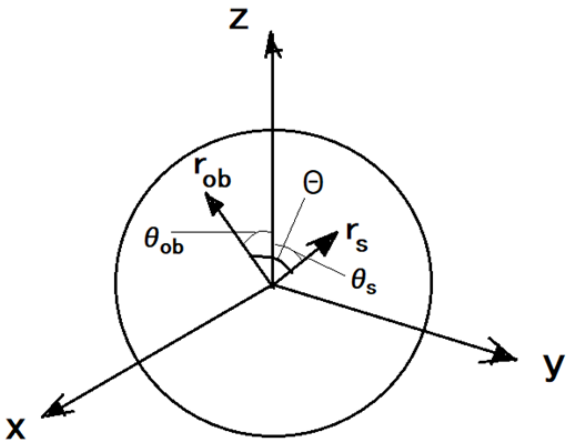

Figure E.
The configuration within an IMSBH describing the source point $\mathbf{r}_s$ and the observation point $\mathbf{r}_{ob}$ on the Cartesian coordinates (x,y,z). Angles between vectors $\hat{\mathbf{z}}$ and $\mathbf{r}_s$, $\hat{\mathbf{z}}$ and $\mathbf{r}_{ob}$, and $\mathbf{r}_{ob}$ and $\mathbf{r}_s$ are given by θ_s, θ_{ob}, and Θ, respectively, for the case where $\mathbf{r}_{ob}$ and $\mathbf{r}_s$ are expressed in spherical coordinates as $(\mathbf{r}_{ob}, \theta_{ob}, \varphi_{ob})$ and $(\mathbf{r}_s, \theta_s, \varphi_s)$, respectively.

Appendix E

Regarding Eq. (2.32) in the main text, the plasma of IMSBH rotates in all regions with constant velocity v_φ around a common axis with different angular velocity Ω as:

$$v_\varphi = r \cdot \sin\theta \cdot \Omega, \qquad \text{with } \Omega = \frac{d\varphi}{dt}. \tag{E1}$$

Associated with this toroidal flow of plasma, toroidal electric currents may easily be raised, as given by Eq. (3.26), which we repeat here as:

$$\mathbf{I} = \alpha_c(r) n N_i e \mathbf{v}, \tag{E2}$$

where α_c (r) expresses the rate of the velocity difference between ions and electrons; we assume that most ions are $Fe^{(n+)}$, with fairly large integer n, because of ionization under extremely high temperatures. We must then consider the electromagnetic Lorentz force $\mathbf{F}_{em}$ = **I**×**B** due to magnetic field **B** generated by the current given in Eq. (E2). Specifically, **B** (=rot**A**) can be found by introducing the vector potential, as:

$$\mathbf{A} = \frac{\mu_0}{4\pi} \int \frac{\mathbf{I}_s}{r_{os}} dV_s, \tag{E3}$$

where $\mathbf{r}_{os}$ is the same as the expression of Eq. (2.31) in the main text, and $\mathbf{I}_s$ is the current at position $\mathbf{r}_s$, where $x = x_s$, $y = y_s$,and $z = z_s$. When we set $\mathbf{r}_{ob}$ within the source region, we cannot avoid including $\mathbf{A}(\mathbf{r}_{ob})$, at $\mathbf{r}_{ob} = \mathbf{r}_s$, then the integration of Eq. (E3) was carried out by applying the expansion of $1/r_{os}$ into the series of polynomials containing Legendre functions. For this expansion purpose, we rewrite $1/r_{os}$, considering the relation of vectors $\mathbf{r}_{ob}$ and $\mathbf{r}_s$ given in Figure E, as follows:

$$\frac{1}{r_{os}} = \frac{1}{r_{ob}\sqrt{1 + \left(\frac{r_s}{r_{ob}}\right)^2 - 2\left(\frac{r_s}{r_{ob}}\right)\cos\Theta}} \quad \text{for } r_{ob} > r_s \tag{E4}$$

and

$$\frac{1}{r_{os}} = \frac{1}{r_s\sqrt{1 + \left(\frac{r_{ob}}{r_s}\right)^2 - 2\left(\frac{r_{ob}}{r_s}\right)\cos\Theta}} \quad \text{for } r_s > r_{ob}, \tag{E5}$$

where $r_{ob} = |\mathbf{r}_{ob}|$, $r_s = |\mathbf{r}_s|$, and

$$\cos\Theta = \cos(\theta_{ob} - \theta_s) \cdot \cos^2\left(\frac{\varphi_{ob} - \varphi_s}{2}\right) + \cos(\theta_{ob} + \theta_s) \cdot \sin^2\left(\frac{\varphi_{ob} - \varphi_s}{2}\right) \tag{E6}$$

For the expressions given by Eqs. (E4) and (E5), the polynomial expansion is established as an application of the Legendre function, P_n (x), of the n-th order by setting the argument x to be cosΘ, corresponding to Eqs. (E4) and (E5), respectively, as:

$$\frac{1}{r_{os}} = \sum_{n=0}^{\infty} \frac{r_s^n}{r_{ob}^{n+1}} P_n(\cos\Theta) \qquad \text{for } r_{ob} > r_s \tag{E7}$$

and

$$\frac{1}{r_{os}} = \sum_{n=0}^{\infty} \frac{r_{ob}^n}{r_s^{n+1}} P_n(\cos\Theta) \qquad \text{for } r_s > r_{ob}. \tag{E8}$$

Because current $\mathbf{I}_s$ is expressed assuming that the current intensity is proportional to the plasma number density and velocity difference factor, it follows that:

$$\mathbf{I}_s = \left(\frac{r_{Mc}}{r_s}\right)^{2+\delta} I_0 \hat{\boldsymbol{\varphi}}, \tag{E9}$$

using the unit vector in the azimuthal direction $\hat{\boldsymbol{\varphi}}$. Then, the vector potential given by Eq. (E3) is expressed by:

$$\begin{aligned} &A_\varphi(\mathbf{r}_{ob}) \\ &= \frac{\mu_0 I_0}{4\pi}\int_0^{\pi}\sin\theta_s d\theta_s \int_0^{2\pi} d\varphi_s \left[\int_0^{r_{ob}} r_s^2 dr_s \cdot \left(\frac{r_{Mc}}{r_s}\right)^{2+\delta}\sum_{n=0}^{\infty}\frac{r_s^n}{r_{ob}^{n+1}}P_n(\cos\Theta)\right. \\ &\left. + \int_{r_{ob}}^{r_{Mc}} r_s^2 dr_s \cdot \left(\frac{r_{Mc}}{r_s}\right)^{2+\delta}\sum_{n=0}^{\infty}\frac{r_{ob}^n}{r_s^{n+1}}P_n(\cos\Theta)\right]. \end{aligned} \tag{E10}$$

Because the dependence of $P_n(\cos\Theta)$ on the arguments θ_s and φ_s is complicated, as expressed by Eq. (E6), we applied numerical integration for integration by $d\theta_s$ and $d\varphi_s$ after finding the analytic formulae for integration by dr_s for Eq. (E10). Then, we arrive at the equations for A_φ/r,$(\partial A_\varphi)/(\partial r)$, and $(\partial A_\varphi)/(r\partial\theta)$, which become elements to calculate $\mathbf{B}=\mathrm{rot}\mathbf{A}$; i.e., by rewriting r_{ob} and θ_{ob} as r and θ, respectively, it follows that:

$$\begin{aligned} \frac{A_\varphi}{r} &= \frac{\mu_0 I_0 r_{Mc}}{4\pi}\left(\frac{r_{Mc}}{r}\right)\int_0^{\pi}\int_0^{2\pi}\left\{\sum_{n=0}^{6}\left[\frac{2n+1}{(n+\delta)(n+1-\delta)}\left(\frac{r_{Mc}}{r}\right)^{\delta}\right.\right. \\ &\left.\left. - \frac{1}{n+\delta}\left(\frac{r}{r_{Mc}}\right)^{n}\right]P_n(\cos\Theta)\right\}\sin\theta_s d\theta_s d\varphi_s, \end{aligned} \tag{E11}$$

$$\begin{aligned} \frac{\partial A_\varphi}{\partial r} &= \frac{\mu_0 I_0 r_{Mc}}{4\pi}\int_0^{\pi}\int_0^{2\pi}\left\{\sum_{n=0}^{6}\left[\frac{-(2n+1)\delta}{(n+\alpha)(n+1-\alpha)}\left(\frac{r_{Mc}}{r}\right)^{1+\delta}\right.\right. \\ &\left.\left. - \frac{n}{n+\delta}\left(\frac{r}{r_{Mc}}\right)^{n-1}\right]\cdot P_n(\cos\Theta)\right\}\sin\theta_s d\theta_s d\varphi_s, \end{aligned} \tag{E12}$$

$$\begin{aligned} \frac{\partial A_\varphi}{r\,\partial\theta} &= \frac{\mu_0 I_0 r_{Mc}}{4\pi}\left(\frac{r_{Mc}}{r}\right)\int_0^{\pi}\int_0^{2\pi}\left\{\sum_{n=0}^{6}\left[\frac{2n+1}{(n+\delta)(n+1-\delta)}\left(\frac{r_{Mc}}{r}\right)^{\delta}\right.\right. \\ &\left.\left. - \frac{1}{n+\delta}\left(\frac{r}{r_{Mc}}\right)^{n}\right]\frac{\partial P_n(x)}{\partial x}\right\}\frac{d(\cos\Theta)}{d\theta}\sin\theta_s d\theta_s d\varphi_s, \end{aligned} \tag{E13}$$

where

$$\frac{d(\cos\Theta)}{d\theta} = -\sin\theta\cos\theta_s + \cos\theta\sin\theta_s \cdot \cos(\varphi - \varphi_s). \qquad (E14)$$

In Eqs. (E11)–(E13), the expansions of the Legendre function P_n (cosΘ) are approximated by stopping the expansion at n = 6, and differentiation $(\partial P_n(x))/\partial x$ was directly performed to the expanded polynomial $P_n(x)$ of the Legendre function.

By the numerical integration of $d\theta_s$ and $d\varphi_s$ with respect to Eqs. (E11)–(E13), we have the results of the generated magnetic field in spherical coordinates as:

$$B_r = (\mathrm{rot}\mathbf{A})_r = \frac{\cos\theta}{\sin\theta}\frac{A_\varphi}{r} + \frac{\partial A_\varphi}{r\,\partial\theta} \qquad (E15)$$

and

$$B_\theta = (\mathrm{rot}\mathbf{A})_\theta = -\frac{A_\varphi}{r} - \frac{\partial A_\varphi}{\partial r}. \qquad (E16)$$

The numerical results of B_r and B_θ are given in Figure 3 for δ=0 in the main text, where quantities are normalized by $\mu_0 I_0 r_{Mc}$, with the unit $4\pi\times10^{-7}$ Wb/m^2 for the current density I_0 (A/m^2) and core radius r_{Mc} (m) of the IMSBH.
The Lorenz force caused by the toroidal currents and generated magnetic fields is:

$$\mathbf{I}\times\mathbf{B} = I_\varphi\left(\frac{A_\varphi}{r} + \frac{\partial A_\varphi}{\partial r}\right)\hat{\mathbf{r}} + I_\varphi\left(\frac{\cos\theta}{\sin\theta}\cdot\frac{A_\varphi}{r} + \frac{\partial A_\varphi}{r\,\partial\theta}\right)\hat{\boldsymbol{\theta}} \qquad (E17)$$

where $\hat{\mathbf{r}}$ and $\hat{\boldsymbol{\theta}}$ are the unit vector in the radial and polar angle directions, respectively.
In the main text, normalized A_φ is expressed by defining A_φ^* as:

$$A_\varphi = I_0 A_\varphi^*. \qquad (E18)$$

Appendix F

Regarding Eqs. (3.37) and (3.38) in the main text, we are concerned here with the θ dependence of the Lorentz force terms F_{Lr} and $F_{L\theta}$ expressed, respectively, by:

$$F_{Lr} = \eta(r)\frac{r}{r_{Mc}}\left(\frac{A_\varphi^*}{r} + \frac{\partial A_\varphi^*}{\partial r}\right) \qquad (F1)$$

and

$$F_{L\theta} = \eta(r)\frac{r}{r_{Mc}}\left(\frac{A_\varphi^*}{r}\frac{\cos\theta}{\sin\theta} + \frac{\partial A_\varphi^*}{r\,\partial\theta}\right). \qquad (F2)$$

To obtain a simple model of the force balance in the IMSBH, the point of interest is focused how the θ dependence of F_{Lr} and $F_{L\theta}$ becomes close to that of mechanical forces of rotating plasma, which is expressed by a constant for F_{Lr} and cosθ/sinθ for $F_{L\theta}$. Then, we calculate F_{Lr} and $F_{L\theta}$ with $\alpha_c(r) = \alpha_0 (r_{Mc}/r)^\delta$ for ten cases of δ in the range of 0≤δ<1, together with A_φ^* and the related terms given in Eqs. (F1) and (F2) (see Appendix E). In these cases, η(r) is expressed as:

$$\eta(r) = \eta_0\left(\frac{r_{Mc}}{r}\right)^\delta. \qquad (F3)$$

In Figure F, the calculation results of F_{Lr} and $F_{L\theta}$ are presented for three example cases of δ=0~0.2. Among these results, we selected the case of δ=0 with a standpoint to evaluate the range of divergence versus r/r_{Mc}. As given in the panels of δ=0, the estimated approximation functions that represent the F_{Lr} and $F_{L\theta}$ functions are:

$$F_{Lr} = 0\,, \qquad \text{(F4)}$$

and

$$F_{L\theta} = \begin{cases} 1.3\dfrac{\cos\theta}{\sin\theta}, & \dfrac{\pi}{6} \le \theta \le \dfrac{5\pi}{6} \\ 0.5\dfrac{\cos\theta}{\sin\theta}, & 0 \le \theta \le \dfrac{\pi}{6} \text{ and } \dfrac{5\pi}{6} \le \theta \le \pi\,. \end{cases} \qquad \text{(F5)}$$

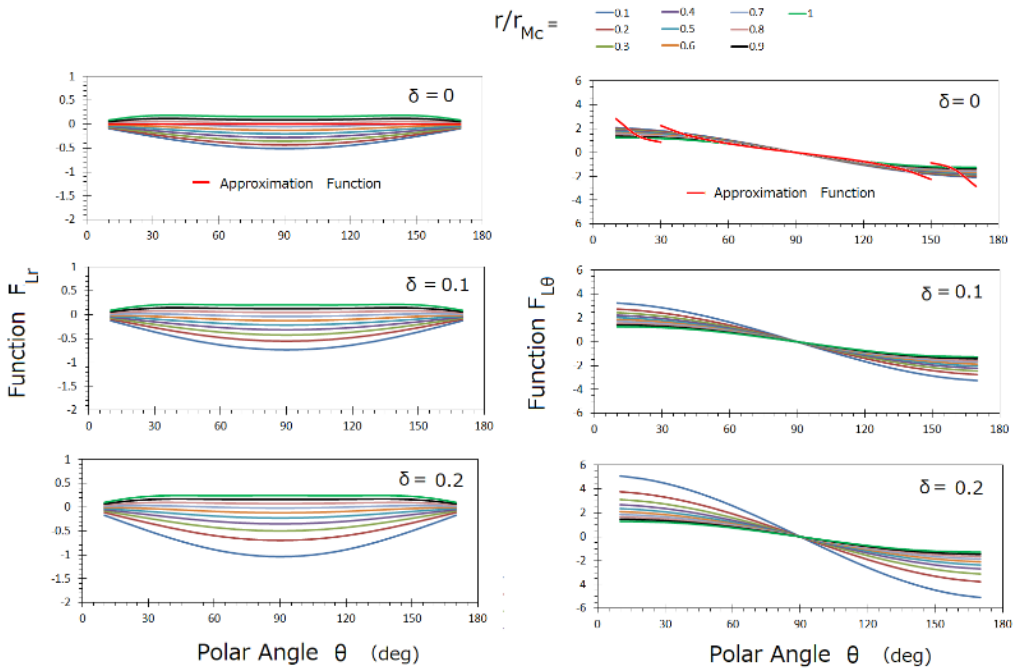

Figure F: Calculation results of functions F_{Lr} and $F_{L\theta}$ versus polar angle θ with radial position r/r_{Mc} as a parameter. Results are shown for three cases of δ from 0 to 0.2, as given in the corresponding panel. The case of δ=0 is selected as the suitable case containing an approximation function of the θ dependence, which is close to that of the mechanical terms in the force balance equations. In these selected cases, the approximation functions are shown in the corresponding panels by pure red curves

Appendix G

Starting with Eq. (5.1) in the main text, the Einstein tensor G_{jk} is realized with the Ricci tensor R_{jk} and scaler Ricci R, which are expressed by:

$$R_{jk} = \frac{1}{2}\left(-\Box h_{jk} + \eta^{nm}\frac{\partial^2 h_{km}}{\partial x^n\,\partial x^j} + \eta^{nm}\frac{\partial^2 h_{jm}}{\partial x^n\,\partial x^k} - \frac{\partial^2 h}{\partial x^j\,\partial x^k}\right) \qquad \text{(G1)}$$

and

$$R = \eta^{jk}R_{jk} = \frac{1}{2}\left(-2\Box h + 2\eta^{jj}\eta^{mm}\frac{\partial^2 h_{jm}}{\partial x^m\,\partial x^j}\right). \qquad (G2)$$

When we introduce a new tensor φ_{jk}, as:

$$\varphi_{jk} = h_{jk} - \frac{1}{2}\eta_{jk}h, \qquad (G3)$$

then the Einstein tensor is expressed by:

$$G_{jk} = R_{jk} - \frac{1}{2}\eta_{jk}R = \frac{1}{2}\left(-\Box\varphi_{jk} + \eta^{mm}\frac{\partial^2\varphi_{km}}{\partial x^j\,\partial x^m} + \eta^{mm}\frac{\partial^2\varphi_{jm}}{\partial x^k\,\partial x^m} + \eta_{jk}\frac{\partial^2\varphi^{jm}}{\partial x^j\,\partial x^m}\right). \qquad (G4)$$

At this stage, we apply gauge selection following the orthodox method of the reduction of GWs. When we follow the Lorentz gauge, which allows

$$\frac{\partial\varphi_{km}}{\partial x^m} = 0, \qquad (G5)$$

it is easily concluded that:

$$\eta^{mm}\frac{\partial^2\varphi_{km}}{\partial x^j\,\partial x^m} = \eta^{mm}\frac{\partial}{\partial x^j}\left(\frac{\partial\varphi_{km}}{\partial x^m}\right) = 0,$$
$$\eta^{mm}\frac{\partial^2\varphi_{jm}}{\partial x^k\,\partial x^m} = \eta^{mm}\frac{\partial}{\partial x^k}\left(\frac{\partial\varphi_{jm}}{\partial x^m}\right) = 0,$$
$$\eta_{jk}\frac{\partial^2\varphi^{jm}}{\partial x^j\,\partial x^m} = \eta_{jk}\cdot\eta^{jj}\eta^{m\,m}\frac{\partial}{\partial x^j}\left(\frac{\partial\varphi_{jm}}{\partial x^m}\right) = 0. \qquad (G6)$$

It follows from Eq. (G4), referring to the Einstein equation of Eq. (2.2) in the main text, that:

$$\Box\varphi_{jk} = -\frac{16\pi G}{c^4}T_{jk}. \qquad (G7)$$

Appendix H

As given in the main text, we introduced a new coordinate system (x'^0, x'^1, x'^2, x'^3), with a small deviation ξ^μ such that:

$$x'^\mu = x^\mu + \xi^\mu. \qquad (H1)$$

By this transformation, the metric tensor $g_{\mu\nu}$ in the x^μ coordinate system changes to g_{ij}' in the x'^μ coordinate system as:

$$g'_{ij}dx'^i dx'^j = g'_{ij}\frac{\partial x'^i}{\partial x^\mu}\cdot\frac{\partial x'^j}{\partial x^\nu}dx^\mu dx^\nu = g_{\mu\nu}dx^\mu dx^\nu. \qquad (H2)$$

Then, $h_{\mu\nu}$, as given by Eq. (5.1) in the main text, is related to h_{ij}' in the transformed coordinates as:

$$\left(\eta'_{ij} + h'_{ij}\right)\frac{\partial x'^{i}}{\partial x^{\mu}} \cdot \frac{\partial x'^{j}}{\partial x^{\nu}} = \eta_{\mu\nu} + h_{\mu\nu} \,. \tag{H3}$$

For Eq. (H2), we have:

$$\frac{\partial x'^{i}}{\partial x^{\mu}} \cdot \frac{\partial x'^{j}}{\partial x^{\nu}} = \left(\delta^{i}_{\mu} + \frac{\partial \xi^{i}}{\partial x^{\mu}}\right)\left(\delta^{j}_{\nu} + \frac{\partial \xi^{j}}{\partial x^{\nu}}\right)$$

$$\approx \delta^{i}_{\mu}\delta^{j}_{\nu} + \delta^{i}_{\mu}\frac{\partial \xi^{j}}{\partial x^{\nu}} + \delta^{j}_{\nu}\frac{\partial \xi^{i}}{\partial x^{\mu}}. \tag{H4}$$

Because $\eta_{ij}' = \eta_{\mu\nu}$, it follows from Eqs. (H3) and (H4) that:

$$h'_{\mu\nu} = h_{\mu\nu} - \eta_{ij}\delta^{i}_{\mu}\frac{\partial \xi^{j}}{\partial x^{\nu}} - \eta_{ij}\delta^{j}_{\nu}\frac{\partial \xi^{i}}{\partial x^{\mu}} = h_{\mu\nu} - \frac{\partial \xi_{\mu}}{\partial x^{\nu}} - \frac{\partial \xi_{\nu}}{\partial x^{\mu}} \,. \tag{H5}$$

Then, the metric $\varphi'_{\mu\nu}$ is transformed as:

$$\varphi'_{\mu\nu} = h_{\mu\nu} - \eta_{ij}\delta^{i}_{\mu}\frac{\partial \xi^{j}}{\partial x^{\nu}} - \eta_{ij}\delta^{j}_{\nu}\frac{\partial \xi^{i}}{\partial x^{\mu}} - \frac{1}{2}\eta'_{\mu\nu}h' \,. \tag{H6}$$

Here, h' is given by:

$$h' = \eta^{\mu\nu}\left(h_{\mu\nu} - \frac{\partial \xi_{\mu}}{\partial x^{\nu}} - \frac{\partial \xi_{\nu}}{\partial x^{\mu}}\right) = h - 2\frac{\partial \xi^{\mu}}{\partial x^{\mu}} \,. \tag{H7}$$

Thus:

$$\varphi'_{\mu\nu} = \varphi_{\mu\nu} - \frac{\partial \xi_{\mu}}{\partial x^{\nu}} - \frac{\partial \xi_{\nu}}{\partial x^{\mu}} + \eta_{\mu\nu}\frac{\partial \xi^{\mu}}{\partial x^{\mu}} \,. \tag{H8}$$

Calculating $\partial\varphi'_{\mu\nu}/\partial x'^{\nu}$ for $\varphi'_{\mu\nu}$ given by Eq. (H6):

$$\frac{\partial \varphi'_{\mu\nu}}{\partial x'^{\nu}} = \frac{\partial \varphi'_{\mu\nu}}{\partial x^{\nu}}\left(\frac{\partial x^{\nu}}{\partial x'^{\nu}}\right) = \frac{\partial \varphi_{\mu\nu}}{\partial x^{\nu}} - \eta_{\mu\nu}\frac{\partial^{2}\xi^{\nu}}{\partial x^{\nu}\,\partial x^{\nu}} - \eta_{\mu\nu}\frac{\partial^{2}\xi^{\mu}}{\partial x^{\nu}\,\partial x^{\mu}} + \eta_{\mu\nu}\frac{\partial^{2}\xi^{\mu}}{\partial x^{\nu}\,\partial x^{\mu}} \,. \tag{H9}$$

More specifically, because $\eta_{\mu\nu} = \eta_{\mu\mu} = \eta_{\nu\nu}$ for nonzero terms, Eq. (H9) is equivalent to:

$$\frac{\partial \varphi'_{\mu\nu}}{\partial x'^{\nu}} = \frac{\partial \varphi_{\mu\nu}}{\partial x^{\nu}} - \Box\xi^{\mu} \,. \tag{H10}$$

For the selection of the Lorentz gauge $\partial\varphi_{\mu\nu}'/\partial x'^{\nu} = 0$ and $\partial\varphi_{\mu\nu}/\partial x^{\nu} = 0$, it is required that:

$$\Box\xi^{\mu} = 0 \,. \tag{H11}$$

To clarify the TT gauge expression for the GW, following the standard processes, we express $\varphi_{\mu\nu}'$, $\varphi_{\mu\nu}$, and ξ^{μ} as propagation functions, as follows:

$$\varphi'_{\mu\nu} = A'_{\mu\nu}\exp\left(\underline{i}k_m x^m\right), \qquad \text{(H12a)}$$

$$\varphi_{\mu\nu} = A_{\mu\nu}\exp\left(\underline{i}k_m x^m\right), \qquad \text{(H12b)}$$

$$\xi^{\mu} = B^{\mu}\exp\left(\underline{i}k_m x^m\right), \qquad \text{(H12c)}$$

where $\underline{i}$ is the imaginary unit, and k_m is a four-dimensional wavenumber of the harmonic waves. In Eq. (H11), $A_{\mu\nu}$',$A_{\mu\nu}$, and B^{μ} are amplitudes of the corresponding harmonic wave expressions. Corresponding to Eq. (H8), therefore, we have:

$$A'_{\mu\nu} = A_{\mu\nu} - \underline{i}\left(\eta_{\mu\mu}k_\nu B^{\mu} + \eta_{\nu\nu}k_\mu B^{\nu} - \eta_{\mu\nu}k_\mu B^{\mu}\right). \qquad \text{(H13)}$$

From this relationship, we can find constraints for $A_{\mu\nu}$' and $A_{\mu\nu}$ as $A_{0\nu}$'= 0 and $A_{o\nu}$ =0, respectively, for suitable values of B^{ν} as functions of B^0 that satisfy:

$$\eta_{00}k_\nu B^0 + \eta_{\nu\nu}k_0 B^{\nu} - \eta_{0\nu}k_0 B^0 = 0. \qquad \text{(H14)}$$

Further constraints to $A_{\mu\nu}$' and $A_{\mu\nu}$ can be found when we investigate the Lorentz gauge given by $\partial\varphi_{\mu\nu}'/\partial x'^{\nu}$)=0 and $\partial\varphi_{\mu\nu}/\partial x^{\nu} = 0$, in terms of Eqs. (H12a) and (H12b), i.e.,

$$\underline{i}k_\nu A'_{\mu\nu} = \underline{i}k_\nu A_{\mu\nu} + k_\nu\left(\eta_{\mu\mu}k_\nu B^{\mu} + \eta_{\nu\nu}k_\mu B^{\nu} - \eta_{\mu\nu}k_\mu B^{\mu}\right) = 0. \qquad \text{(H15)}$$

Then, it is required that:

$$k_\nu A'_{\mu\nu} = k_\nu A_{\mu\nu} = 0. \qquad \text{(H16)}$$

The traces $\eta^{\mu\nu}\varphi_{\mu\nu}$' and $\eta^{\mu\nu}\varphi_{\mu\nu}$ are expressed by:

$$\eta^{\mu\nu}A'_{\mu\nu} = \eta^{\mu\nu}A_{\mu\nu} - \underline{i}\left(\eta^{\mu\nu}\eta_{\mu\mu}k_\nu B^{\mu} + \eta^{\mu\nu}\eta_{\nu\nu}k_\mu B^{\nu} - \eta^{\mu\nu}\eta_{\mu\nu}k_\mu B^{\mu}\right). \qquad \text{(H17)}$$

Then, the traceless condition is confirmed for the case:

$$\left(\eta^{\mu\nu}\eta_{\mu\mu}k_\nu B^{\mu} + \eta^{\mu\nu}\eta_{\nu\nu}k_\mu B^{\nu} - \eta^{\mu\nu}\eta_{\mu\nu}k_\mu B^{\mu}\right) = 0. \qquad \text{(H18)}$$

Specifically, for A'=$\eta^{\mu\nu}$ $A_{\mu\nu}$'= 0, which is equivalent to φ'= 0 and h'=0, it is required that:

$$\eta^{\mu\nu}A'_{\mu\nu} \equiv \eta^{00}A'_{00} + \eta^{11}A'_{11} + \eta^{22}A'_{22} + \eta^{33}A'_{33} = 0. \qquad \text{(H19)}$$

Relative to Eq. (H19), the imaginary part of Eq. (H17) is rewritten as:

$$k_0 B^0 + k_1 B^1 + k_2 B^2 + k_3 B^3 = 0. \qquad \text{(H20)}$$

The relation in Eq. (H19) is rewritten, considering A_{00}'= 0, as follows:

$$A'_{11} + A'_{22} + A'_{33} = 0. \qquad \text{(H21)}$$

Further, considering all possible constraints at this stage, given by $A_{0\nu}$' = 0 and $A_{o\nu}$ = 0, $k_\nu A_{\mu\nu}$'= 0, and Eq. (H.19), we have the following four linear equations:

$$\left.\begin{array}{l} A'_{11} + A'_{22} + A'_{33} = 0 \\ k'_1 A'_{11} + k'_2 A'_{12} + k'_3 A'_{13} = 0 \\ k'_1 A'_{21} + k'_2 A'_{22} + k'_3 A'_{23} = 0 \\ k'_1 A'_{13} + k'_2 A'_{23} + k'_3 A'_{33} = 0 \end{array}\right\} . \qquad \text{(H. 22)}$$

Here, we are allowed the freedom to select two amplitudes of the metric, among $A_{\mu\nu}$', as arbitrary values; then, the remaining $A_{\mu\nu}$' can be fixed by solving Eq. (H.22) as functions of the two selected arbitrary $A_{\mu\nu}$'. We then select A_{11}' and A_{12}' as independent amplitudes to decide φ_{11}' and φ_{12}'. More specifically, the linear equation Eq. (H.22) is rewritten for the four unknowns A_{13}',A_{22}',A_{23}',and A_{33}' as:

$$\begin{pmatrix} 0 & 1 & 0 & 1 \\ k'_3 & 0 & 0 & 0 \\ 0 & k'_2 & k'_3 & 0 \\ k'_1 & 0 & k'_2 & k'_3 \end{pmatrix} \begin{pmatrix} A'_{13} \\ A'_{22} \\ A'_{23} \\ A'_{33} \end{pmatrix} = \begin{pmatrix} -A'_{11} \\ -k'_1 A'_{11} - k'_2 A'_{12} \\ -k'_1 A'_{12} \\ 0 \end{pmatrix}, \qquad \text{(H23)}$$

with solutions:

$$\left.\begin{array}{l} A'_{13} = -\dfrac{k'_1 A'_{11} + k'_2 A'_{12}}{k'_3} \\ A'_{22} = -\dfrac{(k'^2_1 + k'^2_3) A'_{11} + 2k'_1 k'_2 A'_{12}}{k'^2_2 + k'^2_3} \\ A'_{23} = -\left(\dfrac{k'_2}{k'_3}\right) \dfrac{(k'^2_1 + k'^2_3) A'_{11} + k'_1 k'_2 A'_{12}}{k'^2_2 + k'^2_3} \\ A'_{33} = \dfrac{(k'^2_1 + k'^2_2) A'_{11} + 2k'_1 k'_2 A'_{12}}{k'^2_2 + k'^2_3} \end{array}\right\} . \qquad \text{(H. 24)}$$

Whole equations in Eq. (H.24) are given as Eq. (5.15) in the main text.

Appendix I

We start with the retarded potential formulation given as Eq. (5.17) in the main text:

$$h^{TT}_{ij}(r_{ob}) = -\frac{4G}{c^4} \int_s \frac{T_{ij}\left(\mathbf{r}^{(or)}_{ob}, t_{ob} - \frac{r_{os}}{c}\right) \cdot \delta\left(\mathbf{r}^{(or)}_{ob} - \mathbf{r}^{(or)}_{s}\right)}{r_{os}} dV^{(or)}_s . \qquad \text{(I1)}$$

(See the main text for all notations relating to Eqs. (5.17) and (5.18).) As given in Figure I, four Cartesian coordinate systems with supporting spherical coordinates are set to describe an orbiting IMSBH: specifically, the coordinate system ($x^{(or)}$,$y^{(or)}$,$z^{(or)}$) describes the entire binary orbits and coordinate system ($x^{(ts)}$,$y^{(ts)}$,$z^{(ts)}$) describes the interior of the Kerr BH and IMSBH of Gam, where the $y^{(ts)}$ axis rotates with phase angle $\Omega_{orb}\, t_s$:

$$\left.\begin{array}{l} x^{(c)}_s = x^{(or)}_s \cos(\Omega_{orb} t_s) + y^{(or)}_s \sin(\Omega_{orb} t_s) \\ y^{(c)}_s = -x^{(or)}_s \sin(\Omega_{orb} t_s) + y^{(or)}_s \cos(\Omega_{orb} t_s) - R_{Gam} \\ z^{(c)}_s = z^{(or)}_s \end{array}\right\} , \qquad \text{(I2)}$$

where R_{Gam} is the orbital radius of BH Gam. In the coordinate given by Eq. (I2), we rewrite Eq. (I1) as:

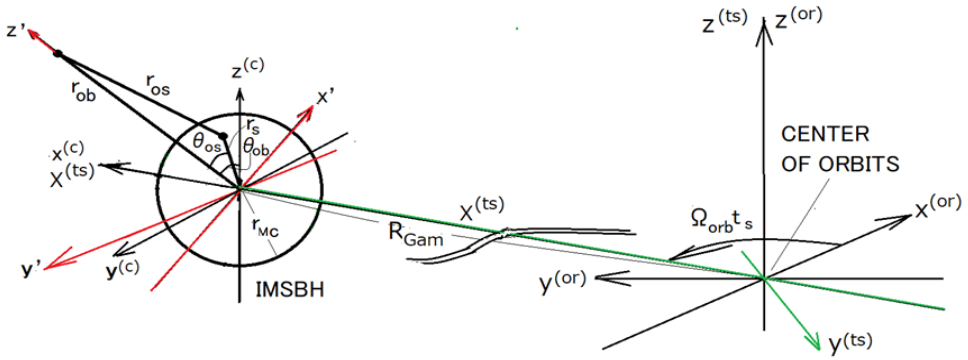

Figure I: Coordinate systems for orbiting IMSBH of the binary supermassive BHs whose orbits are described in the Cartesian coordinate system $(x^{(or)},y^{(or)},z^{(or)})$ with the origin given at the center of the binary orbits. The center of IMSBH that is assumed to be spherical with radius r_{Mc} is located in the direction of the $y^{(ts)}$ axis with distance R_{Gam}, i.e., the orbit radius of BH Gam; the Cartesian coordinate system $(x^{(ts)}),y^{(ts)},z^{(ts)})$, whose origin is set as coinciding with the center of the binary orbits, is defined so that the $x^{(ts)}$ and $y^{(ts)}$ axes are in the orbital plane, setting $y^{(ts)}$ to coincide with the moving radius of the orbiting Gam. The Cartesian coordinate system $(x^{(c)},y^{(c)},z^{(c)})$ is defined by setting the origin at the center of the orbiting IMSBH. The directions of all axes are set parallel to the corresponding axes of the $(x^{(ts)}),y^{(ts)},z^{(ts)})$ coordinate system. The source position in IMSBH given by the position vector $\mathbf{r}_s$ is expressed by the Cartesian coordinate system (x',y',z') defined by rotating the $(x^{(c)},y^{(c)},z^{(c)})$ system with respect to the fixed origin at the center of IMSBH so that the z' axis coincides with vector $\mathbf{r}_{ob}$. In this (x',y',z') coordinate system, the integration of Eq. (I1) can be expressed with simple steps by transforming to spherical coordinates.

$$h_{ij}^{TT}(\mathbf{r}_{ob}) = -\frac{4G}{c^4}\int_s \frac{T_{ij}\left(\mathbf{r}_s^{(c)}, t_{ob} - \frac{r_{os}}{c}\right)}{r_{os}} dV_s^{(t_s)}, \qquad (I3)$$

where $\mathbf{r}_{os}=|\mathbf{r}_{ob}^{(c)}-\mathbf{r}_s^{(c)}|$ for $\mathbf{r}_{ob}^{(c)}$ and $\mathbf{r}_s^{(c)}$ are vectors of the observation point and source position, respectively, defined from the origin of the coordinate at the center of the IMSBH. Considering the relation of the unit vectors in the two coordinate systems $(x^{(c)},y^{(c)},z^{(c)})$ and (x',y',z') whose relations are expressed by:

$$\left.\begin{aligned}
\hat{x}' &= -\sin\varphi_{ob}\hat{x}^{(c)} + \cos\varphi_{ob}\hat{y}^{(c)}\ , \\
\hat{y}' &= -\cos\theta_{ob}\cos\varphi_{ob}\hat{x}^{(c)} - \cos\theta_{ob}\sin\varphi_{ob}\hat{y}^{(c)} + \sin\theta_{0b}\hat{z}^{(c)}\ , \\
\hat{z}' &= \sin\theta_{ob}\cos\varphi_{ob}\hat{x}^{(c)} + \sin\theta_{ob}\sin\varphi_{ob}\hat{y}^{(c)} + \cos\theta_{0b}\hat{z}^{(c)},
\end{aligned}\right\} \qquad (I4)$$

we can write the relation of vectors $\mathbf{r}_{ob}^{(c)}$ and $\mathbf{r}_s^{(c)}$ in terms of $\mathbf{r}_{ob}'$ and $\mathbf{r}_s'$ in the transformed coordinate system, i.e., $\mathbf{r}_{os}=|\mathbf{r}_{ob}^{(c)}-\mathbf{r}_s^{(c)}|=|\mathbf{r}_{ob}'-\mathbf{r}_s'|$. Therefore, when we select r_{ob}' in the direction of $\hat{z}'$, the directional cosine is expressed as follows:

$$\mathbf{r}_{ob}' \cdot \mathbf{r}_s' = r_{ob}.r_s\cos\theta_{0s}, \qquad (I5)$$

where θ_{0s} is the angle between vectors $\mathbf{r}_{ob}'$ and $\mathbf{r}_s'$ observed at the center of the IMSBH. Rewriting this using r_{ob},r_s, θ_{0b},and θ_{0s}, as given in Figure I, i.e.,

$$z_{ob}' = r_{ob}, x_s' = r_s\sin\theta_s\cos\varphi_s, \qquad y_s' = r_s\sin\theta_s\sin\varphi_s, \qquad \text{and}$$
$$z_s' = r_s\cos\theta_s, \qquad (I6)$$

it follows that:

$$r_{os}^2 = |\mathbf{r}_{ob}' - \mathbf{r}_s'|^2 = r_{ob}^2 + r_s^2 - 2r_{ob}r_s\cos\theta_{os}. \qquad (I7)$$

When we rewrite the integration given by Eq. (I3) in coordinates $(x^{(ts)},y^{(ts)},z^{(ts)})$ to the expression in the (x',y',z') coordinate system, it follows that:

$$h_{ij}^{TT}(\mathbf{r}_{ob}) = -\frac{4G}{c^4}\int_s \frac{T_{ij}\left(\mathbf{r}_s', t_{ob} - \frac{r_{os}}{c}\right)}{r_{os}} r_s^2 \sin\theta_{os} dr_s\, d\theta_{os} d\varphi_s, \tag{I8}$$

where r_s,θ_{os},and φ_s are spherical coordinates related to (x',y',z') as:

$$\left.\begin{aligned} x_s' &= r_s \sin\theta_{os}\cos\varphi_s \\ y_s' &= r_s \sin\theta_{os}\sin\varphi_s \\ z_s' &= r_s \cos\theta_{os} \end{aligned}\right\} . \tag{I9}$$

Then, from Eq. (I7), we have:

$$r_{os} = \sqrt{r_{ob}^2 + r_s^2 - 2 r_{ob} r_s \cos\theta_{os}}\ . \tag{I10}$$

Using Eq. (I10), we can rewrite Eq. (I8) by expanding $1/r_{os}$ to the first order of r_s/r_{ob} , as:

$$h_{ij}^{TT}(\mathbf{r}_{ob}) = -\frac{4G}{c^4}\int_s \frac{T_{ij}\left(\mathbf{r}_s', t - \frac{r_{os}}{c}\right)\left(1 + \frac{r_s}{r_{ob}}\cos\theta_{os}\right)}{r_{ob}} r_s^2 \sin\theta_{os} dr_s\, d\theta_{os} d\varphi_s\ . \tag{I11}$$

Using dV_s' for integration of the first term, it follows that:

$$h_{ij}^{TT}(\mathbf{r}_{os}) = -\frac{4G}{c^4}\int_s \frac{T_{ij}\left(\mathbf{r}_s', t - \frac{r_{os}}{c}\right)}{r_{ob}} dV_s'$$

$$-\frac{4G}{c^4}\int_0^{r_{Mc}}\int_0^{\pi}\int_0^{2\pi} \frac{T_{ij}\left(x^s, t - \frac{r_{os}}{c}\right)}{r_{ob}^2} r_s^3 \sin 2\theta_{os}\, dr_s d\theta_{os} d\varphi\ . \tag{I 12}$$

Because the second term on the right-hand side of Eq. (I12) vanishes for integration by θ_{os} in the range of $0 \le \theta_{os} \le \pi$, we have the same result with the case of the remote source approximation, given by:

$$h_{ij}^{TT}(\mathbf{r}_{ob}) = -\frac{4G}{c^4}\int_s \frac{T_{ij}\left(\mathbf{r}_s', t - \frac{r_{os}}{c}\right)}{r_{ob}} dV_s'\ . \tag{I13}$$

Because r_{os} and r_{ob} do not vary when the coordinates are transformed from (x',y',z') to $(x^{(or)},y^{(or)},z^{(or)})$, we can express Eq. (I14) in the form of an orbiting binary as:

$$h_{ij}^{TT}(\mathbf{r}_{ob}) = -\frac{4G}{c^4}\int_s \frac{T_{ij}\left(\mathbf{r}_{ob}^{(or)}, t_{ob} - \frac{r_{os}}{c}\right)\cdot\delta\left(\mathbf{r}_{o\,b}^{(or)} - \mathbf{r}_s^{(or)}\right)}{r_{ob}} dV_s^{(or)}\ . \tag{I14}$$

For the source term in Eq. (I14), we can apply Einstein's quadrupole theorem to the IMSBH of Gam in the binary orbit as:

$$h_{ij}^{TT}(\mathbf{r}_{ob}) = -\frac{2G}{c^4}\cdot\frac{\partial^2}{\partial t_{ob}^2}\int_s \frac{T_{00}\left(\mathbf{r}_s^{(or)}, t_{ob}-\frac{r_{os}}{c}\right)x^i x^j}{r_{ob}}dV_s^{(or)}. \quad (I15)$$

This result is given as Eq. (5.19) in the main text.

Appendix J

For Eqs. (5.19) and (5.20) in the main text, we have approximated expressions by taking $x=R_{Gam}\cos(\Omega_{orb}t_s)$ and $y=R_{Gam}\sin(\Omega_{orb}t_s)$, considering $R_{Gam}\gg x_s^{(c)}$, and $R_{Gam}\gg y_s^{(c)}$, as:

$$h_{xx}^{TT}(\mathbf{r}_{ob})$$

$$= -\frac{2G}{c^4}\int_s \frac{\partial^2}{\partial t_s^2}\left\{\frac{\rho c^2\delta\left(x_s^{(or)}-x,\ y_s^{(or)}-y,\ t_{ob}-\frac{r_{os}}{c}\right)R_{Gam}^2\cdot\left[\frac{1+\cos(2\Omega_{orb}t_s)}{2}\right]}{r_{ob}}\right\}dV_s^{(or)}, \quad (J1)$$

and

$$h_{xy}^{TT}(\mathbf{r}_{ob})$$

$$= -\frac{2G}{c^4}\int_s \frac{\partial^2}{\partial t_s^2}\left\{\frac{\rho c^2\delta\left(x_s^{(or)}-x,\ y_s^{(or)}-y,\ t_{ob}-\frac{r_{os}}{c}\right)R_{Gam}^2\left[\frac{1}{2}\sin(2\Omega_{orb}t_s)\right]}{r_{ob}}\right\}dV_s^{(or)}. \quad (J2)$$

Differentiating by t_s, Eqs. (J1) and (J2) are rewritten as:

$$h_{xx}^{TT}(\mathbf{r}_{ob})$$

$$= -\frac{4G}{C^4}\int_s \frac{\rho c^2\delta\left(x_s^{(or)}-x,\ y_s^{(or)}-y,\ t_{ob}-\frac{r_{os}}{c}\right)\cdot[-R_{Gam}^2\Omega_{orb}^2\cos(2\Omega_{orb}t_s)]}{r_{ob}}dV_s^{(or)} \quad (J3)$$

and

$$h_{xy}^{TT}(\mathbf{r}_{ob})$$

$$= -\frac{4G}{C^4}\int_s \frac{\rho c^2\delta\left(x_s^{(or)}-x,\ y_s^{(or)}-y,\ t_{ob}-\frac{r_{os}}{c}\right)\cdot[-R_{Gam}^2\Omega_{orb}^2\sin(2\Omega_{orb}t_s)]}{r_{ob}}dV_s^{(or)}, \quad (J4)$$

where R_{Gam} and Ω_{orb} are the orbiting radii of the BH Gam and the angular velocity, respectively. We calculated GW in the region inside the event horizon of the Kerr BH, where the radius of the event horizon r_E is in the range of $100r_{Mc}>r_E>10r_{Mc}$, with respect to the radius r_{Mc} of the IMSBH as the source. In this case, the distribution of the source is not simply considered as a point; we should consider the distribution of the source within the range $r_{Mc}\geq r_s$. Then, applying the same processes for treating $\mathbf{r}_{os}=|\mathbf{r}_{ob}-\mathbf{r}_s|$, as is the case in Appendix I, where we selected local spherical coordinates to express $dV_s^{(or)}=dV_s^{(c)}$, Eqs. (J3) and (J4) are rewritten by expanding r_{os} to the first order of r_s/r_{ob} as follows:

$$h_{xx}^{TT}(\mathbf{r}_{ob}) = \frac{4G}{c^4}\int_0^{r_{Mc}}\int_0^{\pi}\int_0^{2\pi}\frac{\rho c^2\delta\left(t_s-\left[t_{ob}-\frac{r_{ob}}{c}\left(1-\frac{r_s}{r_{ob}}\cos\theta_{os}\right)\right]\right)}{r_{ob}}$$

$$\times[R_{Gam}^2\Omega_{Gam}^2\cos(2\Omega_{orb}t_s)]r_s^2\sin\theta dr_s d\theta d\varphi \qquad (J5)$$

and

$$h_{xy}^{TT}(\mathbf{r}_{ob}) = \frac{4G}{c^4}\int_0^{r_{Mc}}\int_0^{\pi}\int_0^{2\pi}\frac{\rho c^2\delta\left(t_s-\left[t_{ob}-\frac{r_{ob}}{c}\left(1-\frac{r_s}{r_{ob}}\cos\theta_{os}\right)\right]\right)}{r_{ob}}$$

$$\times[R_{Gam}^2\Omega_{orb}^2\sin(2\Omega_{orb}t_s)]r_s^2\sin\theta dr_s d\theta d\varphi. \qquad (J6)$$

The relations in Eqs. (J5) and (J6) are further mainpulated to realize:

$$h_{xx}^{TT}(\mathbf{r}_{ob})$$

$$= \frac{8\pi G}{c^4}\int_0^{r_{Mc}}\int_0^{\pi}\frac{\rho\cdot R_{Gam}^2\Omega_{orb}^2\cos\left[2\Omega_{orb}\left(t_{ob}-\frac{r_{ob}}{c}\right)+2\Omega_{orb}\frac{r_s}{c}\cos\theta_{os}\right]r_s^2\sin\theta dr_s d\theta}{r_{ob}}. \qquad (J7)$$

and

$$h_{xy}^{TT}(\mathbf{r}_{ob})$$

$$= \frac{8\pi G}{c^4}\int_0^{r_{Mc}}\int_0^{\pi}\frac{\rho\cdot R_{Gam}^2\Omega_{orb}^2\sin\left[2\Omega_{orb}\left(t_{ob}-\frac{r_{ob}}{c}\right)+2\Omega_{orb}\frac{r_s}{c}\cos\theta_{os}\right]r_s^2\sin\theta dr_s d\theta}{r_{ob}}. \qquad (J8)$$

When we estimate the term $(2\Omega_{orb}\, r_s\cos\theta_{os})/c$ at the phase of the sinusoidal function, the value is clarified to be less than 10^{-3} in the case of the present binary system. Accordingly, we can only consider the term $2\Omega_{orb}(t_{ob}\text{-}r_{ob}/c)$ in the phase of the sinusoidal function. As results of the integration in Eqs. (J7) and (J8), we have:

$$h_{xx}^{TT}(t_{ob},\mathbf{r}_{ob}) = \frac{4GM}{c^2 r_{ob}}\left(\frac{R_{Gam}^2\Omega_{orb}^2}{c^2}\right)\cdot\cos\left[2\Omega_{orb}\left(t_{ob}-\frac{r_{ob}}{c}\right)\right] \qquad (J9)$$

and

$$h_{xy}^{TT}(t_{ob},\mathbf{r}_{ob}) = \frac{4GM}{c^2 r_{ob}}\left(\frac{R_{Gam}^2\Omega_{orb}^2}{c^2}\right)\cdot\sin\left[2\Omega_{orb}\left(t_{ob}-\frac{r_{ob}}{c}\right)\right], \qquad (J10)$$

where M is the total mass of the BH, given by:

$$M = \frac{4\pi}{3}r_{Mc}^3\rho\,, \qquad (J11)$$

with respect to the radius r_{Mc} of the IMSBH, simply assuming a homogeneous state of the matter.
When we apply the Schwarzschild radius $r_g=(2GM)/c^2$, orbital velocity v_{Gam}, and initial average phase Φ_I, the results can be rewritten as follows:

$$h_{xx}^{TT}(t_{ob},\mathbf{r}_{ob}) = 2\frac{r_g}{r_{ob}}\cdot\left(\frac{v_{Gam}}{c}\right)^2\cdot\cos\left[2\Omega_{orb}\left(t_{ob}-\frac{r_{ob}}{c}\right)+\Phi_I\right] \quad \text{(J12)}$$

and

$$h_{xy}^{TT}(t_{ob},\mathbf{r}_{ob}) = 2\frac{r_g}{r_{ob}}\cdot\left(\frac{v_{Gam}}{c}\right)^2\cdot\sin\left[2\Omega_{orb}\left(t_{ob}-\frac{r_{ob}}{c}\right)+\Phi_I\right]. \quad \text{(J13)}$$

Appendix K

Eqs. (6.1) and (6.2) in the main text are given in Cartesian coordinates with the origin at the center of the orbits of the binary BH, as depicted in Figure 10 of the main text, where the spherical coordinates whose origin is at the center of the IMSBH are defined. These two coordinates are related as follows:

$$\left.\begin{aligned} x_s^{(or)} &= R_{Gam}\cos(\Omega_{orb}t+\Phi_0)+r\sin\theta\cdot\cos\varphi \\ y_s^{(or)} &= R_{Gam}\sin(\Omega_{orb}t+\Phi_0)+r\sin\theta\cdot\sin\varphi \\ z_s^{(or)} &= r\cos\theta \end{aligned}\right\}. \quad \text{(K1)}$$

For the spacetime of the GWs h_{xx}^{TT} and h_{xy}^{TT}, we applied the transformation to include expressions in the spherical coordinates at a given plane with a fixed θ. Following the formula of the transformation of the tensor, the transformed tensors h_{rr}^{TT},$h_{r\varphi}^{TT}$,and $h_{\varphi\varphi}^{TT}$ are expressed as:

$$h_{rr}^{TT} = h_{xx}^{TT}\frac{\partial x}{\partial r'}\frac{\partial x}{\partial r'}+2h_{xy}^{TT}\frac{\partial x}{\partial r'}\frac{\partial y}{\partial r'}+h_{yy}^{TT}\frac{\partial y}{\partial r'}\frac{\partial y}{\partial r'}, \quad \text{(K2)}$$

$$h_{r\varphi}^{TT} = h_{xx}^{TT}\frac{\partial x}{\partial r'}\cdot\frac{\partial x}{r'\,\partial\varphi}+h_{xy}^{TT}\frac{\partial x}{\partial r'}\cdot\frac{\partial y}{r'\,\partial\varphi}+h_{xy}^{TT}\frac{\partial x}{r'\,\partial\varphi}\frac{\partial y}{\partial r'}+h_{yy}^{TT}\frac{\partial y}{\partial r'}\frac{\partial y}{r'\,\partial\varphi}, \quad \text{(K3)}$$

$$h_{\varphi\varphi}^{TT} = h_{xx}^{TT}\frac{\partial x}{r'\,\partial\varphi}\cdot\frac{\partial x}{r'\,\partial\varphi}+2h_{xy}^{TT}\frac{\partial x}{r'\,\partial\varphi}\cdot\frac{\partial y}{r'\,\partial\varphi}+h_{yy}^{TT}\frac{\partial y}{r'\,\partial\varphi}\cdot\frac{\partial y}{r'\,\partial\varphi}, \quad \text{(K4)}$$

where $x=x_s^{(or)}$, $y=y_s^{(or)}$, $z=z_s^{(or)}$, and $r'=r\sin\theta$, and the spacetime h_{yy}^{TT} is given as

$h_{yy}^{TT}=-h_{xx}^{TT}$ by local plane wave approximation. From the relations given in Eq. (K1), it follows that:

$$\left.\begin{aligned} &\partial x/\partial r' = \cos\varphi, \\ &\partial x/r'\,\partial\varphi = -\sin\varphi \\ &\partial y/\partial r' = \sin\varphi \\ &\text{and} \\ &\partial y/r'\,\partial\varphi = \cos\varphi \end{aligned}\right\}. \quad \text{(K5)}$$

Inserting the relations in Eq. (K5) into the corresponding terms in Eqs. (K2)–(K4), we have:

$$h_{rr}^{TT} = h_{xx}^{TT}\cos^2\varphi + 2h_{xy}^{TT}\cos\varphi\cdot\sin\varphi + h_{yy}^{TT}\sin^2\varphi = h_{xx}^{TT}\cos 2\varphi + h_{xy}^{TT}\sin 2\varphi$$
$$= 4\frac{r_g}{r_{ob}}\cdot\left(\frac{v_{Gam}}{c}\right)^2\cdot\cos\left[2\Omega_{orb}\left(t_{ob}-\frac{r_{ob}}{c}\right)+\Phi_I-2\varphi\right], \qquad (K6)$$

$$h_{r\varphi}^{TT} = -h_{xx}^{TT}\cos\varphi\cdot\sin\varphi + h_{xy}^{TT}\cos^2\varphi - h_{xy}^{TT}\sin^2\varphi + h_{yy}^{TT}\sin\varphi\cdot\cos\varphi$$
$$= -h_{xx}^{TT}\sin 2\varphi + h_{xy}^{TT}\cos 2\varphi$$
$$= 4\frac{r_g}{r_{ob}}\cdot\left(\frac{v_{Gam}}{c}\right)^2\cdot\sin\left[2\Omega_{orb}\left(t_{ob}-\frac{r_{ob}}{c}\right)+\Phi_I-2\varphi\right], \qquad (K7)$$

and

$$h_{\varphi\varphi}^{TT} = h_{xx}^{TT}\sin^2\varphi - 2h_{xy}^{TT}\sin\varphi\cdot\cos\varphi + h_{yy}^{TT}\cos^2\varphi = -h_{xx}^{TT}\cos 2\varphi - h_{xy}^{TT}\sin 2\varphi$$
$$= -h_{rr}^{TT}. \qquad (K8)$$

To determine the above relations, we utilized the expressions in Eqs. (5.26) and (5.27) in the main text for h_{xx}^{TT} (=$-h_{yy}^{TT}$) and h_{xy}^{TT}, respectively. The relations in Eqs. (K6) and (K7) are given as Eqs. (6.6) and (6.7), respectively, in the main text, setting φ to be an arbitrary constant φ_0. Notably, the phase is rewritten in the expression of Eqs. (6.6) and (6.7) through the argument given in Eq. (6.4).

Appendix L

As expressed by Eq. (6.9) in the main text, we have a compact form that describes the two basic components of GW as:

$$H = h_{rr}^{TT} + \underline{i}\, h_{r\varphi}^{TT} = A\cdot\cos(2\Omega_{orb}t_{ob} - \mathbf{k}_{ob}\mathbf{r}_{ob} + \Phi_I - 2\varphi_{0b})$$
$$+\underline{i}\, A\cdot\sin(2\Omega_{orb}t_{ob} - \mathbf{k}_{ob}\mathbf{r}_{ob} + \Phi_I - 2\varphi_{0b})\,. \qquad (L1)$$

Because the GW equation given by Eq. (L1) is an expression in QMST, transformation is required for the expression in spacetime of the Kerr BH for the vacuum region inside the event horizon to determine the real amplitude of GW in the BH. To prepare for this purpose, we rewrite H in Eq. (L1) as:

$$\overline{h_{rr}^{TT}} = h_{rr}^{TT}\left(1 + \underline{i}\frac{h_{r\varphi}^{TT}}{h_{rr}^{TT}}\right)$$
$$= h_{rr}^{TT}\left[1 \quad + \underline{i}\tan(2\Omega_{orb}t_{ob} - \mathbf{k}_{ob}\mathbf{r}_{ob} + \Phi_I - 2\varphi_{0b})\right]. \qquad (L2)$$

This is a kind of degenerated expression of GW in the observation frame, where we can observe the spin motion of Kerr BH in QMST (QM in following equations). Between the QMST and the spacetime of the vacuum region inside the event horizon of Kerr BH (B), the four-dimensional proper length is co-occupied as:

$$-c^2\left(1-\frac{v_\varphi^2}{c^2}\right)\cdot dt_{QM}^2 + dr_{QM}^2 = -c^2 dt_B^2\cdot F^2 + \frac{\Sigma}{\Delta}dr_B^2\,. \qquad (L3)$$

The GW spacetime (h_{rr}^{TT}) in QMST is transformed to the expression in the Kerr spacetime as:

$$h_{(B)rr}^{TT} = \overline{h_{rr}^{TT}} \frac{\partial r_{QM}}{\partial r_B} \cdot \frac{\partial r_{QM}}{\partial r_B} . \qquad (L4)$$

From Eq. (L3), we calculated $(\partial r_{QM})/(\partial r_B)$ considering the relation given in Eq. (6.13) in the main text; the result gives:

$$h_{(B)rr}^{TT} = \overline{h_{rr}^{TT}} \cdot \frac{\Sigma}{\Delta} . \qquad (L5)$$

By translating the spacetime in Eq. (L2) to the Kerr spacetime, we obtained the results for the amplitude given by Eq. (6.15) in the main text.